MANUFACTURING OF A FAST-DISSOLVING DOSAGE FORM – INVESTIGATING POWDER HANDLING & CONTROL OF SURFACE CHARACTERISTICS

OMAR SHEZAD ASLAM

A Thesis Submitted to the Department of Chemical Engineering, University of Birmingham for the Degree of Master of Research (MRes)

JUNE 2009

DEPARTMENT OF CHEMICAL ENGINEERING, UNIVERSITY OF BIRMINGHAM

MANUFACTURING OF A FAST-DISSOLVING DOSAGE FORM – INVESTIGATING POWDER HANDLING & CONTROL OF SURFACE CHARACTERISTICS

By

Omar Shezad Aslam

2009

ABSTRACT

An early stage in the manufacture of a proprietary fast dissolving dosage form (FDDF), involves dissolution/suspension of the active agent in an aqueous solution. To allow use of aqueous labile drugs and/or coated drug particles in the FDDF, the development of an alternative approach is sought i.e. that which allows independent dosing of drug powders and liquid components. The focus of this work is on the powder dosing aspect. A vacuum based filling system was investigated and was generally shown to be capable of delivering accurate 50 mg and 400 mg doses of model drug particles with high precision (RSD <2 %). The investigated model materials included coated sugar spheres, paracetamol, ibuprofen and excipient powders with typical diameters between 100 μm-500 μm. The strength of vacuum used to collect the powder was seen to affect the dose weight for certain materials more than others; the magnitude of this effect was linked to the Carr's Index. The dosing equipment was shown to be capable of collecting doses rapidly (< ½ second), hence being suitable for a potential, future automated process. In a discrete investigation into the manufacture of the same FDDF, the presence of surface imperfections (known as nodules) was known to affect a small number of manufactured units which led to lost product. The occurrence of these nodules was shown to be linked to the relative concentrations of the major constituents (biopolymer and saccharide) and also to irregular freezing rates. Formulations with low biopolymer content and high saccharide content appeared to be more prone to small surface imperfections due to a weaker structure. However the presence of large nodules (on all formulations) was linked to temperature fluctuations that have the effect of creating irregular freezing rates during the freezing process.

ACKNOWLEDGEMENTS

I am grateful to my academic supervisors Dr Rachel Bridson and Dr Serafim Bakalis for their support and guidance throughout this project. I would also like to thank my industrial supervisor Dr Desmond Wong for his invaluable input and support.

I wish to acknowledge the EPSRC and Catalent Pharma Solutions for financial support during the period of study.

I would also like to thank Catalent Pharma Solutions for providing equipment, support and training. In particular I would like to thank Mr Kerri Mallindine for his technical expertise.

Finally, I would like to thank my family for their trust and encouragement and my friends for helping me get through the difficult periods throughout my time of study.

"Verily, when He intends a thing, His command is 'Be!' and it is!" – Qur'an, 36:82

CONTENTS

LIST OF FIGURES

LIST OF TABLES

ABBREVIATIONS

ACR (prefix)	Sugar spheres coated with Acryleze
APAP (prefix)	Acetaminophen (paracetamol)
BH	Birmingham
CA	Cellulose acetate phthalate
CI	Carr's index
E100	Eudragit® 100
FC (technology)	Floor Console (Powder Filling Machine)
FC or σ_c	Unconfined yield stress
FDDF	Fast dissolving dosage form
FFC	Flow function
ID	Inner diameter
MCC	Microcrystalline cellulose
PSD	Particle size distribution
RHOB	Bulk density
RSD	Relative standard deviation
SD	Standard deviation
SIGMA1 or σ_1	Major principle stress
SUR (prefix)	Sugar spheres coated with Surelease

1.0 INTRODUCTION TO POWDER DOSING

1.1 Aims of this work

In the manufacture of a proprietary fast dissolving dosage form (Figure 1 a), the formulation process involves the dissolution/suspension of a drug in an aqueous solution consisting of a biopolymer such as gelatine and a saccharide such as mannitol. The drug must be stable in this aqueous environment for up to several hours, while the mixture is formulated, moved to the main production line (and sometimes queued there), dosed and subsequently frozen and freeze-dried. The biopolymer and saccharide are important because they help create a porous matrix which encourages fast dissolution of the dosage form.

It is now proposed that a two-stage dosing system be developed (Figure 1 b); a system which would allow the dosing of powdered drug to be carried out separately to the aqueous solution before being frozen. This type of system would limit the exposure of a drug to the aqueous solution to a few minutes, allowing the use of a wider range of drugs in the manufacturing process. Furthermore, a two stage dosing system would increase flexibility to allow the use of coated, powdered/granulated drug particles designed for modified/targeted release or taste-masking.

The greatest challenge here lies in the dosing of the powdered drug and how such a system would be combined with a liquid dosing system to produce a viable product.

The aims for this project are:

- To identify suitable technology that will meet the sponsor's requirements, by carrying out a theoretical and experimental appraisal of the available options.
- To investigate the applicability of the technology and explore its capabilities in some depth using experimental trials with a range of typical pharmaceutical bulk materials.
- To provide recommendations with regard to equipment and materials providing a foundation from which a new manufacturing process could potentially be developed.

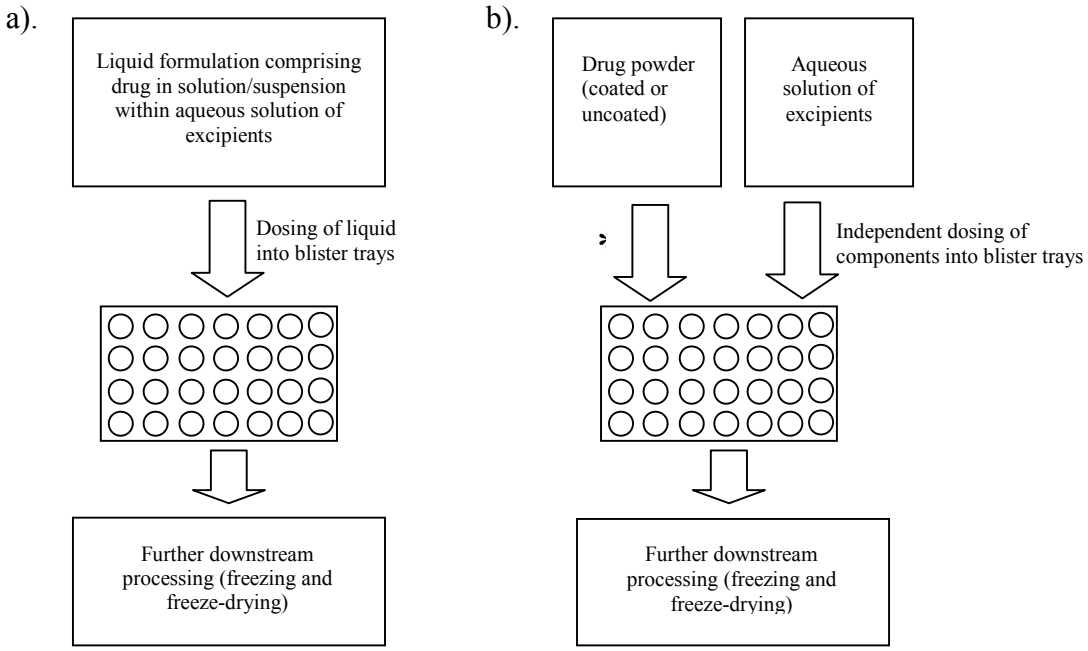

Figure 1 – a) The current manufacturing process; b) The manufacturing process to be explored.
*** The powder dosing operation is the focus of work presented in the main part of this thesis.**

In this chapter, characteristics of particles and powders are introduced that are likely to be important in the development of the powder dosing system. Next, general methods for powder dosing are considered along with an introduction to the requirements of the industrial sponsor. Finally, the author's choice of equipment, which has been evaluated in subsequent chapters, is presented.

1.2 Particle characteristics

Particles are individual solid elements which interact with a continuous medium that may surround them. A powder is the whole medium consisting of many particles which combines all the interactions, particularly particle-particle contacts. The powder is highly heterogeneous but can be considered to be a homogeneous solid with the same density as the mean density of the whole medium (Deleuil *et al*, 1994).

The behaviour of a collection of particles (i.e. the bulk properties) will be dependent on the overall interactions between many particle properties where small changes in one particle property can have considerable effects on the behaviour of a bulk material. Furthermore, each population of particles will always be slightly different in terms of average particle size, size distribution and particle shape. A material's bulk properties can be affected by many particle properties some of which are (Hawkins *et al*, 1990):

- Size/size distribution
- Agglomerate/aggregate state
- Surface texture
- Shape
- Density
- Hardness/crush strength
- Melting point
- Particle porosity
- Surface area

This is not an exhaustive list, and some of these properties will be more important than others depending on the application. In this literature review, it is important to develop an understanding of how bulk materials behave and the properties that may be important in the handling, measurement and dosing of small amounts (<500 mg) of pharmaceutical grade bulk materials. The first two properties in the above list (size and agglomeration) have been chosen for further consideration.

1.2.1 Particle size/size distribution

The particle size defines the magnitude of a whole range of inter-particular forces that may be present (an extensive review is given in Israelachvili *et al*, 1991). These forces may be in the form of Van der Waal's, electrostatic, capillary or frictional and their magnitude is defined by composition of the particles and the surface texture. The origins and methods for calculating the magnitude of the forces are beyond the scope of this text and are given in Seville *et al*, 1997. It is important to understand however that as the particle size decreases, the mass also decreases and hence the gravitational force acting on the particle decreases. At particle sizes below 100 μm, the inter-particulate forces begin to have an effect and at very small sizes, (<10 μm) the effects of the forces are considerable. This results in the materials becoming very cohesive and very difficult to handle. The force required to separate two such particles is a very important powder characterisation parameter because it has an important effect on bulk flowability (Li *et al*, 2004). For particles much greater than 100 μm, the gravitational forces are dominant and the effect of the inter-particular forces becomes less prevalent with the effect that the material becomes more free-flowing.

Another bulk property that is dependent on particle size is the powder bed porosity (also known as void fraction). This is also shown to be influenced by the inter-particle forces, especially for very fine materials (Yu *et al*, 2003).

The particle size distribution (PSD) influences the way in which particles fit together in a powder bed. Furthermore, the PSD can also influence the way in which particles slide over one another when the material flows. There have been many investigations into the packing characteristics of materials; however these have been limited to packing of spheres (e.g. Cheng *et al*, 2000, or Webb *et al*, 2006). A full description of all the types of packing arrangements is beyond the scope of this text but it is important to outline how particle packing can be affected by PSD because this will be important when considering powder beds of various pharmaceutical grade materials in later chapters.

In a powder bed consisting of spherical particles all of the same size, a number of "regular" packing arrangements can occur (e.g. cubic, orthorhombic etc. full details given in Fayed *et al*, 1997). These arrangements are well defined and repeatable. In practice, one arrangement does not occur exclusively since there is a tendency in localised regions for preference of one packing arrangement over another. Each type of arrangement will have an associated powder bed porosity, or void fraction. The arrangements (and hence porosity) can be affected by tapping or vibration or other types of compaction processes. Particles however are not always spherical, nor always the same size. In cases where two distinct sizes are present, smaller particles can fill the spaces between the larger particles to reduce the porosity. When the spread of the PSD is large, the packing arrangement becomes very complicated and difficult to predict and more crucially, difficult to repeat. Furthermore, with a large spread of particle size, there is a tendency for particles to segregate. Even if the powder bed is considered to be well mixed, localised segregation of particles can still occur. Some areas will contain more large particles and other areas will contain more small particles (Schulze *et al*, 1994; Williams *et al*, 1990; Harnby *et al*, 1985).

In the pharmaceutical application of powder dosing, small amounts of powder (<500 mg) must be measured accurately. If this measurement is carried out by mass (e.g. using a balance) the packing arrangement is unimportant, however if the measurement is carried out by volume, a repeatable packing arrangement is crucial to ensure that the volume of powder measured equates to the same mass each time. If the void fraction of the powder

contained in the dose volume varies significantly from one dose to the next, the repeatability (by mass) of the doses will be poor. When the spread of the PSD is large, localised segregation will occur as described above and each dose will consist of different packing arrangements with the overall effect of reducing the repeatability of each dose.

1.2.2 Agglomerate/aggregate state

The amount of agglomeration or aggregation in a material is dependent on the nature of the cohesive forces between particles. Cohesive forces can arise as a result of Van der Waals interactions, hydrogen binding, electrical attraction between charged particles or capillary forces that arise due to the presence of moisture between the particles (Deleuil *et al*, 1994). The inter-particle forces only have a significant effect on flow behaviour if the particles are small and the gravitational forces are small compared to the inter-particle forces (Seville *et al*, 1997). The effect of aggregation and agglomeration is that a material becomes less free flowing and more difficult to handle. Furthermore, if some particles clump together, they no longer behave as small particles but can be considered as one larger irregular particle. The result is that the material contains mainly fine particles with a great deal of larger aggregates dispersed within the bulk. This in effect is like increasing the spread of the particle size distribution. The result on the particle packing arrangement is therefore similar to that described in the previous section.

1.3 Powder dynamics and powder flow

Powder characterisation and flow properties are widely documented in general terms (Sutton *et al*, 1976 and Yokoyama *et al*, 1991) and for cohesive powders (Molerus *et al*, 1982). The flowability of a powder depends on a wide range of factors. Particle size, electrostatic forces, particle shape, moisture content, cohesion forces and bulk density are just some of the particle properties that determine the flowability. Flowability must be consistent in separating a powder for a consistent volume; this is simple only for liquids. Due to the complexity of the processes involving powders, there are no reliable quantitative relationships between primary properties like particle size and distribution, particle shape, etc and secondary properties such as flow properties or bulk density (Hawkins *et al*, 1990). Therefore, reliable process design can only be done on the basis of laboratory or pilot-scale tests on the actual powder.

There are various methods which can be used to determine flowability, some of which are described in Cumberland *et al*, 1987, and Iinoya *et al*, 1988. Two common approaches are described below.

The first method is proposed by Carr *et al* (Carr, 1965) in which the change in apparent density of a bed of powder in response to tapping or vibration can be quantified. The Carr's compressibility index is thus defined as:

$$CI = \frac{\rho_{tapped} - \rho_{poured}}{\rho_{tapped}} \times 100 \qquad (1)$$

Although the name suggests it measures compressibility, the Carr's index more usefully describes the flowability as discussed in Chulia *et al*, 1985. Particles which are considered to be freely mobile have a Carr index of less than 15%, whereas cohesive materials with low particle mobility have a Carr index of over 22%. The Carr's method is a simple but effective way of measuring the flowability of materials and it allows a material to be assigned with a numerical value. This may therefore allow one to observe quantitative relationships between powder behaviour under various processing conditions (e.g. the dosing process) and Carr's index.

A second widely used method for flow characterisation is to use shear testing (Jenike *et al*, 1964). The basis of shear testing is to find the shear stress required to make a material fail (or flow) under a defined consolidating stress. When the consolidating stress is varied, a range of shear stresses are obtained. A yield locus can then be obtained by plotting the shear stresses against the consolidating stresses. The unconfined yield strength, σ_c, is defined as the stress required to make a material flow when the normal stress is zero and is obtained by drawing a Mohr's stress circle which is tangential to the material yield locus and goes through the origin. A second Mohr's circle that is tangential to the end point of the yield locus describes the major consolidation stress, σ_1 as shown in Figure 2. The use of Mohr circles to describe the stresses in a bulk material is described in many powder technology texts, e.g. Deleuil *et al*, 1994, Seville *et al*, 1997 or Schulze, 2008.

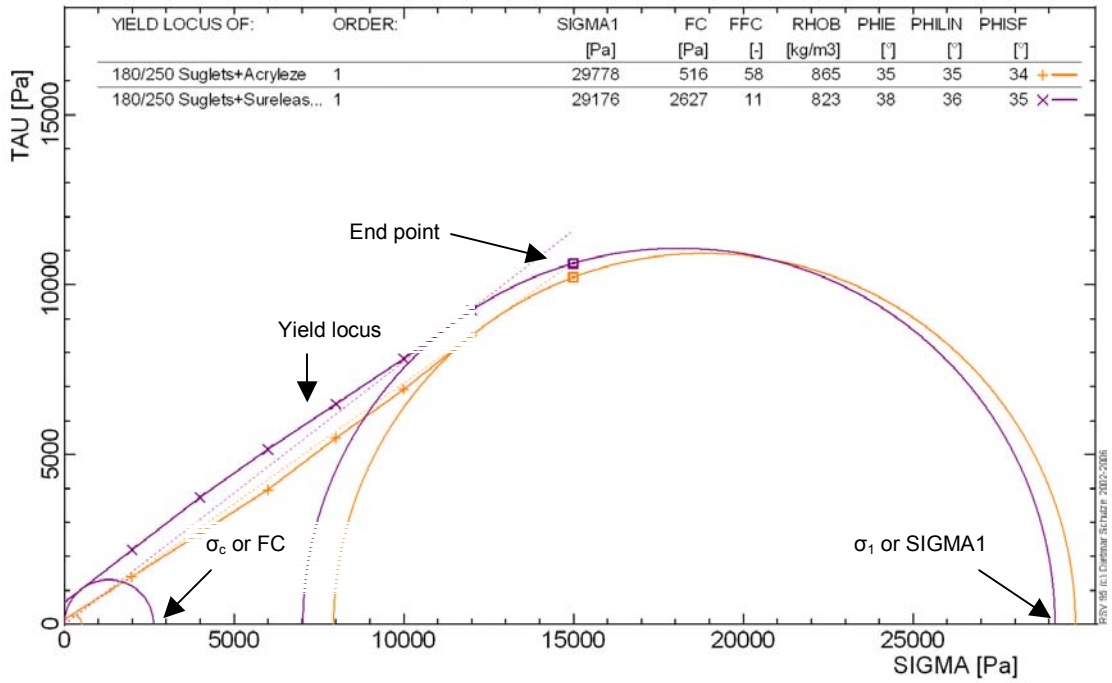

Figure 2 – Graph showing the yield locus for two materials tested using the Schulze Shear Tester and the associated σ_c and σ_1 values.

Shear testing is used to obtain a flow function for a material which was defined by Jenike *et al* as:

$$\text{Flow Function (FFC)} = \frac{\sigma_1}{\sigma_c} = \text{major consolidating stress/unconfined yield strength.} \quad (2)$$

It would be very simple if the flow function was a single value for all consolidation stresses, however in reality, the flowability of a material will change depending on the level of consolidation experienced. In general, the larger FFC is, the better a bulk solid flows (Schulze, 2008) however a material may have a high FFC value at low consolidation stresses and a low FFC value at high consolidation stresses, and vice versa. Therefore, the flow function is more accurately described by plotting a curve such as the one in Figure 3. The diagram shows that the FFC value is dependent on the consolidation stress. With some materials, FFC varies with σ_1 as shown by curve B and with others it will vary as shown by curve A (Schulze, 2008). The flowability of a material at a given consolidation stress will depend on many properties, such as particle shape, hardness, surface characteristics, friction, attractive forces, and elastic/plastic deformation to name just a few. With each consolidation stress, a different value of FFC is obtained. For materials that behave as described by curve A, FFC will usually be larger (i.e. better flowability) at a greater consolidation stress and for most bulk solids there will be an

extremely low consolidation stress at which the bulk solid flows poorly. In other words, most materials have a flow function curve that passes between the flow regimes described in Figure 3. Because of this dependence on consolidation stress, it is not possible to describe the flowability of a bulk solid with only one numerical value.

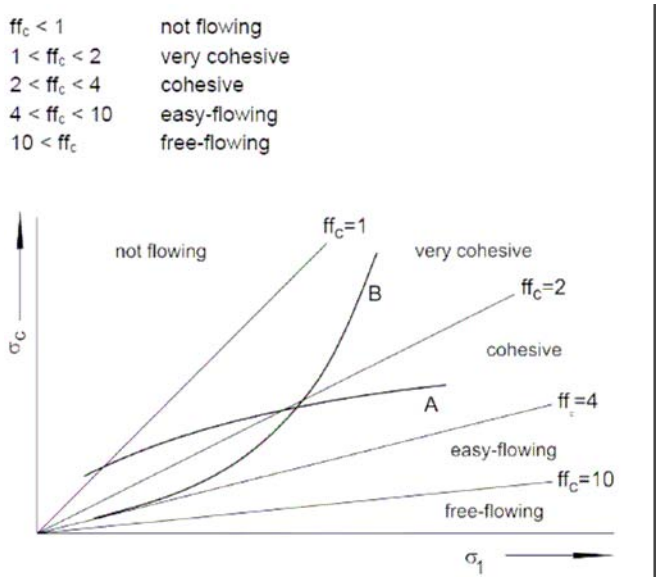

Figure 3 – Figure showing how the numerical value of flow function (FFC) relates to a description of the flow behaviour. Curves A and B show how a materials' flowability can vary depending on the consolidation stress. (Schulze, 2008).

1.4 Powder dosing

The process of filling into capsules is widely carried out in the pharmaceutical industry, but in this project, blister filling is required. Capsule filling and filling into blister packs are largely the same; the major difference being that blister trays have an array of pockets over a rectangular area which need to be filled, however capsules can be conveyed in single file which means that the dosing head can remain stationary.

Powder dosing systems essentially involve four operations; collection/picking from the source, conveying, dispensing to the target and measuring the dose. Sometimes the four stages may be more or less distinct. The first operation, powder collection from the source, can be achieved by feeding from a silo, aspirating from a powder bed or picking up by electrostatic collectors. In the second operation, conveying of the powder can be achieved by pneumatic means or mechanical means e.g. auger screw or robotic motion. The dispensing can then be carried out under the influence of gravity, electrostatic or Van der Waal's forces. The trickiest operation can often be the measurement of the dose and

this may be embedded in the first three operations e.g. by controlling the rotation speed in screw feeding or using a controlled volume to collect the powder. The only truly accurate and reliable method for measuring is weighing by balance. This is less convenient and slower than volumetric methods, which are more commonly used (Yang *et al*, 2007). The main disadvantage of volumetric methods is the likelihood of error induced by the variability of the powder packing density (see section 1.2.1). The apparent density of powders is affected dramatically by the powder characteristics (size, shape etc) and the environmental conditions (Deleuil *et al*, 1994).

1.5 Measurement and dispensing methods

There are primarily two methods for measuring a powder dose. Material can either be measured gravimetrically using an accurate balance or alternately using a control volume (volumetric method) to measure a volume of powder. The latter process is therefore dependent on a powder packing in the same way for each dose. The packing is in turn dependent on the particle size distribution as described in section 1.2. Slight differences in the size distribution between batches can significantly affect the particle packing efficiency. There are several types of volumetric methods, some of which use plungers to compact a powder into a volume such as the arrangement in Figure 4.

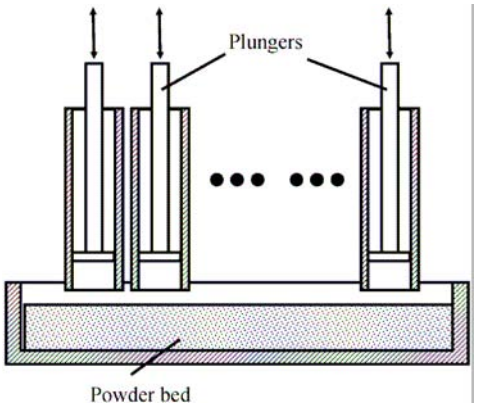

Figure 4 - Collection of powder plugs from a powder bed using controlled volumes (taken from Yang *et al*, 2007)

Another volumetric method is to use vacuum suction to collect material into a dosing chamber as shown in Figure 5. The material is restricted to the dosing chamber by using an air filter and is dispensed to a receiving container by a small blast of air creating positive pressure. The disadvantage of this method is its inability to provide continuous

automatic measuring and dispensing of powder i.e. motion of the instrument must be carried out from the powder bed to the target.

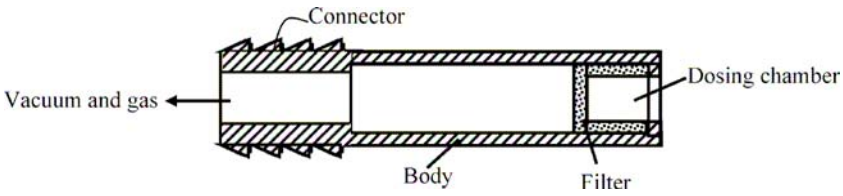

Figure 5 – A vacuum based dosing head (taken from Yang *et al*, 2007)

Another type of volumetric method is the screw or auger dosing method. The dose in this method is measured by controlling the rotation of the screw as shown in Figure 6. Augers have been developed to overcome some of the problems with cohesive materials (Ionadi *et al*, 2000 and Alexande *et al*, 1999). However, with small doses, powders tend to cake and dosing becomes difficult. One method to resolve this is to use a system of concentric augers (Gaalswyk *et al*, 1999) where a large auger provides rapid transfer to a weighing system but shuts off before the predetermined amount is reached. A small concentric auger would then provide the exact dose.

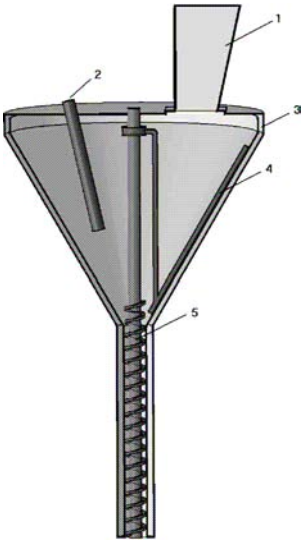

Figure 6 – Diagram of an auger filling system (type SD1, Optima). (1) Opening with funnel for filling powder into hopper; (2) Product sensor; (3) Plexiglass hopper; (4) Agitator; (5) Auger. (taken from Klous, 2004).

Gravimetric methods are much preferred for precision dosing however volumetric dosing is usually faster. There is currently a need for automatic weighing devices that can dispense precise amounts of powder in a mass production process at high speed (Yang *et*

al, 2007). For the dosing of a drug in a blister, it is important to weigh precise masses of the active ingredient. Conventional weighing balances (both manual and automated) are too slow and volumetric methods can encounter problems of inaccuracy which are often highly dependent on the material characteristics. Therefore, a balance must be achieved by using volumetric methods but proceeding with caution to ensure that accuracy is maintained by using materials with the correct characteristics.

1.6 Equipment requirements (acceptance criteria)

The equipment must be able to deliver accurate and precise doses. The measure for precision is the relative standard deviation (RSD). This is the standard deviation (SD) of a sample of doses expressed as a percentage of the sample mean.

$$RSD = \frac{SD}{mean} \times 100 \qquad (3)$$

The industrial sponsor's requirement is that the equipment must deliver doses with a precision of RSD ± 2 % or better. The accuracy of the equipment is measured by the deviation of the mean fill weight from the target fill weight.

The equipment must be able to deliver particles in the size range of 100 μm-500 μm diameter with fill weights between 50 mg-400 mg. This particle size range was chosen because:

- Materials greater than 100 μm diameter are relatively free-flowing when compared to very fine materials (<<100 μm) (Deleuil *et al*, 1994).
- Materials greater than 100 μm are easily coated (for modified release etc.) using fluid-bed coating methods. With smaller materials, clumping and agglomeration can occur with individual particles being difficult to separate in the fluidised bed (Seville *et al*, 1997, Richardson *et al*, 2002).
- Materials less than 500 μm do not leave a gritty mouth-feel when used in an oral dosage method.
- Materials in this size range are large enough to minimise surface forces (such as van der Waal's forces, electrostatic attraction and the effect of moisture) which can give rise to substantial attraction between particles and cause agglomeration (Israelachvili *et al*, 1991).

The fill weight range of 50 mg-400 mg was chosen to meet the typical fill weight range for a pharmaceutical drug (e.g. in tablets).

The throughput of the equipment must also be considered. There must be the potential for the chosen equipment (when fully automated) to deliver at high speeds such as would be required in a manufacturing process. To satisfy this need, the collection, measurement and dispensing of the powder must therefore be very rapid processes that can be carried out within a few seconds.

1.7 Summary of equipment options

Prior to commencing the main experimental phase of this project, (Chapters 2-3), it was necessary to identify a suitable powder dosing technology for investigation. Table 1 is a summary of the author's evaluation of equipment shortlisted on the basis of the requirements described in section 1.6. Based on an assessment of advantages and disadvantages, the "Floor Console" Powder Filling Machine (M&O Perry Industries, USA) was selected. The full selection process for the equipment is detailed in Appendix I.

Table 1 – Table summarising the equipment options that were evaluated.

	Company	Equipment	Advantages	Disadvantages	Outcome
1	Symyx	Powdernium	- Automated powder dispensing system. - Compatible with a wide range of materials and physical properties (inc. low-density, free-flowing, cohesive and micronised). - RSD 1-5% accuracy depending on flow properties of powder etc. - Compatible with different containers. - Minimum dose is 20mg. - Many powders stored on the machine online. - Each powder dose weighed and recorded automatically. - Monitors powder properties and optimises dosing automatically.	- Cannot handle full size blister trays. - Throughput is slow; each dispense will take 20-60 seconds. - Acceptable purely as a lab based research tool however may not be suitable for production. - Cost; cheapest system quoted at $120k. Customised changes will increase the cost.	Not feasible due to slow throughput and high cost.
2	All-Fill Tech, UK	Series 1, Micro-Fill Auger device	- Volumetric dosing system, designed for dosing foodstuffs and pharmaceuticals. - Capable of desired speeds (up to 300 doses/min). - Can be operated manually and automatically. - Capable of dosing into blister trays. - A pocket as small as 10mm diameter can be dosed. - Can be free standing or incorporated into an existing line. - Cost; system can be ordered for £12000-15000. - UK supplier.	- Volumetric dosing may compromise somewhat on the accuracy although company claimed it was very accurate. - Auger not suitable for cohesive powders.	Visited All Fill Tech to see equipment demonstration. Precision of auger did not match the RSD of ±2%.
4	**M&O Perry, USA**	**Floor Console (FC) Powder Filling Machine**	- **Uses "Accofil" dosing principle.** - **A manual system capable of dosing via a needle/gun.** - **Cost; system is cheap (~£5-10k depending on dosing gun options).** - **Can be used as a set of 8 needles to dose multiple containers. System has a precision between 0.5% (free flowing) – 3% (cohesive powders). Guns available in sizes from 1/8", 3/16", ¼" and larger. Dosing weight and particle size both within range of the instrument.** - **M&O Perry held original patent for Accofil® technology.**	- **The fully automated version of the system is designed for dosing into vials, the equipment is not set up to work with blister packs so the company may not be able to supply a fully automated machine in the future.**	**Chosen as the recommended system ahead of KControls because M&O Perry held the original patent for Accofil®.**
5	Kinematic Controls, USA	Semi-automatic dosing device	- Identical system to the Floor Console from M&O Perry, however it was invented by the latter.	- As above.	See above.

2.0 MATERIAL, EQUIPMENT AND METHODS

2.1 Introduction

One of the key drivers for this project is to allow use of powdered materials that are coated for either taste masking, modified/targeted release of drug, or simply to protect the drug from contact with water. The first part of this chapter describes the materials chosen for study, the reasons for selecting them and the techniques used to characterise the materials. The characterisation techniques were to measure the following powder properties:

- Particle size distribution
- Powder bulk density
- Flow characteristics (or "flowability") of the powders

The remainder of the chapter describes the experimental investigations that were carried out with the chosen dosing equipment (section 1.7).

2.2 Materials

2.2.1 Coated sugar spheres (SUGLETS®)

Three sizes of highly spherical sugar spheres were obtained from NP Pharm, France, with nominal sizes of 180-250 μm, 355-425 μm and 500-600 μm. The particles were then coated (with a mass increase of 10 %) under the instruction of the author using a fluidised bed coater (Wurster Coater) by Colorcon, Dartford, UK. Two types of coating were applied to separate batches of each size range. The coatings were Acryleze® (enteric coating containing Eudragit® L100-55) and Surelease® (modified release coating containing ethylcellulose); see Appendix II for details and Appendix III for images.

2.2.2 Coated paracetamol (APAP) and ibuprofen

A limited amount (20 g-500 g per batch) of coated paracetamol (APAP) and ibuprofen were supplied by the sponsoring company. Three batches of APAP were selected along with one batch of ibuprofen. Table 2 summarises the coating types (details in Appendix

II) and amount of each material available. These materials were neither very spherical, nor highly irregular. See Appendix III for images.

Table 2 – The selection of APAP and ibuprofen for dosing studies.
E100 – Eudragit E100; CA – Cellulose Acetate Phthalate; Coatings applied for a 20% mass increase.

Material Name	Coating Composition	Ratio of E100:CA	Quantity (g)
APAP1624	E100 and CA	9:1	298.5
APAP1627	E100 and CA	9:1	501
APAP1776	E100 and CA	8:2	467.5
Ibuprofen 1618	Only CA	N/A	332

2.2.3 Excipients

Lactose and microcrystalline cellulose (MCC) were also used for powder dosing studies (both uncoated). Lactose was obtained from Freisland Foods, Netherlands and MCC was obtained from FMC Biopolymer under the brand name Avicel PH102. They were chosen because it was suspected that these materials would be more challenging in terms of powder handling since they do not comprise idealised, spherical particles. Both are commonly used pharmaceutical excipients. See Appendix III for images.

2.2.4 Materials summary and abbreviations

Table 3 lists all the materials and abbreviations that will be used hereafter.

Table 3 – Table showing materials, reason for selection and abbreviations.

Material description	Reason for selection	Abbreviation
180-250 µm sugar spheres coated with Acryleze®	Model enteric coated material – small	ACR180
355-425 µm sugar spheres coated with Acryleze®	Model enteric coated material – medium	ACR355
500-600 µm sugar spheres coated with Acryleze®	Model enteric coated material – large	ACR500
180-250 µm sugar spheres coated with Surelease®	Model controlled release material – small	SUR180
355-425 µm sugar spheres coated with Surelease®	Model controlled release material – medium	SUR355
500-600 µm sugar spheres coated with Surelease®	Model controlled release material – large	SUR500
Paracetamol (80 µm diameter) coated with Eudragit® and cellulose acetate phthalate	Typical coated drug – small	APAP1627
Paracetamol (130 µm diameter) coated with Eudragit® and cellulose acetate phthalate	Typical coated drug – medium	APAP1624
Paracetamol (320 µm diameter) coated with Eudragit® and cellulose acetate phthalate	Typical coated drug – large	APAP1776
Ibuprofen (80 µm nominal diameter) coated with cellulose acetate phthalate	Alternative coated drug – small	IBU1618
Lactose (80 µm nominal diameter), uncoated	Cohesive material, none spherical	Lactose
Microcrystalline cellulose (80 µm nominal diameter), uncoated	Alternative cohesive material, none spherical	Avicel

2.3 Equipment

The Floor Console (FC) was purchased from M&O Perry Industries, California, USA. It is a filling machine that uses the Accofil® fill gun (see Appendix I). To dose powder, the operator inserts the fill gun into a bulk supply of product. Subsequently, during the vacuum cycle of the machine, product is drawn in to fill the barrel of the fill gun and additional powder forms a "mushroom" of product on the gun's tip (Figure 7), which the operator then wipes off prior to dosing. Product is then dispensed into the receiving container by the reversal of the machine's vacuum cycle to a positive pressure cycle, which is initiated by the operator depressing a footswitch. According to the manufacturer, the equipment is capable of dosing particles up to 500 µm in diameter and fill weights as low as 20 mg with a precision lower than ± 2 % RSD. The equipment was

procured after successful trials by the manufacturer (M&O Perry Industries) using coated sugar spheres under the instruction of the author (section 2.5.1).

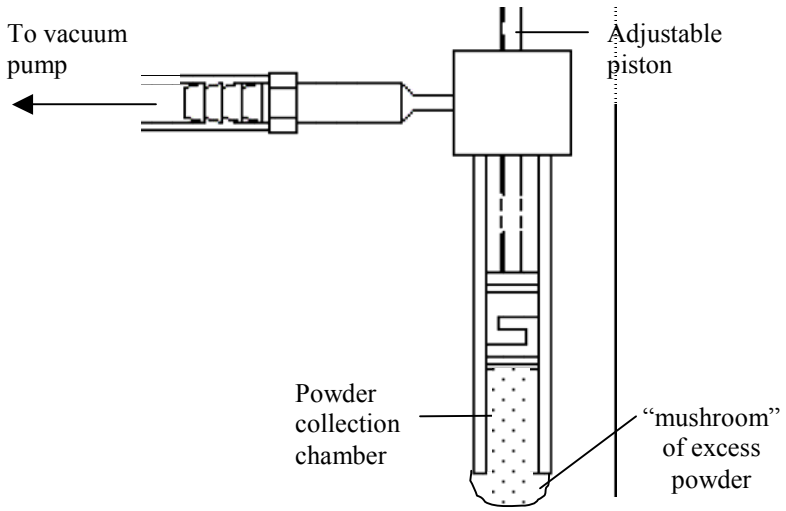

Figure 7 – Diagram showing a filling gun with a "mushroom" of excess powder (M&O Perry Ind.).

2.4 Methods (powder characterisation)

2.4.1 Particle size distribution

The particle size distribution (PSD, by volume) for each material was found using dry powder laser light diffraction (HELOS sensor with RODOS dispersion unit, Sympatec, Germany) at a dispersion pressure of 2 bar. Since some materials were in excess of 500 μm diameter, the R5 lens with a focal length of 500 mm was used, which allowed measurement in the range of 4.5-875 μm. Each measurement was repeated on three independent samples. The d_{90}, d_{50}, d_{10} and d_5 were all output values from the laser diffraction measurements. The span of the PSD was then calculated as:

$$Span = \frac{d_{90} - d_{10}}{d_{50}} \qquad (4)$$

The span is a measure of the spread of data about the median value; the higher the span, the greater the spread. Hence a low span value indicates a relatively narrow size distribution.

2.4.2 Bulk and tapped density

A 100 ml measuring cylinder was used in the estimation of the bulk density of each material. The empty cylinder was placed on a balance and tared. The powder was then poured into the cylinder up to the 100 ml mark and weighed again enabling the poured density to be calculated. After recording the mass, the cylinder was tapped manually 200 times. The final volume was recorded and the resulting tapped density then calculated. This process was repeated three times to obtain an average poured density and average tapped density. The values were then used to calculate the Carr's index (CI) as:

$$CI = \frac{\rho_{tapped} - \rho_{poured}}{\rho_{tapped}} \times 100 \qquad (5)$$

2.4.3 Shear testing

Shear testing was carried out using a Schulze Ring Shear Tester (RST XS), Dietmar Schulze, Germany. Figure 8 shows the schematic of the shear cell used to measure powder flow characteristics.

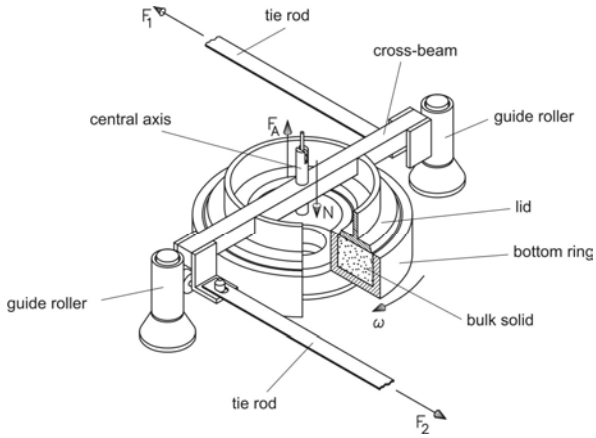

Figure 8 – Schematic of a shear cell from the Schulze Ring Shear Tester (taken from Schulze, 2008)

On the control PC, the RST control software (RST-CONTROL 95) was opened as shown in Figure 9. The name of the material was entered in the *Bulk solid* box. The relevant shear cell number was chosen (in this case, number 4) and the normal loads were entered by clicking on *Enter normal load(s)*. In the new window, 5 kPa was entered as the preshear normal load and the test points were 4 kPa, 3 kPa, 2 kPa, 1 kPa, and 0.5 kPa. After selecting the normal loads, the shear cell was filled with powder and the surface levelled with a straight edged steel scraper. The mass of the filled shear cell was then

entered in the box labelled *m, tot (g)*. The test procedure was initiated by clicking on *Start*. When prompted by the on-screen commands, the shear cell was placed on the tester, the lid positioned into place and the loading rods placed in the correct positions. The remainder of the test (preshear and shear) was carried out automatically according to the normal loads that were specified. When the test was completed, the data were saved and analysed to create the yield loci and the Mohr's circles using the analysis software, RSV-95.

The test procedure was then repeated with preshear normal loads of 10 kPa and 15 kPa with associated test points as shown in Table 4. This enabled a family of yield loci to be obtained. From each yield locus, an associated consolidation stress (σ_1 or SIGMA1) and unconfined yield stress (σ_c or FC) were determined. The ratio of σ_1 to σ_c was calculated to give the flow function of the material (FFC). The values of σ_1 versus σ_c from each yield locus for a material were plotted to show the flow function over a range of consolidation stresses. The shear testing was repeated on 3 independent samples of each material, and the flow functions for all the materials were plotted on the same axes.

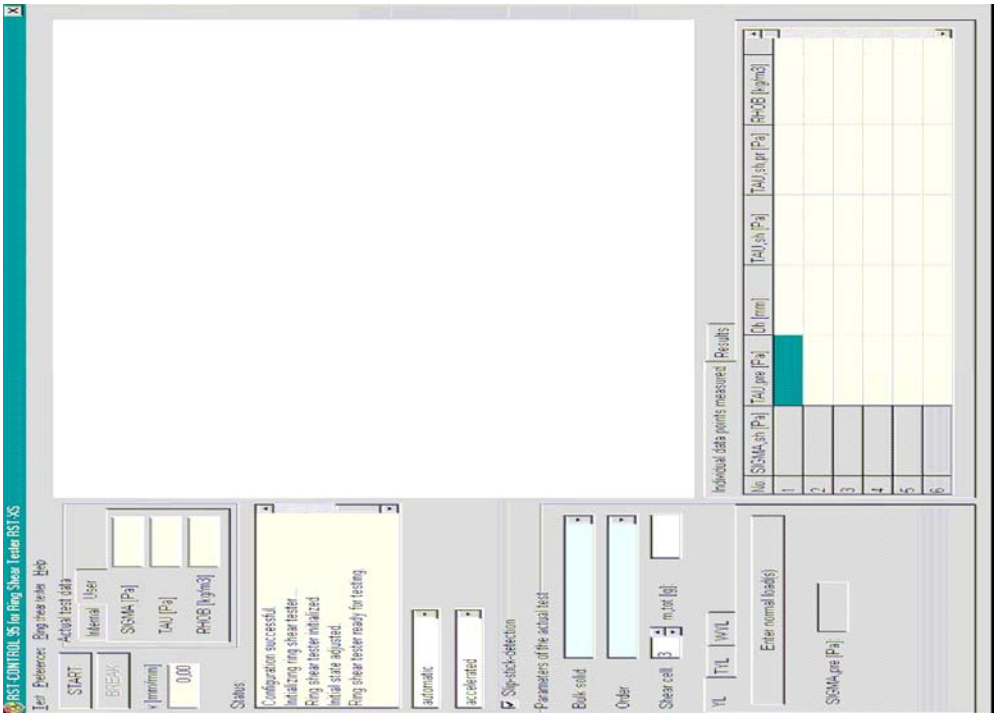

Figure 9 – Screen view of the RST-CONTROL 95 software

Table 4 – Table showing the normal loads for pre-shear and the associated test points

Preshear normal load	**5 kPa**	**10 kPa**	**15 kPa**
Test points (kPa)	0.5	1	2
	1	2	4
	2	4	6
	3	6	8
	4	8	10
			12

2.5 Methods (powder dosing studies)

2.5.1 Preliminary validation experiments

The objective of these experiments was to qualify the operation of the FC Powder Filling Machine using coated sugar spheres and to compare the results with those obtained by M&O Perry Industries during the initial practical appraisal prior to purchasing the machine.

The materials used were ACR180, ACR355 and ACR500 at two fill weights, 50 mg (1/8 inch and 3/16 inch guns) and 400 mg (1/4 inch gun). Twenty doses were taken with each gun for each powder and measured on a balance from which the sample mean and RSD were calculated. The various machine settings are summarised in Table 5. The dose pressure (purge pressure) varied between 0.5 and 4.5 inches Hg depending on the size of the fill gun in use. In general, the smallest filling gun (1/8 inch ID) required the highest dose pressure (4.5 inHg) and the largest filling gun (1/4 inch ID) required the smallest dose pressure (0.5 inHg). Note, the equipment originated in the US and used imperial units, therefore the use of imperial units was continued throughout to provide consistency and also "convenient" numbers.

The experiments were carried out in a laboratory where temperature and humidity were controlled and remained relatively constant with temperature between 20°C-22°C and relative humidity less than 15 %.

Table 5 – Table showing the settings used for preliminary assessments on the FC Powder Filler.

Materials	ACR180, ACR355 and ACR500
Vacuum strength (inches Hg)	-20
Dose pressure (inches Hg)	0.5-4.5
Temperature (°C)	20-22
Lab humidity (%)	<15%

2.5.2 Investigating the effect of vacuum strength using the FC Powder Filler

The FC Powder Filler has a variable vacuum strength setting which can be adjusted depending on the powder that is being used.

The objective for this investigation was to develop an understanding of how the vacuum strength used in the filling gun affects the accuracy and precision of the dose weight for a range of powders. Furthermore, a range of powders was used (Table 6). This allowed the combined effect of the vacuum strength and powder properties such as particle size, particle size distribution and the flowability of the materials, to be evaluated.

Table 6 – Materials used for vacuum strength investigation. Size, ρ_p ρ_t , Carr Index and flow description are discussed in Chapter 3.

Material	Size (d_{50}) µm	Average poured density (ρ_p, kg/m^3)	Average tapped density (ρ_t, kg/m^3)	Carr Index (%)	Flow Description
ACR180	228 ± 2	849 ± 3	874 ± 1	3 ± 0.2	Free flowing
SUR180	228 ± 2	776 ± 6	809 ± 2	4 ± 0.6	Free flowing
ACR355	431 ± 3	853 ± 4	879 ± 2	3 ± 0.3	Free flowing
SUR355	450 ± 1	784 ± 6	808 ± 3	3 ± 0.4	Free flowing
APAP 1627	80 ± 5	440 ± 15	517 ± 5	15 ± 2.1	Free flowing
APAP 1624	134 ± 7	459 ± 12	544 ± 4	16 ± 2.1	Free flowing
APAP 1776	327 ± 5	719 ± 8	757 ± 3	5 ± 0.7	Free flowing
IBU1618	79 ± 3	510 ± 16	573 ± 5	11 ± 2.6	Free flowing
Lactose	68 ± 1	647 ± 18	862 ± 6	25 ± 1.5	Easy flowing
Avicel	81 ± 11	362 ± 14	437 ± 5	17 ± 2.2	Easy flowing

The speed of collection, defined as the time taken to dip and remove the gun from the powder bed, was "intermediate" i.e. the process of collection was carried out in <1 second. "Fast" and "slow" collection speeds are defined in section 2.5.3. Twenty doses were taken from each powder to calculate a mean and RSD. Four vacuum set-points were used: -20inHg, -15inHg, -10inHg and -5inHg. In order to compare the sample means between experiments, the fill gun settings were maintained constant i.e. the position of the adjustable piston on the fill gun was not altered between the four vacuum strengths for each material.

With materials APAP1627, APAP1624, IBU1618, lactose and Avicel, the removal of the filling gun after collecting a dose left behind a well defined cavity in the powder bed. Therefore, doses for these materials were collected from 20 separate locations within the powder bed. After collecting 20 doses, the powder bed was returned to its original

"poured" state by pouring to and from a separate container. Figure 10 shows this in a bed of APAP1627 after 20 doses had been collected.

With materials ACR180, ACR355, SUR180, SUR355, and APAP1776, the powder flowed freely into the cavity after removing the gun so a well defined cavity did not remain. Hence, doses for these materials were collected randomly from any location in the powder bed.

The experiments were carried out at two fill weights for each material. For ACR180, ACR355, SUR180 and SUR355, the fill weights were 50 mg ($1/8^{th}$ inch gun) and 400 mg (¼ inch gun). The remaining materials were less dense and the volume of powder required for a fill weight of 400 mg was very close to the maximum volume of the ¼ inch filling gun. Therefore, for all APAP, ibuprofen, lactose and Avicel, the fill weights were 50 mg and 300 mg.

The results were grouped accordingly to analyse the effect of:

- Particle size. Comparisons were made between the following materials which had the same coating but different particle sizes:
    - ACR180 versus ACR355
    - SUR180 versus SUR355
    - APAP1627 versus APAP1624 and APAP1776
- Flowability. Comparisons were made between the following materials which had similar mean particle sizes but different flow characteristics:
    - ACR180 versus SUR180
    - ACR355 versus SUR355
    - IBU1618 versus lactose and Avicel

Figure 10 – Image showing the cavities left behind after 20 doses had been collected from a bed of APAP1627.

2.5.2.1 Development of hypotheses and statistical analysis

Statistical analysis of variance (ANOVA) was used to identify if any of the means ($\overline{X}$) between samples were significantly different (Jones D *et al*, 2002).

The null hypothesis assumed that there was no difference in the sample means for the four treatments groups, i.e. the means of the treatment groups were identical. In light of this, the null hypothesis (H_0) was therefore:

$$H_0: \overline{X}_{20inHg} = \overline{X}_{15inHg} \text{ and } \overline{X}_{15inHg} = \overline{X}_{10inHg} \text{ and } \overline{X}_{10inHg} = \overline{X}_{5inHg}$$

The alternative hypothesis took the opposite outcome to the null hypothesis. Hence, the alternative hypothesis (H_a) assumed that there was a significant difference in the sample means for the four treatments, i.e. the four means were not identical:

$$H_a: \overline{X}_{20inHg} \neq \overline{X}_{15inHg} \text{ or } \overline{X}_{15inHg} \neq \overline{X}_{10inHg} \text{ or } \overline{X}_{10inHg} \neq \overline{X}_{5inHg}$$

Finally, the level of significance (α) for all statistical tests was set to 0.05.

To identify the treatment groups that were significantly different, a post-hoc comparison was carried out using Tukey's honestly significant difference (HSD) test (Jones D *et al*, 2002). In this test, only adjacent sample means were compared to assess the importance of incremental increases in vacuum strength, i.e. $\overline{X}_{20inHg}$ versus $\overline{X}_{15inHg}$, $\overline{X}_{15inHg}$ versus $\overline{X}_{10inHg}$ and $\overline{X}_{10inHg}$ versus $\overline{X}_{5inHg}$.

2.5.3 Investigating the effect of collection speed using the FC Powder Filler

Manual use of the FC Powder Filler by an operator is a relatively slow process. It was not yet known whether the equipment was capable of rapid powder collection and dosing as would be experienced in a potential automated production process. Therefore, the objective for this investigation was to develop an understanding of the effect of collection speed on the accuracy and precision of the fill weight. The collection speed is defined by measuring the time taken for insertion and removal of a filling gun to a depth of 2 cm in a powder bed.

The materials used for this investigation were the same as those shown in Table 6 in the previous section. Also as before, the fill weights investigated were 50 mg and 400 mg for

ACR180, ACR355, SUR180, SUR355, and 50 mg and 300 mg for all others materials. The vacuum strength was kept constant at -20 inHg and the variable in this investigation was collection (or plunging) speed. The time taken for the insertion and removal of the gun was used to define the speed as:

SLOW:	1-2 seconds
INTERMEDIATE:	< 1 second
FAST:	< ½ second

It must be noted that since the dosing guns were handled manually, it was not possible to accurately measure the time taken to dip the gun and remove it by hand using standard laboratory equipment. Therefore, the above criteria for slow, intermediate and fast speeds were devised to ensure that the collection process will take no longer than the time stated in the above definition. More accurate measurements of collection speed are possible only with fully automated equipment with variable speed control, especially in the timescale of <1 second.

3.0 RESULTS & DISCUSSIONS

3.1 Powder characterisation

3.1.1 Particle size distribution

The PSDs for materials with prefix ACR (Acryleze coating) and SUR (Surelease coating) were expected to be the same since the samples shared the same core, taken from the same uncoated batch prior to coating. Furthermore, the PSD was expected to be relatively narrow with very little fines and no contamination with larger particles. The results indeed were as expected, and so Figure 11 to Figure 13 are representative of both Acryleze and Surelease coated sugar spheres. Figure 14 to Figure 19 show the PSD for APAP, IBU1618, lactose and Avicel. The PSD is then summarised for all the materials in Table 7.

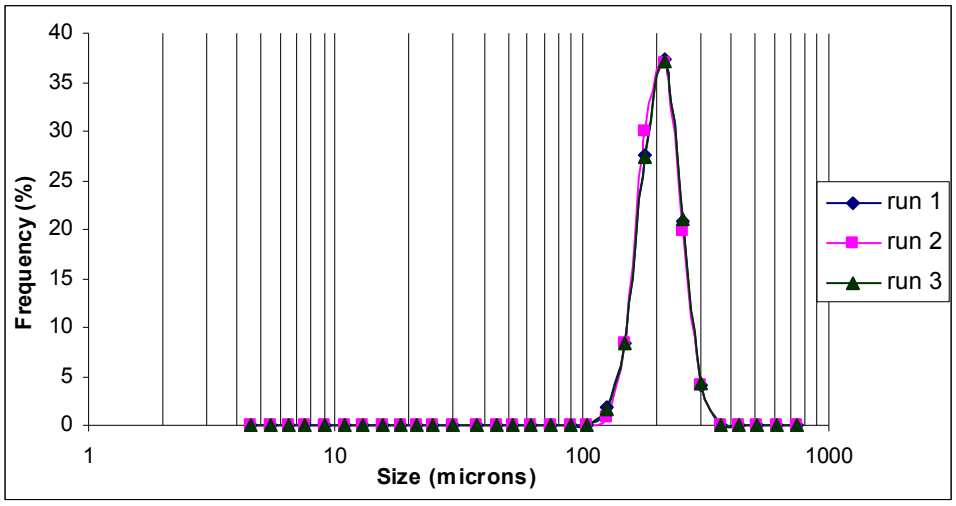

Figure 11 – Graphs showing the particle size distribution for ACR180. D_{50}: 228µm; d_{90}: 291µm; d_{10}: 180µm; span=0.49

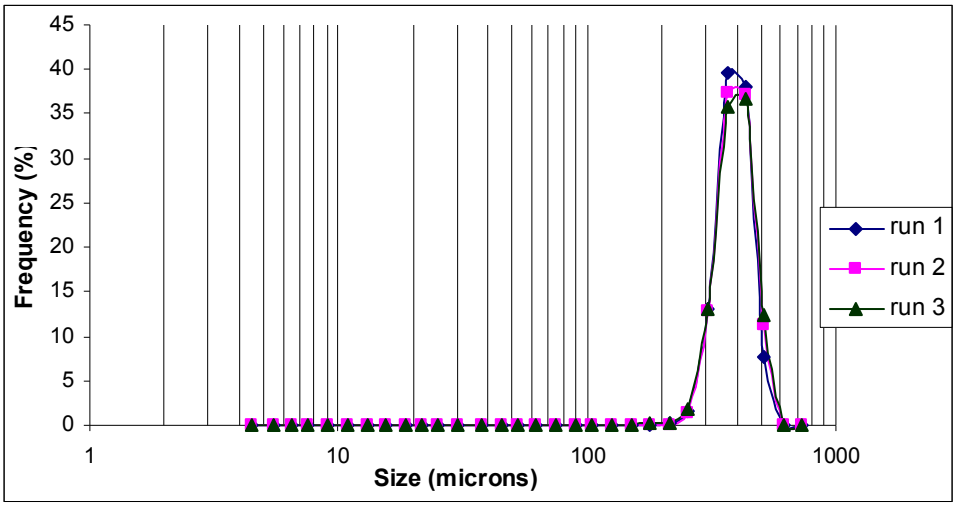

Figure 12 – Graph showing the particle size distribution for ACR355. D_{50}: 431µm; d_{90}: 523µm; d_{10}: 343µm; span=0.42

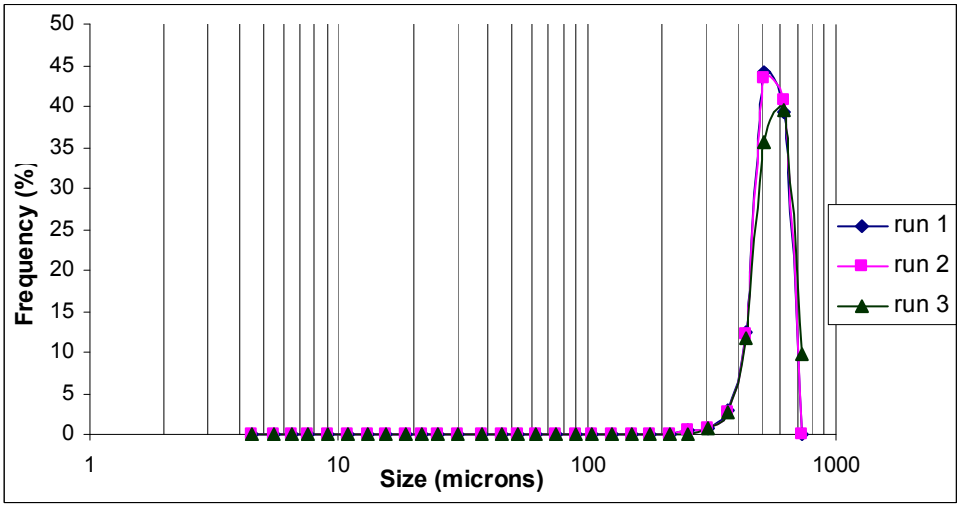

Figure 13 – Graph showing the particle size distribution for ACR500. D_{50}: 599µm; d_{90}: 715µm; d_{10}: 476µm; span=0.40

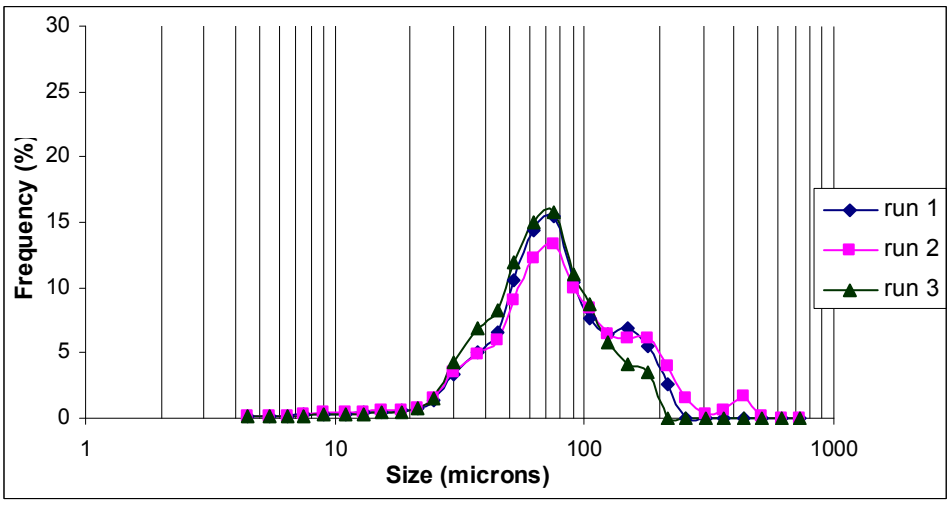

Figure 14 – Graph showing the particle size distribution for APAP1627. D_{50}: 80µm; d_{90}: 172µm; d_{10}: 39µm; span=1.66

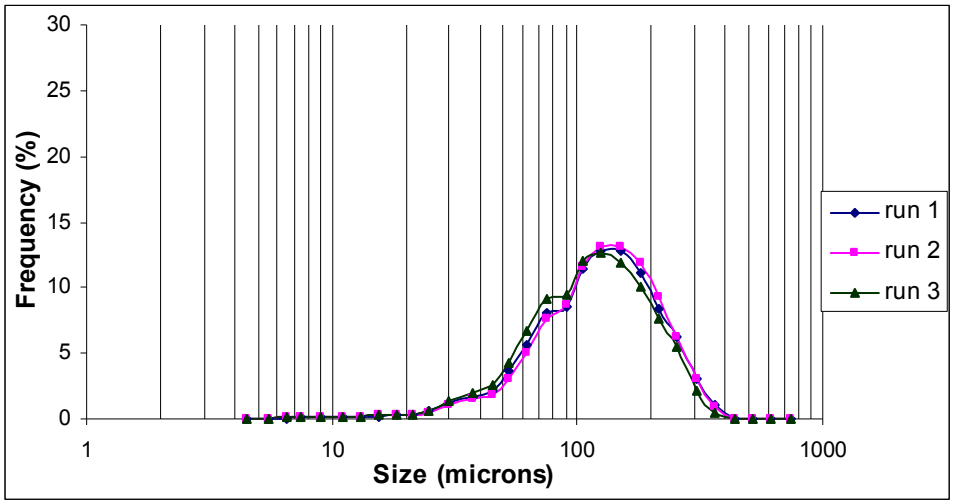

Figure 15 – Graph showing the particle size distribution for APAP1624. D_{50}: 133µm; d_{90}: 253µm; d_{10}: 60µm; span=1.45

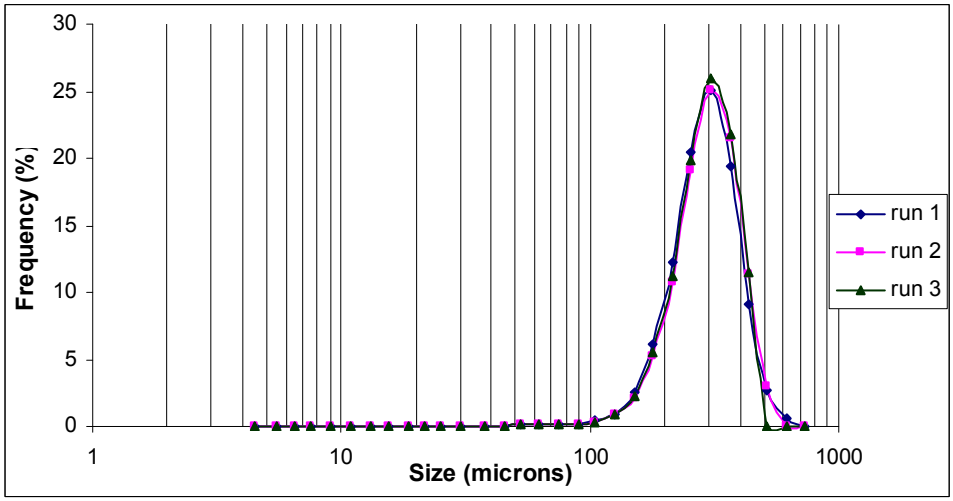

Figure 16 – Graph showing the particle size distribution for APAP1776. D_{50}: 327µm; d_{90}: 456µm; d_{10}: 216µm; span=0.73

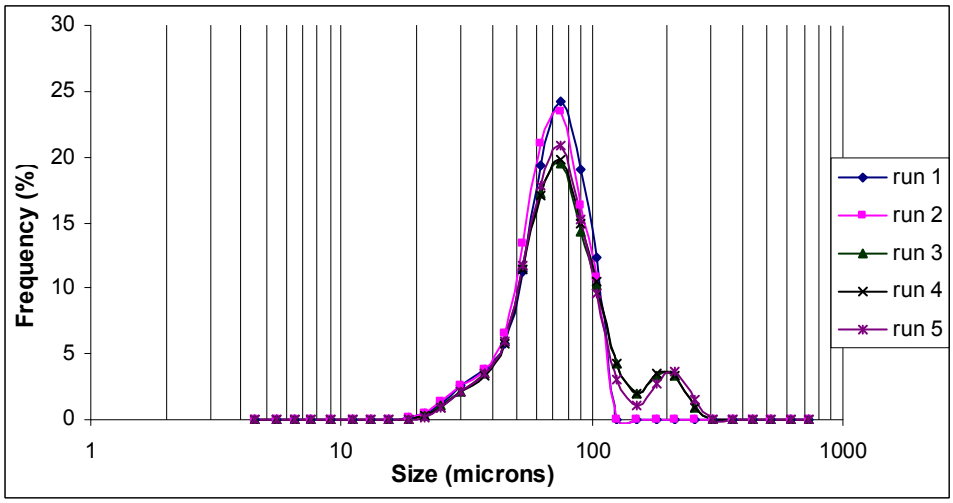

Figure 17 – Graph showing the particle size distribution for IBU1618. D_{50}: 79µm; d_{90}: 131µm; d_{10}: 48µm; span=1.04

A

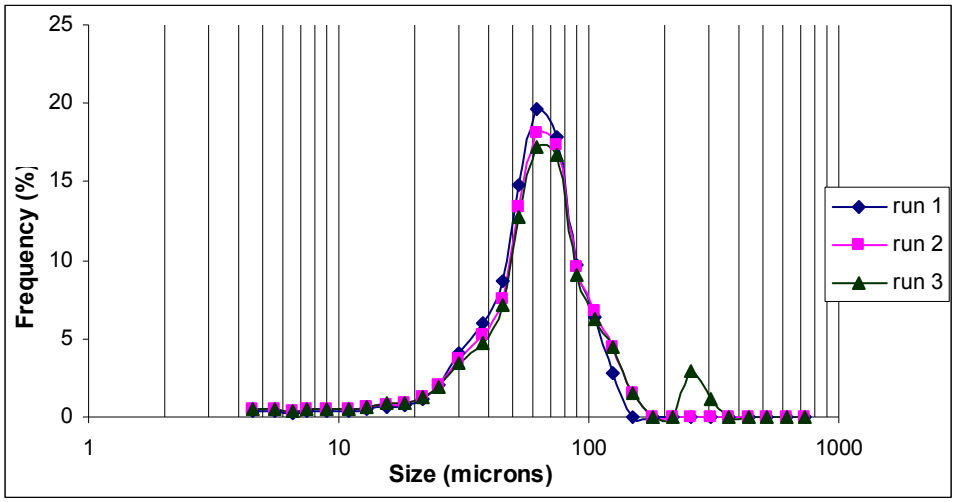

B

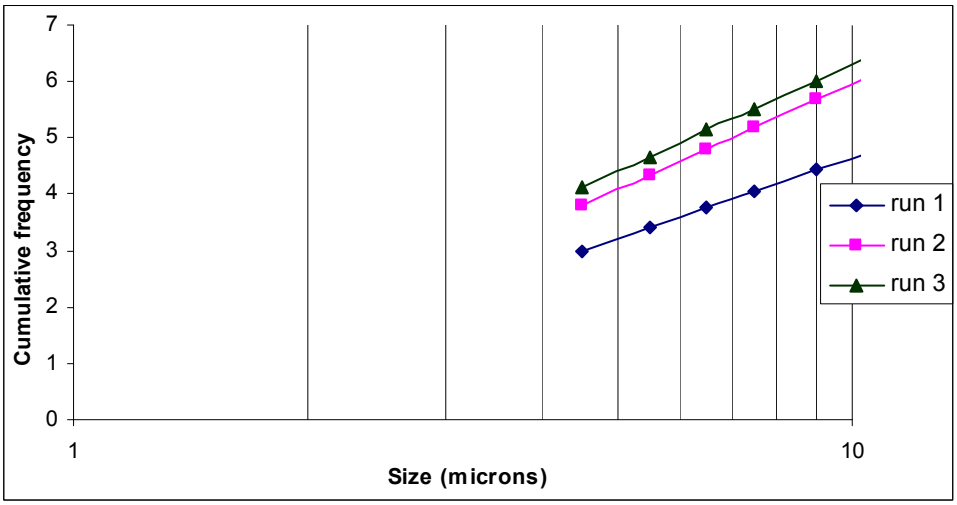

Figure 18 – (A) Graph showing the particle size distribution for lactose. D_{50}: 68µm; d_{90}: 114µm; d_{10}: 26µm; span=1.30. (B) Graph showing the proportion of material <10µm.

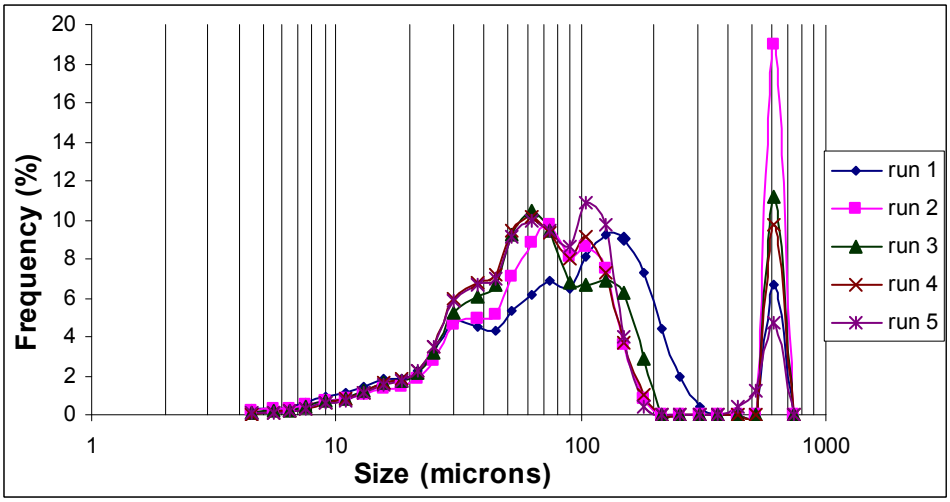

Figure 19 – Graph showing the particle size distribution for Avicel. D_{50}: 81µm; d_{90}: 650µm; d_{10}: 26µm; span=7.7

Table 7 – PSD for coated Suglets, APAP, ibuprofen, lactose and Avicel. Each value represents the mean from 3 independent measurements ± one standard deviation of the mean. ** 5 independent measurements taken.*

Material	D10 (µm)	D50 (µm)	D90 (µm)	Span
ACR180	180 ± 1	228 ± 2	291 ± 1	0.49
SUR180	181 ± 1	228 ± 2	291 ± 2	0.48
ACR355	343 ± 2	431 ± 3	523 ± 12	0.42
SUR355	345 ± 4	450 ± 1	559 ± 3	0.48
ACR500	476 ± 3	599 ± 12	715 ± 17	0.40
SUR500	484 ± 34	601 ± 16	712 ± 11	0.38
APAP1627	39 ± 1	80 ± 5	172 ± 33	1.66
APAP1624	60 ± 3	134 ± 7	253 ± 7	1.45
APAP1776	216 ± 3	327 ± 5	456 ± 10	0.73
IBU1618*	48 ± 1	79 ± 3	131 ± 21	1.04
Lactose	26 ± 3	68 ± 1	114 ± 11	1.30
Avicel*	26 ± 2	81 ± 11	381 ± 248	4.4

In Figure 11 to Figure 13, it can be seen that the PSDs for coated sugar spheres are narrow with a span of between 0.4-0.5 and a maximum frequency peak of around 40%. The coated sugar spheres do not contain particles that are much greater than the mean size (>2 × d_{50}) or very fine particles (<0.5 × d_{50}). Also, the inter-sample variability is very small with each sample showing excellent reproducibility. With this in mind, it is reasonable to expect that these materials will behave in a reproducible manner under experimental conditions. In Figure 14 to Figure 16, the maximum frequency peak is much lower (15-25%) suggesting a broader particle size range for coated APAP powders. These powders also have greater spans than coated sugar spheres. APAP1627 has the lowest mean diameter (80 µm) and is expected to be the most cohesive material of the three. APAP1776 has the largest mean diameter (327 µm) and is therefore expected to be the most free-flowing of the three APAP powders.

Figure 17 shows the PSD for IBU1618. The distribution is relatively narrow with a span of 1.04 however a small amount (~5%) of the material is around 200 µm, indicated by the small peak.

Figure 18(A) shows the PSD for uncoated lactose. The mean particle diameter is 68 μm and the material contains a proportion of "fines" (material less than 10 μm, shown in Figure 18(B)) which is reflected in the greater span value of 1.30 compared to 1.04 for IBU1618 which does not contain any fines. Lactose also has some larger particles around 250 μm (approximately 3%) which were seen in two out three measured samples.

Finally, Figure 19 shows the PSD for Avicel which has been selected as the material with the widest spread of particle size. Avicel contains two distinct regions of particle size, shown by one broad peak between 50-150 μm and a sharp peak at around 600 μm. It is unclear before any experimentation whether the two distinct particle populations would benefit particle packing or be a hindrance. There is inter-sample variability in Figure 19 and it is reasonable to expect that powder filling performance may not be very repeatable with Avicel due to segregation as described in section 1.1.1.

The PSD information now shows that a wide range of material sizes are available from lactose (mean size 68 μm) to ACR500 (mean size 599 μm) which broadly covers the original specified range for investigation of 50-500 μm. The effect of PSD on the filling performance will be discussed in the relevant experimental sections.

3.1.2 Bulk and tapped density

The average poured and tapped densities are shown in Table 8 along with the calculated Carr's index values. The materials coated with Acryleze and Surelease all have Carr's index values less than 5 %; these are considered to be very free flowing. APAP1776 also has a Carr's index of 5%, this is likely to be because the particles are relatively large and the material is also very free flowing. The final free flowing material is IBU1618 with a Carr's index of 11 %. The remaining materials have Carr's index values above 15%. These materials are considered to be less free flowing. In general, the smaller materials have greater Carr's indexes and are more cohesive than the larger materials.

Table 8 – Table showing the poured and tapped densities alongside the Carr's index for each material. Each density value represents the average from three measurements ± standard deviation.

Material	Average poured density (ρ_p , kg/m^3)	Average tapped density (ρ_t , kg/m^3)	Carr Index (%)
ACR180	849 ± 3	874 ± 1	3 ± 0.2
SUR180	776 ± 6	809 ± 2	4 ± 0.6
ACR355	853 ± 4	879 ± 2	3 ± 0.3
SUR355	784 ± 6	808 ± 3	3 ± 0.4
ACR500	818 ± 1	847 ± 1	3 ± 0.0
SUR500	764 ± 4	790 ± 3	3 ± 0.3
APAP 1627	440 ± 15	517 ± 5	15 ± 2.1
APAP 1624	459 ± 12	544 ± 4	16 ± 2.1
APAP 1776	719 ± 8	757 ± 3	5 ± 0.7
IBU1618	510 ± 16	573 ± 5	11 ± 2.6
Lactose	647 ± 18	862 ± 6	25 ± 1.5
Avicel	362 ± 14	437 ± 5	17 ± 2.2

3.1.3 Shear testing

Figure 20 shows an example of 9 shear tests (3 for each normal load) carried out with lactose. The full shear test result data from which the flow functions have been calculated are shown in Appendix IV. The figure shows a family of yield loci along with the Mohr's circles. From the Mohr's circles, the consolidation stresses and the unconfined yield stresses were estimated and are shown in the table. The FC and SIGMA1 figures show that the unconfined yield stress increases when the preshear compacting stress increases.

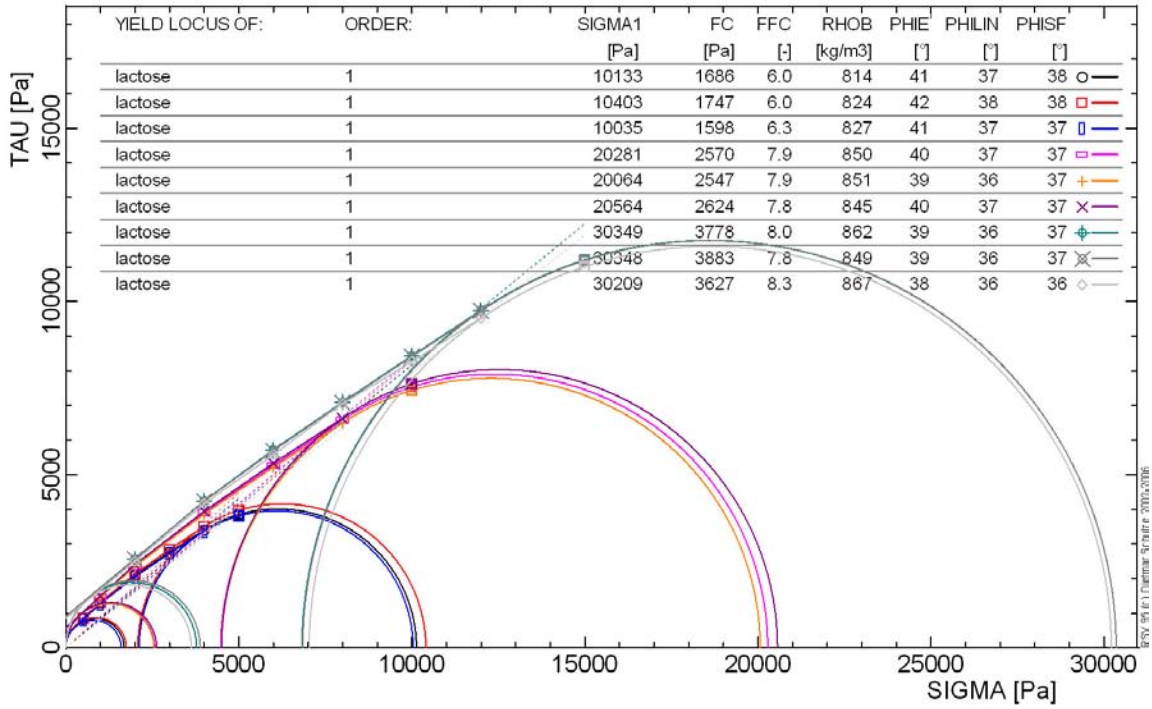

Figure 20 - Figure showing a family of yield loci for lactose when tested with pre-shear normal loads of 5kPa, 10kPa and 15kPa. From the Mohr's circles, σ_1 and σ_c can be found. These in turn are used to plot the flow function.

The flow functions from the shear tests are calculated and plotted on one set of axes (Figure 21). The regions that show a specific type of flow behaviour (e.g. cohesive, easy flowing) are marked for reference. These regions are not rigid and should only be considered as general guidelines. Most of the curves for the materials have a flow function curve which lies in the *free-flowing* segment. Avicel and lactose have curves which lie in the *easy-flowing* segment. The figure is also depicted with the flow function for a very cohesive material (calcium carbonate) to illustrate how relatively free flowing all the materials actually are. Nevertheless, there is still a marked difference in flow behaviour between the most cohesive of the chosen materials (lactose and Avicel), when compared to the most free flowing materials (ACR180 and ACR355). Figure 22 shows this more clearly; lactose and Avicel have FFC values less than 10 whereas all the other materials have FFC values over 10 indicating that they are free-flowing.

Figure 22 also raises an interesting observation for SUR180 and SUR355. The flow functions for these materials curve upwards when the consolidation stress rises above 20000 Pa. It is likely that the Surelease coating creates a textured surface which promotes the adhesion of particles when compressed together. This is important because at higher consolidation stresses, SUR180 and SUR355 will become more cohesive and this may have an adverse affect on the process. However, it is not expected at this stage that

powder dosing applications will involve large consolidation stresses that cause the material to become cohesive.

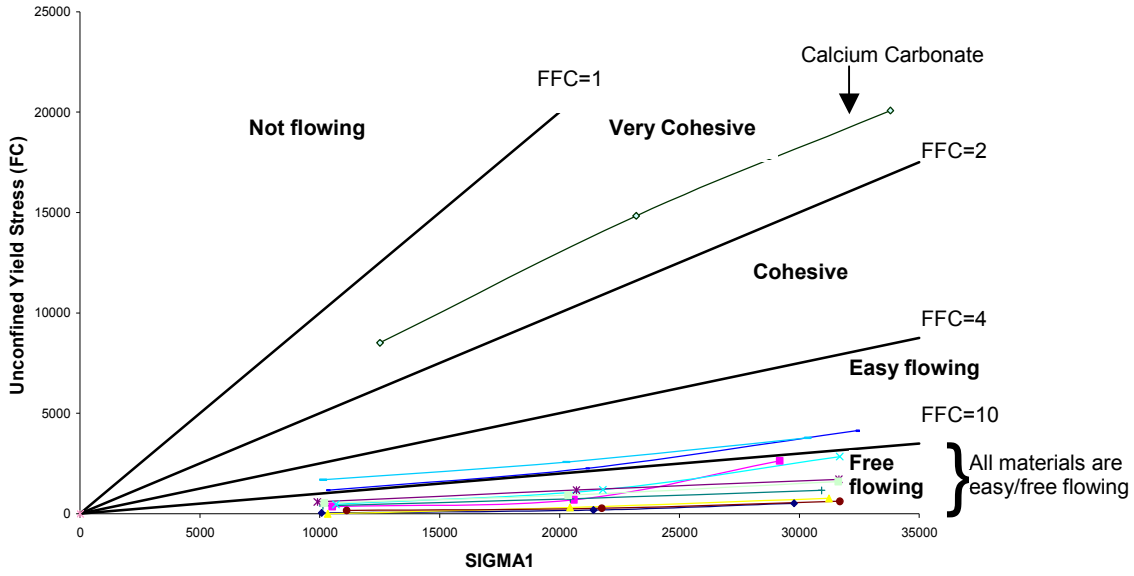

Figure 21 – Graph showing the relative position of the flow function of each material alongside that of a very cohesive material such as calcium carbonate. Most of the materials are within the free flowing section with Avicel and lactose being the only two materials with a flow function less than 10.

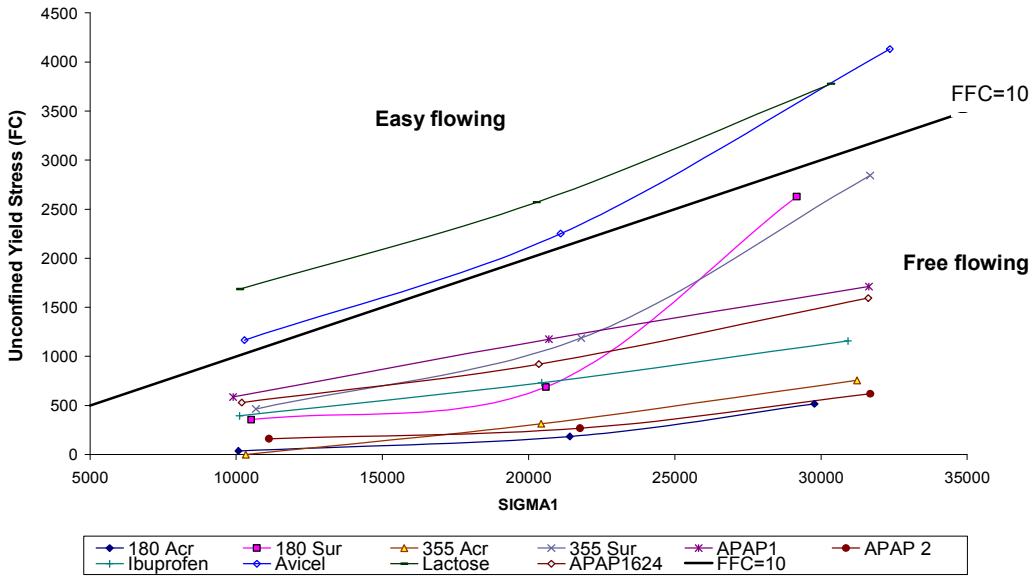

Figure 22 – Graph showing the flow functions of each material. Most materials lie within the free-flowing segment. Lactose and Avicel are the most cohesive from the selection and lie within the easy-flowing segment. Note: this figure is for a single set of shear tests and is representative of the repeats which are shown in Appendix IV.

A summary of the powder characterisation is shown in Table 9. In general, the larger materials are the freest flowing and have the lowest Carr's Index values. The smallest materials are the most cohesive (APAP 1627, lactose, Avicel and IBU1618).

Table 9 – Table summarising the power characteristics

Material	Size (d_{50}) µm	Average poured density (ρ_p, kg/m^3)	Average tapped density (ρ_t, kg/m^3)	Carr Index (%)	Flow Description
ACR180	228 ± 2	849 ± 3	874 ± 1	3 ± 0.2	Free flowing
SUR180	228 ± 2	776 ± 6	809 ± 2	4 ± 0.6	Free flowing
ACR355	431 ± 3	853 ± 4	879 ± 2	3 ± 0.3	Free flowing
SUR355	450 ± 1	784 ± 6	808 ± 3	3 ± 0.4	Free flowing
ACR500	599 ± 12	818 ± 1	847 ± 1	3 ± 0.0	Free flowing
SUR500	601 ± 16	764 ± 4	790 ± 3	3 ± 0.3	Easy/Free flowing
APAP 1627	80 ± 5	440 ± 15	517 ± 5	15 ± 2.1	Free flowing
APAP 1624	134 ± 7	459 ± 12	544 ± 4	16 ± 2.1	Free flowing
APAP 1776	327 ± 5	719 ± 8	757 ± 3	5 ± 0.7	Free flowing
IBU1618	79 ± 3	510 ± 16	573 ± 5	11 ± 2.6	Free flowing
Lactose	68 ± 1	647 ± 18	862 ± 6	25 ± 1.5	Easy flowing
Avicel	81 ± 11	362 ± 14	437 ± 5	17 ± 2.2	Easy flowing

3.2 Preliminary validation experiments

The aim of the preliminary experiments (section 2.5.1) was to repeat the assessments carried out by M&O Perry Industries and validate the operation of the FC Powder Filling Machine. The industrial requirements for the equipment were:

- to dose 100-500 μm diameter particles.
- to dose fill weights from 50 mg to 400 mg.
- to deliver the required dose with a precision of ±2 % RSD.

The RSD values obtained for the preliminary experiments are show in Table 10, along with details of the operability ranges stated by the manufacturer. These are compared with values obtained by M&O Perry (selected rows from Table 18 in Appendix I). The side-by-side comparison is shown in Table 11.

There are a number of important observations that can be made from the results. Firstly, the RSD values obtained by the author were consistently higher than those obtained by the M&O Perry technician, for any material. This could be due to operator differences because the use of a filling gun is a manual process and the results are dependent on how the operator uses the gun (e.g. operator differences could include different plunging depths or plunging speeds). An equally plausible explanation for the differences is the inherent difference between the two different machines. Nevertheless, the performance and precision achieved by the author was still very good for some of the materials and the equipment still managed to meet the performance criteria in these instances. The 1/8 inch gun performed well with materials ACR180 and ACR355 to deliver 50 mg. The ¼ inch gun similarly performed well with materials ACR180 and ACR355 to deliver 400 mg. The 3/16 inch gun performed well with material ACR180 to deliver 50 mg, but did not perform well with ACR355. This may be because the gun was operating at the lowest fill weight for the gun's capability; the operability range of the 3/16 inch gun was 50 mg-200 mg. At a fill weight of 150 mg, the gun performed well with both ACR180 and ACR355 as expected.

Table 10 – Table showing % RSD values for Suglets coated with Acryleze. *Fail* indicates that the powder could not be picked up with the gun. *Out of range* indicates that the target dose is outside the manufacturer's stated operability range for the particular gun size.

Gun I.D.	Stated operability range, mg	Target Dose (mg)	RSD (%)		
			ACR180	ACR355	ACR500
1/8	15-85	50	1.27	1.6	1.89*
3/16	50-200	50	1.36	11.38*	Fail
¼	125-450	50	Out of range	Out of range	Out of range
3/16	50-200	150	0.41	0.60	Fail
1/8	15-85	400	Out of range	Out of range	Out of range
3/16	50-200	400	Out of range	Out of range	Out of range
¼	125-450	400	0.43	0.63	0.93*

*** Material pick-up in these experiments was weak, with powder often falling out of the gun before discharge.**

Table 11 – Side-by-side comparison of RSD values achieved by external (M&O Perry) and internal assessments (the author) using sugar spheres coated with Acryleze. *Fail* indicates that the powder could not be picked up with the gun.

Gun I.D.	Dose (mg)	RSD (%) for ACR180		RSD (%)for ACR355		RSD (%)for ACR500	
		Internal	M&O P.	Internal	M&O P.	Internal	M&O P.
1/8	50	1.27	0.60	1.60	1.39	1.89*	Fail
3/16	50	1.36	0.60	11.36*	Not tested	Fail	Fail
3/16	150	0.41	Not tested	0.60	Not tested	Fail	Not tested
¼	400	0.43	0.17	0.63	0.25	0.93*	Not tested

*** Material pick-up in these experiments was weak, with powder often falling out of the gun before discharge.**

The second observation is the poor pick-up quality of the largest material, ACR500. Although two good RSD values were achieved by the author (1.89, and 0.93), the quality of the pick-up was very weak. The gun was moved slowly from the powder container to the receiving container when full with powder however any sudden movements caused the powder to leak from the gun. This is important because if the gun was operated with a robotic arm with rapid movements, the weak pick-up would result in powder leakage and poor dosage accuracy. In the case of the 3/16th inch filling gun, ACR500 failed to pick up altogether.

The reason for this can be understood if one considers a bed of particles in a section of pipe (Figure 23, Rhodes *et al*, 1990); if frictional forces are neglected a simple momentum balance on the powder will give:

Net force acting on powder = Rate of increase in momentum of powder (6)

Therefore:

Pressure force – gravitational force = increase in momentum of powder (7)

And for successful pickup of the powder, the increase in momentum must be positive, hence: *pressure force* > *gravitational force* for successful pickup.

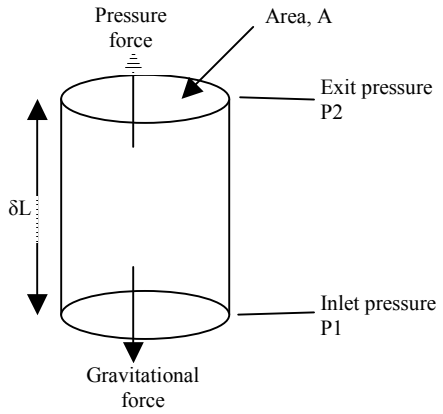

Figure 23 – Section of conveying pipe used for the momentum equation (adapted from Rhodes *et al*).

The pressure force is applied by the vacuum where P1 – P2 is the gauge pressure of the machine; assume this remains constant. The gravitational force per unit area of the powder (static head of powder) is given by (Rhodes *et al*, 1990):

Gravitational force per unit area = $\rho_s L(1-\varepsilon)g$ (8)

Where ρ_s is the solid density, L is the length of the pipe section, ε is the powder bed porosity and g is the gravitational acceleration. As the particle size decreases, ε will increase (Fayed *et al*, 1997) and so the gravitational force will decrease. Conversely, if the particle size increases, ε will decrease and the gravitational force will increase. At some point, the particles will be so large that the gravitational force is greater than the pressure force and the particles fail to pick up. Another way of looking at the same problem is to consider the ratio of mass to surface area. For a single large particle, the pressure force will act in an upward direction on the available surface area of the particle.

If the particle mass is too large, the weight of the particle will exceed the pressure force and the particle will fall. If the same mass were to be distributed over many smaller particles, the combined surface area of the particles would be greater than the single large particle. Therefore, the pressure would have a greater surface area to act upon, thereby allowing the pressure force to exceed the combined weight of the particles. The gravitational force is also dependent on the particle density. For successful pickup, the combined effect of particle density and particle size on the gravitational force must not outweigh the pressure force. For sugar spheres with a solid density of 1570 kg/m^3, the critical size for successful pickup is around 500 μm.

Table 10 also shows that the RSD achieved for the higher fill weight (400 mg) is consistently lower than at 50 mg. This can be expected because the gun performance is always subject to standard experimental error. The error by mass will be relatively constant however as the fill weights get lower and lower, the standard error will lead to an ever increasing percentage error. The acceptable standard error at 50 mg is ±1 mg, whereas at 400 mg, the acceptable error increases to ± 8 mg.

3.2.1 Conclusions

Based on the experimental evidence, it was concluded that all the guns were able to successfully pick up materials ACR180 and ACR355 when operating in the middle of their respective operability ranges and delivered within the required precision of RSD ± 2 %. When operating at the boundary of it operability range, the 3/16th inch gun was only able to pick up the smallest particles (ACR180) but was not able to pick up the larger material (ACR355) very well. It is therefore not recommended that a gun should be used to deliver relatively large particles with a dose weight very close to the operability boundaries for that particular gun (e.g. for a dose weight of 50 mg, it is recommended to use the 1/8th inch gun, but for a dose weight of 85 mg, it is recommended to use the 3/16th inch gun). Finally, the guns are incapable of strong pickup with very coarse materials that greatly exceed 500-600 μm.

3.3 Investigating the effect of vacuum strength using the FC Powder Filler

The aim of these experiments was to investigate how the accuracy and precision of the fill weight is affected by increasing the vacuum strength. Materials were affected in different

ways depending on the powder characteristics. The results in this section are grouped to show the effect of particle size and the effect of flowability.

For each material, the RSD values and sample means were calculated and plotted against vacuum strength. To recap, the industrial requirements for the equipment were:

- to dose 100-500 μm diameter particles.
- to dose fill weights from 50 mg to 400 mg.
- to deliver the required dose with a precision of ± 2% RSD.

3.3.1 The effect of vacuum strength on particles of different sizes

To investigate the effect of vacuum strength on particles with different sizes the results for the following materials are compared:

- ACR180 vs ACR355
- SUR180 vs SUR355
- APAP1627 vs APAP1624 and APAP1776

For materials consisting of spherical particles and a narrow size distribution, it was expected that the smaller particles (180 μm) would give a better precision (lower RSD) than the larger (355 μm) particles. This is because with smaller particles, the mass of each particle is much smaller. Therefore it is possible to achieve the desired target mass more closely. This is also more likely to be significant for a smaller fill weight (50 mg) than a larger one (400 mg) because the smaller volume of powder will consist of a smaller number of particles and will be more sensitive to small changes in particle numbers.

In considering the effect of vacuum strength, it was expected that the effect on the fill weight will be related to the Carr's index of the material. In other words, increasing the vacuum strength can be likened to the tapping process described in 2.4.2. Both actions cause particles to come closer together; filling any voids to create a tighter packing arrangement. Therefore, if a material has a very low Carr index, (e.g. 3 % for ACR180) it was hypothesised that the mean fill weight would increase by up to 3 % as the vacuum strength increased. Cohesive materials would therefore be affected the most by the vacuum strength. Also, materials ACR180, ACR355 and SUR180, SUR355 have a similar Carr's index (3-4 %), therefore it was expected that the effect of vacuum strength

would be the similar on these materials. APAP1627 and APAP1624 have similar Carr's index (15-16 %) therefore, the effect of vacuum strength on these two is expected to be similar and greater than the affect on APAP1776, which has a Carr's index of 5 %.

3.3.1.1 Effect of vacuum strength on ACR180 & ACR355

Figure 24(A) shows the results for ACR180 at a fill weight of 50 mg in which the mean fill weights are not affected significantly by a change in vacuum strength. Figure 24(B) shows the results for ACR180 with a fill weight of 400 mg. At this fill weight, the sample mean gradually decreases as the vacuum strength increases, however statistically the differences between means are insignificant. These results are not quite as expected; assuming that the voidage at low vacuum strength is the same as it would be for a powder in the poured state, and at high vacuum it is as if the powder has been tapped, it follows that if the Carr's index is 3 % for ACR180, the fill weight would also be expected to increase by 3 % for increasing vacuum strength. However, it may be that the increase in vacuum strength from 5 inHg to 20 inHg is not great enough to cause the material to pack any tighter. Another possibility is that when the gun is dipped into the powder bed, the powder immediately conforms into its most tightly packed arrangement in the gun and increasing the vacuum strength has no further effect on the material.

Figure 24(C) shows the results for ACR355 at a fill weight of 50 mg. There is a trend for the mean to increase as the vacuum strength increases. Figure 24(D) shows the results for ACR355 at a fill weight of 400 mg. The sample means again increase as the vacuum strength increases before levelling off at a vacuum strength of -20 inHg. The results for ACR355 at both fill weights show that the material is affected by vacuum strength and that fill weight will generally increase as vacuum strength increases. However, the amount by which the mean increases is not as great as expected.

Figure 24(E) and (F) show how the precision (% RSD) is affected for both materials at fill weights of 50 mg and 400 mg. For both materials, the RSD remains relatively constant around 0.5 % at 400 mg as the vacuum strength increases. At 50 mg, there is greater variability in the RSD because the fill weight is smaller therefore small errors appear amplified as a percentage error, but the RSD is still within acceptable limits. The RSD is generally lower for ACR180 than ACR355 at both fill weights as expected because the

larger particles give rise to a greater mass error as described earlier. Finally, there does not seem to be a trend in the RSD as the vacuum strength increases.

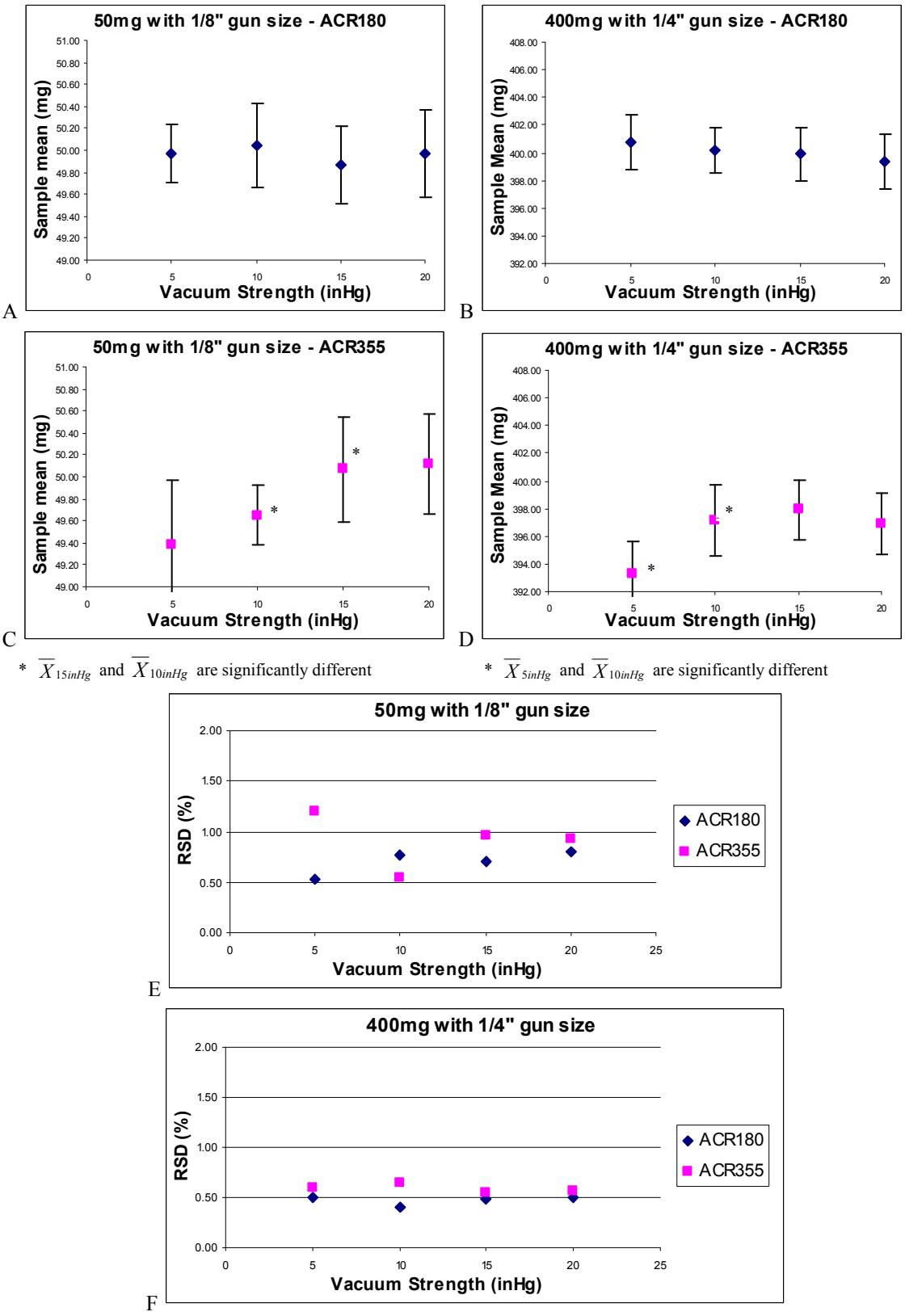

Figure 24 – Figure showing the change in sample mean with increasing vacuum strength for ACR180 and ACR355 at (A) 50mg and (B) 400mg. Also, figures C & D show the change in RSD with vacuum strength for the same materials at 50mg and 400mg.

3.3.1.2 Effect of particle size and vacuum strength with SUR180 & SUR355

Figure 25(A) shows the results obtained for SUR180 at a fill weight of 50 mg. At this fill weight there does not seem to be a trend as the vacuum strength increases. Statistically, two points are significantly different however this is practically unimportant because the means are still very close to the target and there is no trend. Figure 25(B) shows the results for SUR180 at a fill weight of 400 mg. The mean fill weight decreases slightly as the vacuum strength is increased but there is no significant difference between the adjacent means. Nevertheless, the decrease in mean is only slight and the deviation of the mean is very small ($\overline{X}_{20inHg} = 399.4\,\text{mg}$ and $\overline{X}_{5inHg} = 400.6\,\text{mg}$).

Figure 25(C) shows that at a fill weight of 50 mg, SUR355 is not affected by an increase in vacuum strength. Figure 25(D) shows that at 400 mg, there is a slight trend for the sample mean to increase as expected with increasing vacuum strength. As for ACR355 earlier, the increase is not a great as expected (a 3 % increase was arguably expected in line with the Carr's index).

Figure 25(E) and (F) show the RSD versus increasing vacuum strength for SUR180 and SUR355. At both fill weights and with both materials, the RSD is not affected greatly and remains relatively constant. These results are very similar to the results obtained for ACR180 and ACR355 earlier. At 50 mg fill weight, the RSD for SUR180 is generally lower than for SUR355 because the larger particles lead to a greater error and this difference is less pronounced at the higher fill weight. Also, the RSD at 400 mg is generally lower than at 50 mg fill weight.

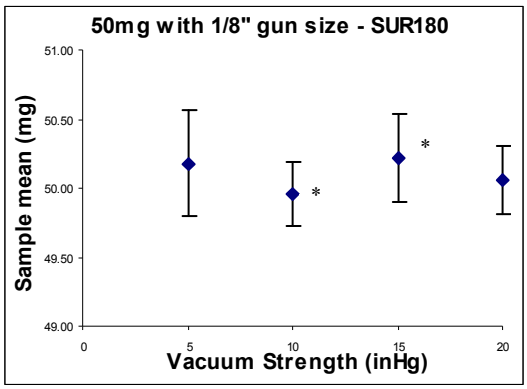

A

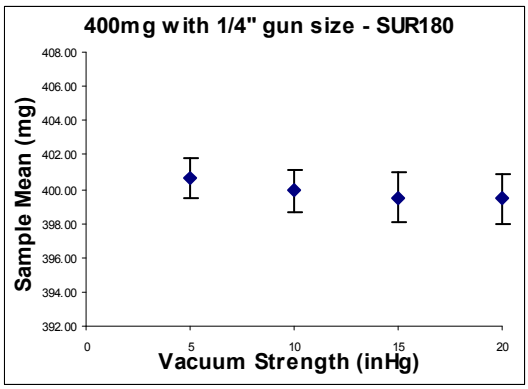

B

* $\overline{X}_{15inHg}$ and $\overline{X}_{10inHg}$ are significantly different.

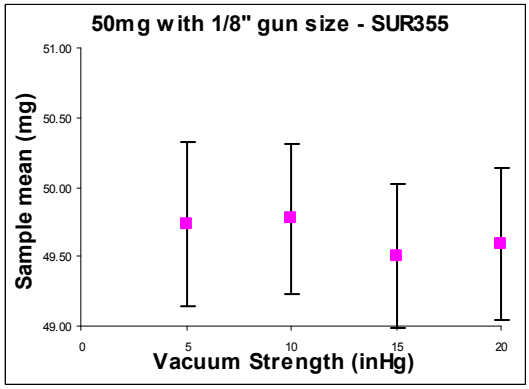

C

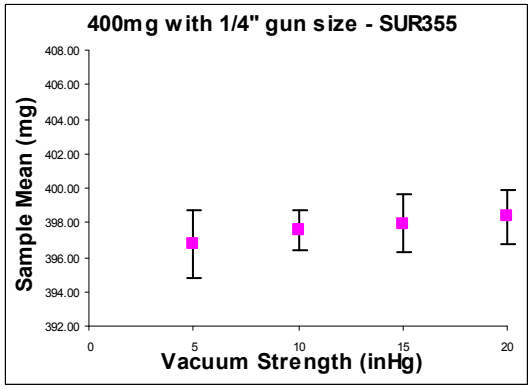

D

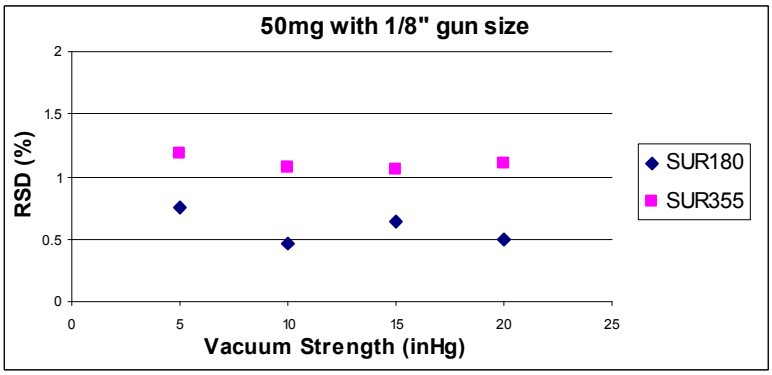

E

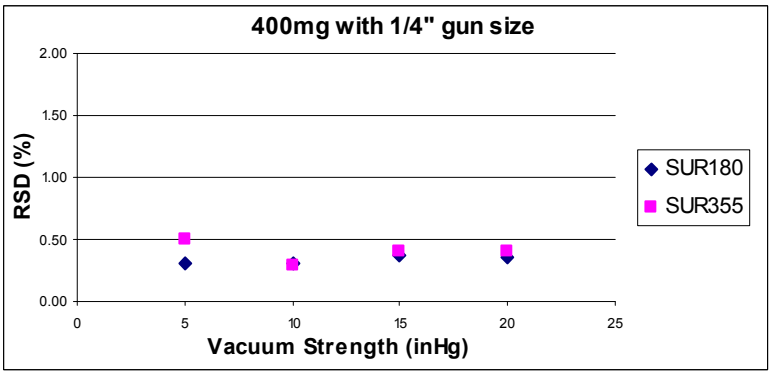

F

Figure 25 - Figure showing the change in sample mean with increasing vacuum strength for SUR180 and SUR355 at (A) 50mg and (B) 400mg. Also, figures E & F show the change in RSD with vacuum strength for the same materials at 50mg and 400mg.

3.3.1.3 Effect of particle size and vacuum strength with APAP1627, APAP1624 & APAP1776

With APAP1627 and APAP1624, it was hypothesised that the mean would increase by up to 15% as the vacuum strength increased from 5 inHg to 20 inHg. Figure 26(A) shows the results for APAP1627 at 50 mg fill weight. The sample mean increases by around 2 % as the vacuum strength increases. At a fill weight of 300 mg, (Figure 26(B)), the mean increases with vacuum strength by around 4 %. As with the previous materials, ACR180, ACR355, SUR180 and SUR355, the effect of vacuum strength is not as great as anticipated but is still significant.

Figure 26(C) shows the results obtained for APAP1624 at a fill weight of 50 mg. The sample mean again increases with vacuum strength by approximately 4 %. At 300 mg fill weight, the mean increases by 1.5 %. Both APAP1627 and APAP1624 performed similarly to each other, because the powder properties were similar for both materials, i.e. similar span of the PSD (1.66 for APAP1627 and 1.45 for APAP1624), similar flow characteristics from shear testing and similar Carr's index (15 % for APAP1627 and 16 % for APAP1624).

Figure 26(E) shows the results obtained for APAP1776 at a fill weight of 50 mg. The general trend in this graph is for the sample mean to decrease as the vacuum strength increases. This is interesting behaviour and it is not clear why it happens; the differences are significant and the actual decrease in the mean is 1.4 %. At a fill weight of 300 mg, (Figure 26(F)), the sample means remain relatively constant as the vacuum strength increases. Again, this is unexpected, and it is not like the results seen with APAP1627 and APAP1624.

Figure 26(G) shows how the RSD is affected by vacuum strength for the three materials at a fill weight of 50 mg. At this fill weight, the RSD values are more variable than at 300 mg fill weight which can be expected because the smaller fill weight will inevitably experience greater percentage variations. For a fill weight of 300 mg, the RSD for all three materials either remains relatively constant or increases as the vacuum strength increases. In all cases, the RSD is acceptable and the differences are practically not important as long as it is well below the 2 % limit.

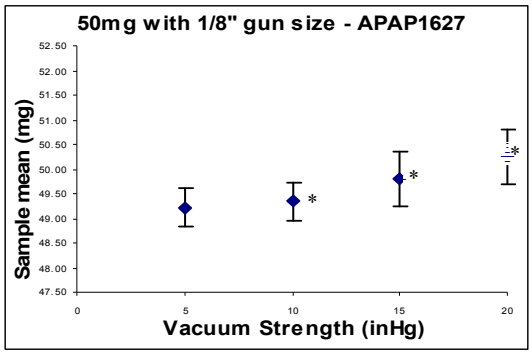

A

* $\overline{X}_{20inHg}$ and $\overline{X}_{15inHg}$ are significantly different

* $\overline{X}_{15inHg}$ and $\overline{X}_{10inHg}$ are significantly different

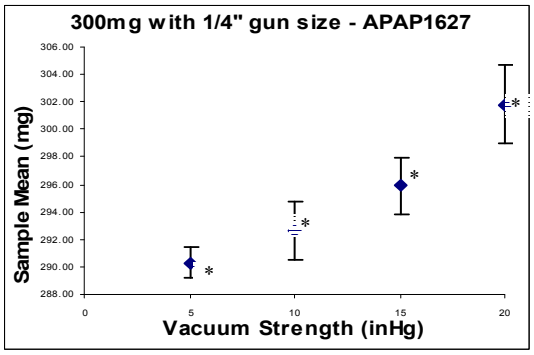

B

* All adjacent means are significantly different

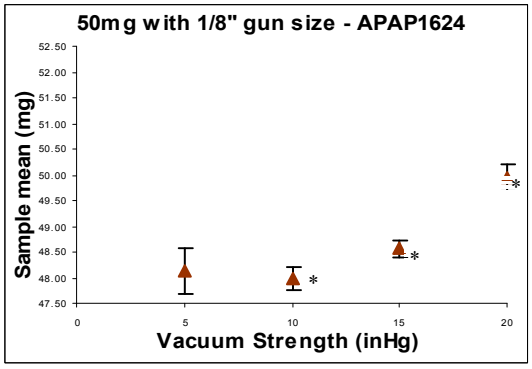

C

* $\overline{X}_{20inHg}$ and $\overline{X}_{15inHg}$ are significantly different

* $\overline{X}_{15inHg}$ and $\overline{X}_{10inHg}$ are significantly different

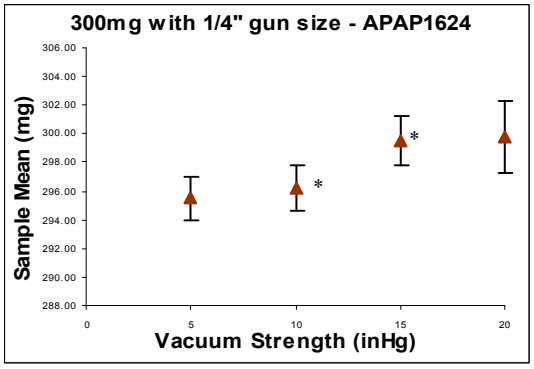

D

* $\overline{X}_{15inHg}$ and $\overline{X}_{10inHg}$ are significantly different

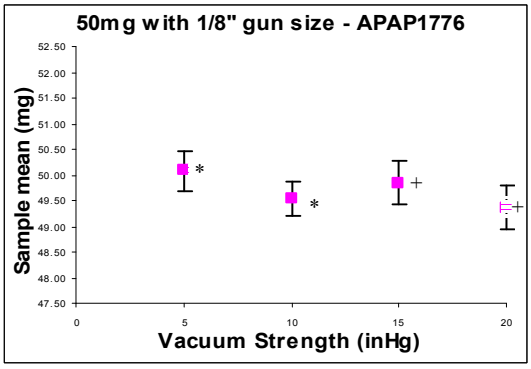

E

* $\overline{X}_{10inHg}$ and $\overline{X}_{5inHg}$ are significantly different

\+ $\overline{X}_{20inHg}$ and $\overline{X}_{15inHg}$ are significantly different

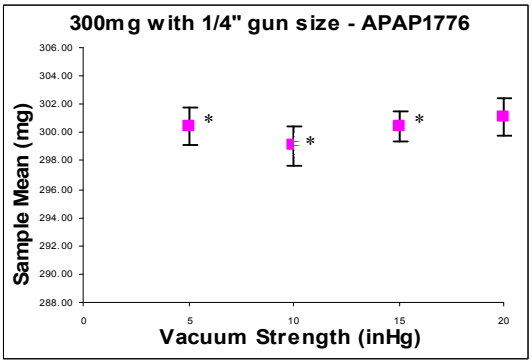

F

* $\overline{X}_{10inHg}$ is significantly different to $\overline{X}_{5inHg}$ and $\overline{X}_{15inHg}$

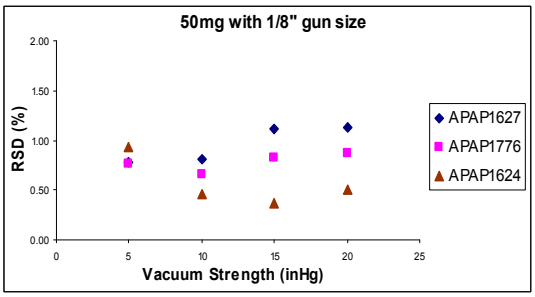

G

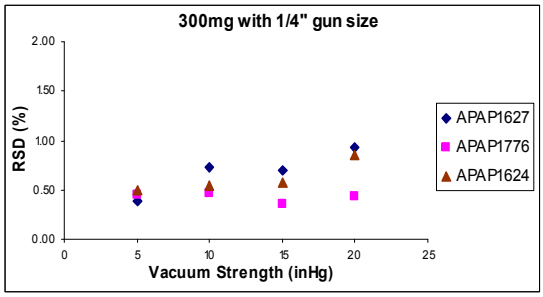

H

Figure 26 - Figure showing the change in sample mean with increasing vacuum strength for 3 size ranges of coated APAP at fill weights of 50 mg and 300 mg. Also, figures G & H show the change in RSD with vacuum strength for the same materials at 50 mg and 300 mg.

3.3.1.4 Effect of vacuum strength on particles of different sizes – discussion

It was hypothesised that all materials would be affected by vacuum strength and the magnitude by which the sample mean would change would be the same as the Carr's index for the material. The results have shown that the effect is certainly not as great as the Carr's index however there is still some relation to Carr's index.

The smallest materials, APAP1627 (80 μm) and APAP1624 (134 μm) in general were affected the most by vacuum strength. The largest materials, ACR355 (431 μm) and SUR355 (450 μm) were also affected somewhat by the vacuum strength. However, the materials in between, ACR180 and SUR180 were affected very little by the vacuum strength. The smallest materials have the highest Carr's index values and therefore are more cohesive. Inter-particular forces (Israelachvili *et al*, 1991) are the greatest in smaller materials and are dominant over the gravitational forces (Seville *et al*, 1997 and Li *et al*, 2004) for materials around 100 μm and smaller. The result is that these materials are not in the most tightly packed arrangement under low vacuum conditions and the packing arrangement changes by increasing the vacuum strength. For ACR180 and SUR180, the gravitational forces dominate so the materials are in a well packed state even under low vacuum conditions. However as the particle size gets close to the limit of around 500 μm (ACR355 and SUR355) where the pick-up becomes weaker, the gravitational forces are such that the material will pack in a very loose arrangement under low vacuum conditions. Therefore increasing the vacuum strength overcomes the gravitational force to make the materials pack in a tighter arrangement. Figure 27 proposes how the vacuum strength may affect particles of different sizes. The results do not unanimously support this idea, for example SUR355 was not affected in the same way as ACR355. This is because there are other factors at play (e.g. surface texture, shape, friction etc) and not just the particle size that affects the flowability and performance of the materials.

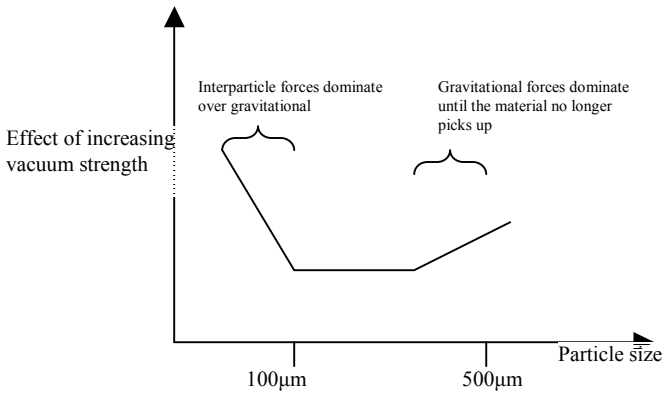

Figure 27 – Figure showing the effect of increasing vacuum strength on different sized particles based on experimental observations.

3.3.2 The effect of vacuum strength on materials with different flow characteristics

In the previous section, the effect of particle size and vacuum strength was investigated. In this section, the results for materials with similar particles sizes, but different flow characteristics are compared. It must be noted that flow characteristics cannot strictly be isolated from the particle size because the flowability depends largely on the particle size. Smaller particles are known to be more cohesive than larger ones. However, the following comparisons are nonetheless carried out:

- ACR180 vs SUR180
- ACR355 vs SUR355
- IBU1618 vs lactose and Avicel

3.3.2.1 The effect of vacuum strength on ACR180 and SUR180

The results for ACR180 and SUR180 (Figure 24(A) and Figure 25(A)) at 50 mg fill weight did not follow a trend and the effects on the sample means that were seen were practically insignificant. At 400 mg fill weight, the results for both materials are almost identical with a slight trend for the mean to decrease but the trend is statistically insignificant. The results are not quite as expected; SUR180 was shown to be slightly more cohesive than ACR180, particularly when the material has been compressed under a higher consolidation load (as shown in shear tests, section 3.1.3). Therefore it was expected that the materials would behave differently to each other, however results have shown they perform in a very similar way.

3.3.2.2 The effect of vacuum strength on ACR355 and SUR355

At 50 mg fill weight, ACR355 (Figure 24(C)) was affected more than SUR355 (Figure 25 (C)) by the increase in vacuum strength. Similarly at 400 mg fill weight, ACR355 (Figure 24(D)) was affected more by the increase in vacuum strength whereas SUR355 (Figure 25(D)) was affected much less. The reason for the differences between the two materials is not clear. It could be related to the greater cohesivity of SUR355. Where ACR355 may have been affected by gravitational forces that caused a loose packing arrangement at a low vacuum strength, it is possible that the greater cohesion in SUR355 particles meant that the effect of inter-particular forces was great enough to overcome the gravitational forces in order to pack the particles in tight arrangement. This is only speculation because the size and PSD of both ACR355 and SUR355 is very similar and the only difference is the surface coating. Therefore, it is possible that the Surelease coating causes greater cohesion between particles either because of greater friction between particles or some other difference in surface chemistry.

3.3.2.3 The effect of vacuum strength on IBU1618, lactose and microcrystalline cellulose (Avicel)

Figure 28(A) shows the results for IBU1618 at a fill weight of 50 mg. Statistically there is no significant difference between any of the means in figure (A). At a fill weight of 300 mg, (Figure 28(B)) $\overline{X}_{15inHg}$ is significantly different to $\overline{X}_{10inHg}$ and $\overline{X}_{20inHg}$ but the practical importance of this is very little because there is no trend for increasing vacuum strength. At both fill weights, the standard error is relatively large and at 50 mg it even exceeds the 2 % RSD limit. These results are surprising because IBU1618 has a Carr's index of 11 % and it was expected that the performance would be similar to APAP1627 or lactose because of the similarity in particle size and PSD.

Figure 28(C) and (D) show the results for lactose at fill weights of 50 mg and 300 mg respectively. At both fill weights, increasing the vacuum strength causes the sample mean to increase significantly. At 50 mg fill weight, the sample mean increases by 2.2 % and at 300 mg fill weight, the mean increases by 3.3 %. The Carr's index for lactose is around 25 %, therefore it was hypothesised that the mean would increase more than it did. As with APAP1627 and APAP1624 in the previous section, the effects of vacuum strength are not as great as expected because either the change in vacuum strength is not

great enough to pack the powder particles very tightly or the particles may be in a tightly packed state at the outset, therefore further increase in vacuum strength does not cause the particles to pack any closer together.

Figure 28(E) and (F) show the results for Avicel at fill weights of 50 mg and 300 mg respectively. At 50 mg fill weight, the sample means do not vary greatly, and statistically only $\overline{X}_{10inHg}$ and $\overline{X}_{15inHg}$ are significantly different. It is unclear why this happens because the material was arguably expected to perform in a similar fashion to APAP1627 and lactose due to their similarity of mean particle size and the relatively high Carr's index (17 %). At 300 mg fill weight, the material performs similarly to lactose as expected because there is a trend for the sample means to increase as the vacuum strength increases.

The plots of RSD versus vacuum strength are shown in Figure 28 (G) and (H). At 50 mg fill weight, the RSD for lactose is generally lower than for Avicel and IBU1618. The RSD for IBU1618 varies considerably and does not meet the ± 2% requirement for every vacuum strength. At 300 mg fill weight, the RSD is generally the lowest for lactose and highest for IBU1618 and again there is much variability with IBU1618. For lactose, the RSD is the best because the material has a relatively narrow PSD therefore the packing arrangement is similar every time a dose is collected. With IBU1618 the same could be expected, but it is unclear why the material exhibits a poorer RSD than lactose (which has a similar mean particle size and span) or APAP1627 (similar mean particle size and PSD) With Avicel, the PSD has a very wide span and the material contains particles from very fine (<10 μm) to very coarse (>600 μm). In such a material, a great deal of segregation can be expected to occur (Thomson *et al*, 1997). If a very small volume of powder is taken from the powder bed (e.g. equivalent to 50 mg) then the actual mass will vary a great deal depending on the relative amount of each particle size within that small volume. In other words, with such a wide ranging PSD, it is very difficult to ensure dose uniformity and a low RSD.

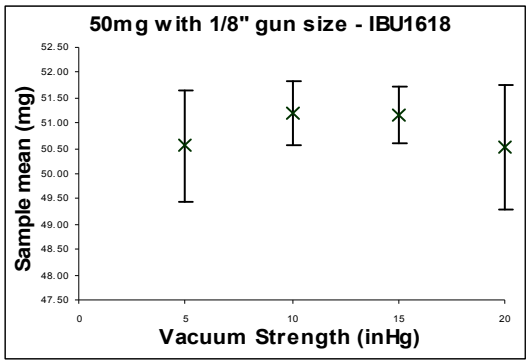

A

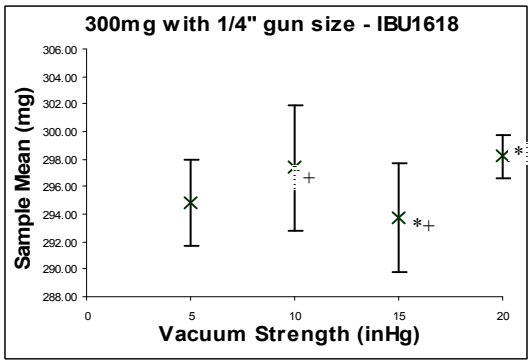

B

* $\overline{X}_{20inHg}$ and $\overline{X}_{15inHg}$ are significantly different

\+ $\overline{X}_{15inHg}$ and $\overline{X}_{10inHg}$ are significantly different

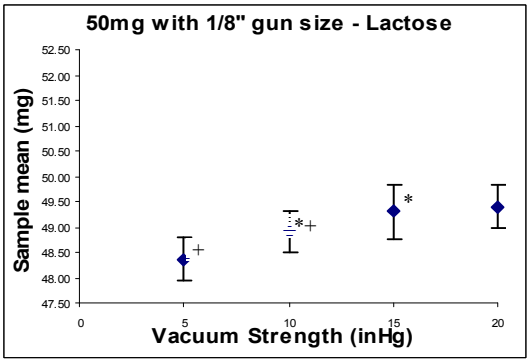

C

* $\overline{X}_{15inHg}$ and $\overline{X}_{10inHg}$ are significantly different

\+ $\overline{X}_{10inHg}$ and $\overline{X}_{5inHg}$ are significantly different

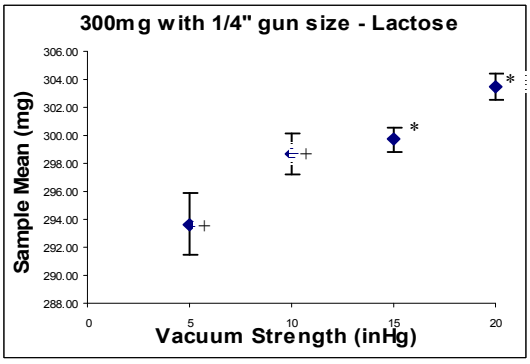

D

* $\overline{X}_{20inHg}$ and $\overline{X}_{15inHg}$ are significantly different

\+ $\overline{X}_{10inHg}$ and $\overline{X}_{5inHg}$ are significantly different

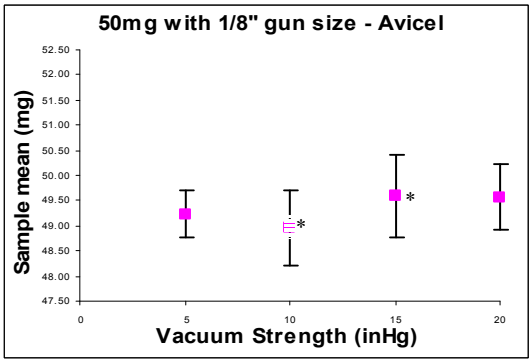

E

* $\overline{X}_{15inHg}$ and $\overline{X}_{10inHg}$ are significantly different

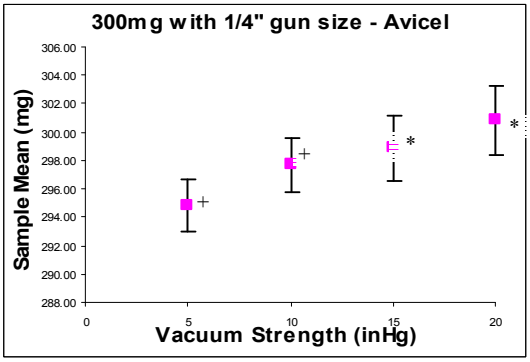

F

* $\overline{X}_{20inHg}$ and $\overline{X}_{15inHg}$ are significantly different

\+ $\overline{X}_{10inHg}$ and $\overline{X}_{5inHg}$ are significantly different

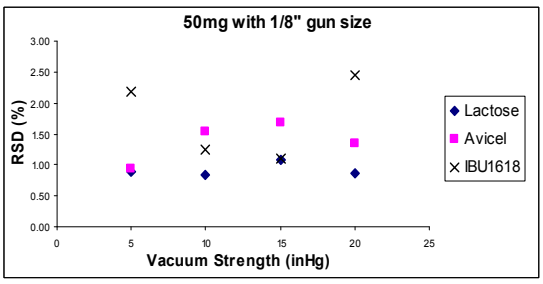

G

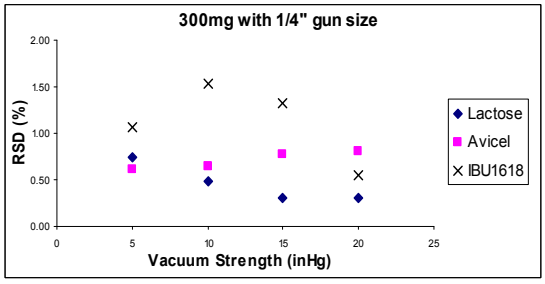

H

Figure 28 - Figure showing the change in sample mean with increasing vacuum strength for coated IBU1618, lactose and Avicel at fill weight of 50 mg and 300 mg (A-F). Also, figures G & H show the change in RSD with vacuum strength for the same materials at 50 mg and 300 mg fill weights.

3.3.2.4 Effect of vacuum strength on materials with different flow characteristics - discussion

For materials where the sample mean increased significantly with increasing vacuum strength (ACR355, APAP1627, APAP1624, lactose and Avicel), the effect was not as great as expected but was still significant to cause the accuracy of the fill weight to alter by up to 4 %. It may be that the increase in vacuum strength was not great enough to cause the materials to pack any tighter or that the powder was already quite close to its tightest packing arrangement at the lowest vacuum strength (5 inHg) and thus increasing the vacuum strength did not have as great an effect as expected. With the exception of ACR355, these materials all have Carr's index values over 15 %.

The most free flowing materials i.e. those with a low Carr's index (ACR180, SUR180, SUR355, APAP1776 and IBU1618) were affected the least by the increasing vacuum strength. These materials generally gave very consistent RSD values (with the exception of IBU1618) and relatively consistent dose weights (i.e. the accuracy was relatively consistent). These results are similar to those by Irwin *et al* (1970) who used similar dosing guns (without vacuum, called a dosator) to dose powders and found that free flowing powders gave the best fill weight uniformity. This correlation was related to the fact that free flowing powders in a dosing hopper reformed better after the dosator had removed its plug and so resulted in a well packed bed to receive the returning dosator.

If the performance of the materials is linked to the Carr's index, then the results seen with ACR355 are an exception. It is possible that with ACR355 at a low vacuum strength (5 inHg), the higher weight of the particles meant that the particles were not packed in the tightest arrangement when the gun was held vertically. As the vacuum then increased, the packing arrangement became tighter. The same was not seen with SUR355 because SUR355 is slightly more cohesive. With ACR355, this behaviour could be associated with the material being too free-flowing. This was shown to be a problem by Kurihara *et al*, (1978), who found that the most free-flowing powders were too free-flowing and were not able to form a sufficiently solid plug of powder to allow accurate volumetric measurement. .

To summarise the effect of vacuum strength on all the materials used, the percentage by which the mean increases as the vacuum strength increases is calculated as:

$$\% \text{ mean increase} = \frac{\overline{X}_{20inHg} - \overline{X}_{5inHg}}{\overline{X}_{5inHg}} \times 100 \qquad (9)$$

This method is not without its errors because for some of the experiments, the mean did not actually increase but in fact decreased slightly. However, it still provides a reasonable approximation of how much the sample mean is affected. The percentage mean increase is calculated for 300mg fill weights (or 400mg where appropriate). Figure 29 is a scatter graph that shows the percentage increase of the sample mean versus the Carr's index. The figure shows that there is a link between the Carr's index (i.e. flowability) and the amount by which a material is affected by the vacuum strength.

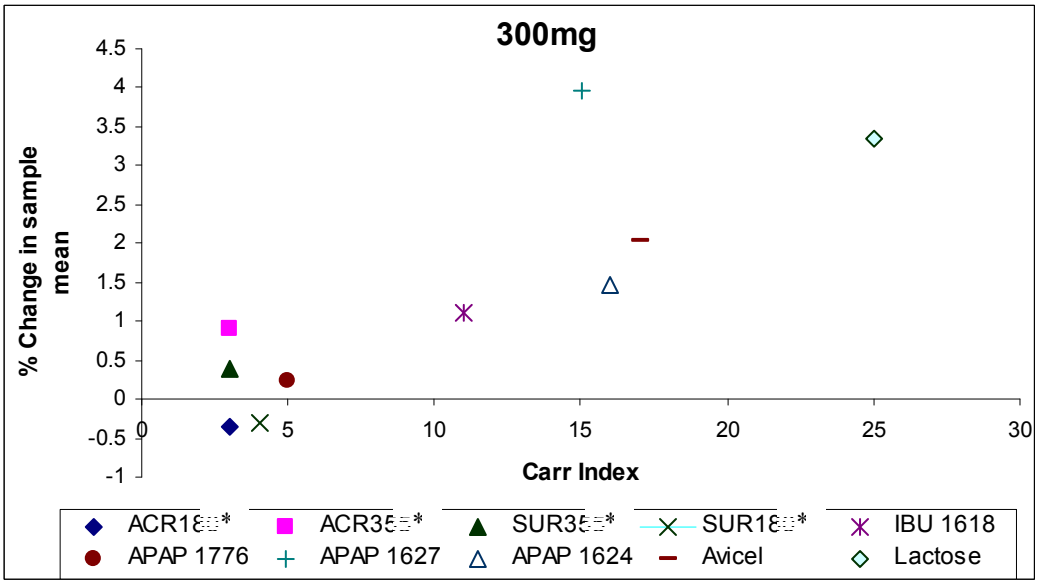

Figure 29 – Graph showing the % increase in the sample mean as the vacuum increases from 5inHg to 20inHg plotted against the Carr Index. Each point represents the percentage by which the mean is affected by vacuum strength at a fill weight of 300mg. * The fill weight used for these materials was 400mg.

3.3.3 Recommendations

In light of the results obtained, the best materials are those between 150-350 µm because these are not affected by changes in vacuum strength. Materials as small as 50 µm and up to 500 µm can be used, with the knowledge that the dose weight may be affected by changing the vacuum strength. Therefore, if the vacuum strength is changed, the filling gun must be recalibrated to deliver the correct dose weight. It is also recommended that materials with a relatively narrow size distribution are used to ensure that localised segregation does not occur and that the particle packing arrangement is repeatable for each dose. The FC Powder Filler is quite tolerant of the particle shape because it

performed adequately with materials such as lactose and Avicel which are known to have very irregular particle shapes (see images in Appendix III). It seems the most important particle characteristics are particle size, and PSD. If these are controlled well, then there is a strong likelihood of a reproducible packing arrangement inside the dosing gun which will lead to a low RSD. To summarise, the powder flowability is affected by a whole range of particle characteristics, yet the bulk flowability can be characterised by the Carr's index. This can be used as a quick assessment as to how well a material will perform and how it will be affected by the vacuum strength. However, it should not be used exclusively without the support of PSD data which is crucial for ensuring good dosing precision.

3.4 Investigating the effect of collection speed using the FC Powder Filler

The aim of these experiments was to investigate how fast an acceptable dose can be taken and how the accuracy and precision of the dose weight is affected by a change in the collection speed (plunging speed) of the filling gun. This could be important in the design of an automated system for the manufacturing line. The time taken for the insertion and removal of the gun was used to define the speed as:

SLOW:	1-2 seconds
INTERMEDIATE:	< 1 second
FAST:	< ½ second

The results in this section are grouped to show the effect of particle size and the effect of flowability.

Particle size:

- ACR180 versus ACR355
- SUR180 versus SUR355
- APAP1627 versus APAP1624 and APAP1776

Flowability:

- ACR180 versus SUR180
- ACR355 versus SUR355
- IBU1618 versus lactose and Avicel

3.4.1 The effect of collection speed on particles of different sizes

When considering the effect of collection speed, it was initially hypothesised that there would be no difference in the dose weight accuracy or the precision as long as the gun was dipped into the powder bed to the same depth each time and sufficient residence time was allowed for powder collection.

3.4.1.1 Effect of collection speed on ACR180 and ACR355

The first set of results for ACR180 at 50 mg fill weight is shown in Figure 30(A). There is a statistically significant difference between the first two data points however there is no trend as the plunging speed increases. Similarly at 400 mg fill weight (Figure 30B), the first two data points are statistically different, but again there is no clear trend.

Practically, the differences in the data points are unimportant because the fill weights (at both 50 mg and 400 mg) are still very close to the target and the RSD is fairly constant and remains below 1%. For ACR355 at 50 mg fill weight (Figure 30(C)), the mean fill weight decreases as the collection speed increases. This suggests that when the material is collected using "fast" speed, the packing arrangement is not as tight as when using the "slow" collection speed. Alternatively, the "fast" operation did not allow sufficient residence time to allow maximum pick up. At 400 mg fill weight (Figure 30(D)), the opposite is seen i.e. the mean fill weight increases with collection speed. This might suggest that the faster collection speed causes the particles to pack more tightly than when using slow collection speed. It is interesting that opposite trends occur with the two different fill weights and it is not clear why this happens. For both materials and both fill weights, the RSD values remain relatively constant and are always below 1%. The important outcome is that both materials can be dosed with acceptable precision and accuracy using a fast collection speed. This is crucial for a potential, future automated process.

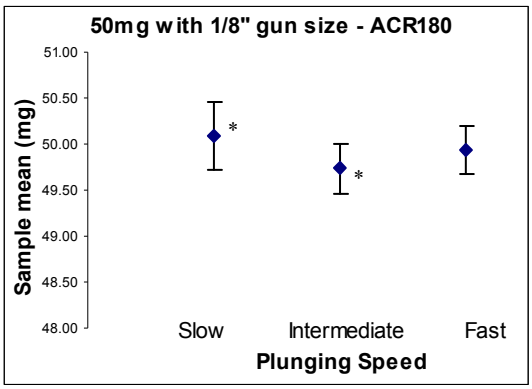

A

* $\overline{X}_{Slow}$ and $\overline{X}_{Int}$ are significantly different.

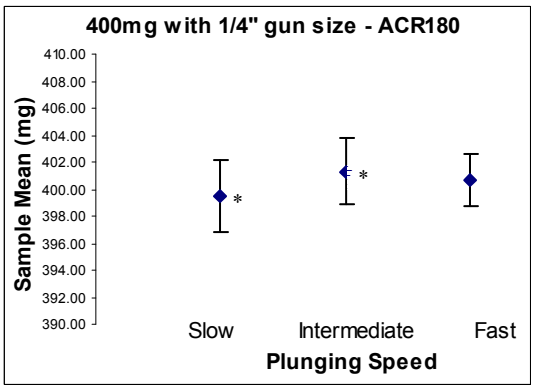

B

* $\overline{X}_{Slow}$ and $\overline{X}_{Int}$ are significantly different.

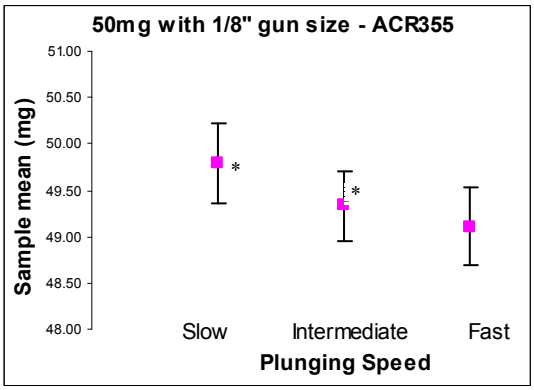

C

* $\overline{X}_{Slow}$ and $\overline{X}_{Int}$ are significantly different.

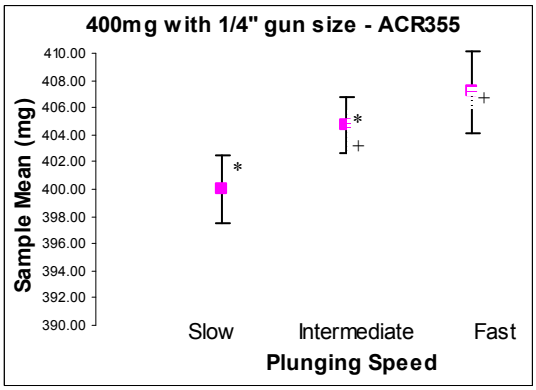

D

*+ $\overline{X}_{Slow}$ and $\overline{X}_{Int}$ and $\overline{X}_{Fast}$ are significantly different.

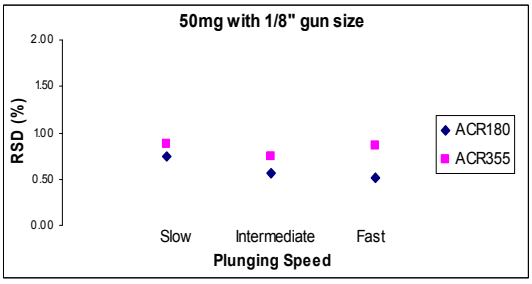

E

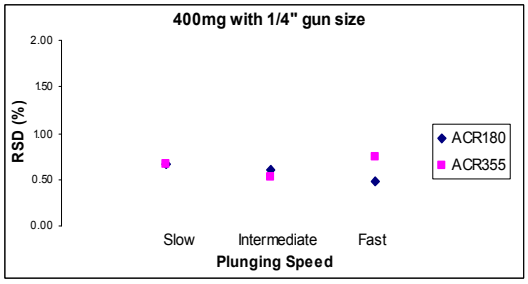

F

Figure 30 - Figure showing the change in sample mean with increasing collection speed for ACR180 and ACR355 at 50 mg and 400 mg fill weights. Also, figures E & F show the change in RSD with collection speed for the same materials at 50 mg and 400 mg.

3.4.1.2 Effect of collection speed on SUR180 and SUR355

Figure 31(A) and (B) show the results for SUR180 at 50 mg and 400 mg fill weights. At 50 mg fill weight, $\overline{X}_{Fast}$ and $\overline{X}_{Int}$ are significantly different, and there is a general trend for the mean fill weight to increase with increasing collection speed. However, the same trend is not seen at 400 mg fill weight. With SUR355 at 50 mg fill weight, there is a tendency for the mean fill weight to decrease as the collection speed increases but the decrease is small and there is no significant difference between adjacent means. At 400 mg fill weight, a similar decrease in the mean is seen. The reason for this behaviour is not clear, but it is possible that the larger particles require the gun to remain in the powder for a slightly longer period of time to allow a tight packing arrangement to form inside the gun. Hence, this would explain why the mean dose weight is highest when using slow collection speed. The RSD for both materials at both fill weights remains relatively constant and is not adversely affected by the collection speed.

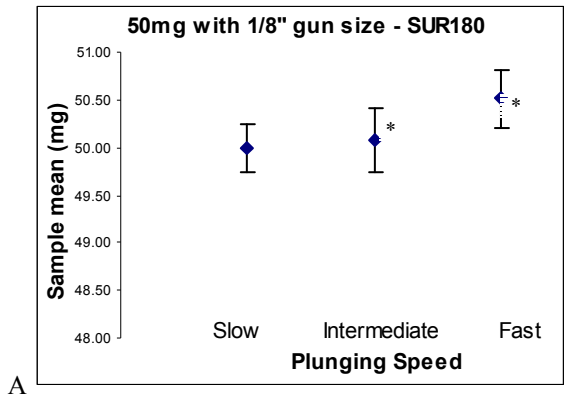

A

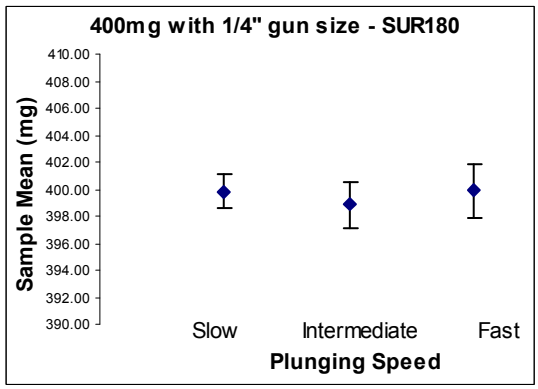

B

* $\overline{X}_{Int}$ and $\overline{X}_{Fast}$ are significantly different.

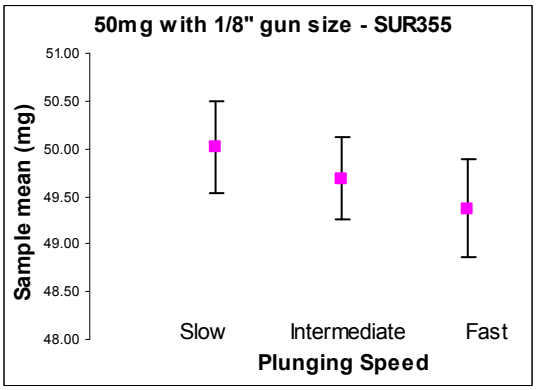

C

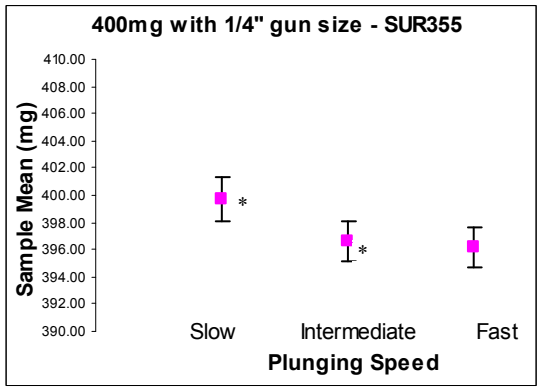

D

* $\overline{X}_{Slow}$ and $\overline{X}_{Int}$ are significantly different.

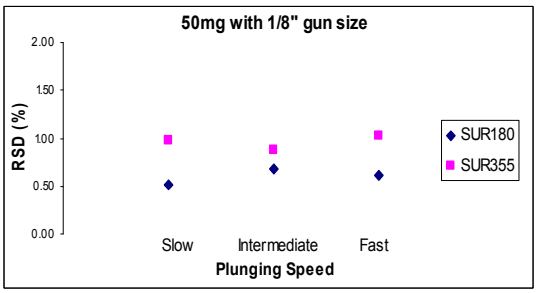

E

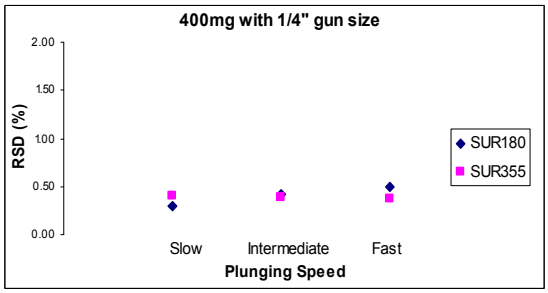

F

Figure 31 - Figure showing the change in sample mean with increasing collection speed for SUR180 and SUR355 at 50 mg and 400 mg fill weights. Also, figures E & F show the change in RSD with collection speed for the same materials at 50 mg and 400 mg.

3.4.1.3 Effect of collection speed on APAP1627, APAP1624 and APAP1776

Figure 32(A) and (B) shows the results for APAP1627 at 50 mg and 300 mg fill weights. At 50 mg fill weight, the mean decreases for the first two data points, but then it levels off. In both graphs, the difference between the first two data points is statistically significant however there is no clear trend at either fill weight. Therefore, practically the differences are unimportant because they are very small.

With APAP1624 at 50 mg fill weight (Figure 32(C)) the first two data points are statistically different but again there is no clear trend. At 300 mg fill weight (Figure 32(D)) there is also no trend although $\overline{X}_{Int}$ and $\overline{X}_{Fast}$ are significantly different. With both APAP1627 and APAP1624, it appears that the sample mean can be affected significantly by the collection speed however it is not clear why on some occasions the mean decreases but on others the mean increases. The fact that there are no clear trends suggests that the results are possibly affected by another factor other than the collection speed. For example, it may be that the method of insertion and removal of the gun is not exactly the same each time. If the gun is dipped a few millimetres further into the bed on some occasions, it may lead to extra compaction of the powder inside the gun and hence a higher dose weight.

Figure 32(E) and (F) show the results for APAP1776 at 50 mg and 300 mg fill weights. At both fill weights, $\overline{X}_{Slow}$ and $\overline{X}_{Int}$ are not significantly different but $\overline{X}_{Fast}$ is significantly greater than the other means. With this material, it could be that the fast collection speed results in compaction of the material inside the gun which leads to a higher fill weight.

At 300 mg fill weight (Figure 32(H)), the RSD for all three materials is very low (around 0.5 %) and remains relatively constant. However at 50 mg fill weight (Figure 32(G)), the RSD varies more and is affected more by the collection speed. However, RSD is still acceptable for all materials and is well below the 2 % limit for all three materials.

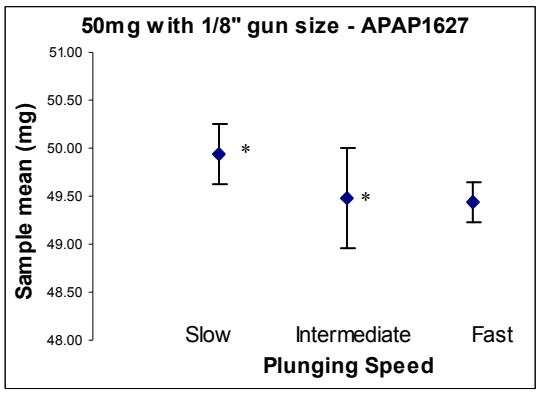

A

* $\overline{X}_{Slow}$ and $\overline{X}_{Int}$ are significantly different.

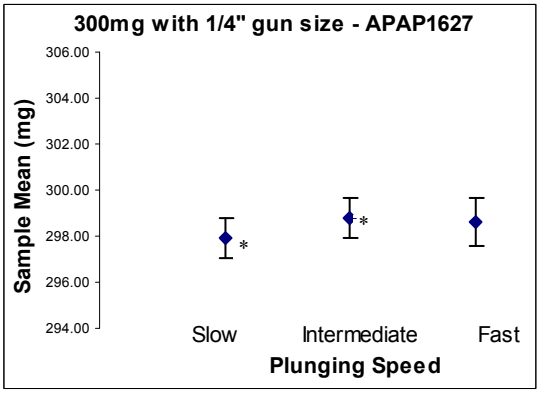

B

* $\overline{X}_{Slow}$ and $\overline{X}_{Int}$ are significantly different.

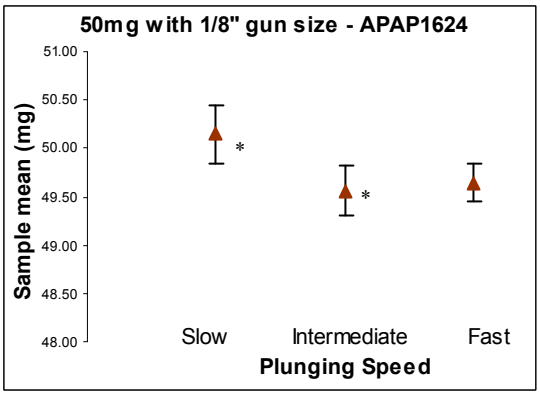

C

* $\overline{X}_{Slow}$ and $\overline{X}_{Int}$ are significantly different.

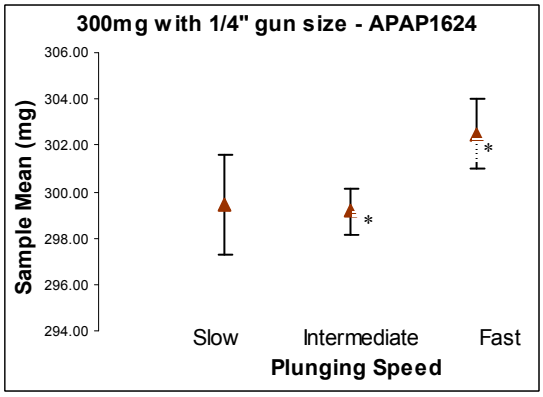

D

* $\overline{X}_{Int}$ and $\overline{X}_{Fast}$ are significantly different.

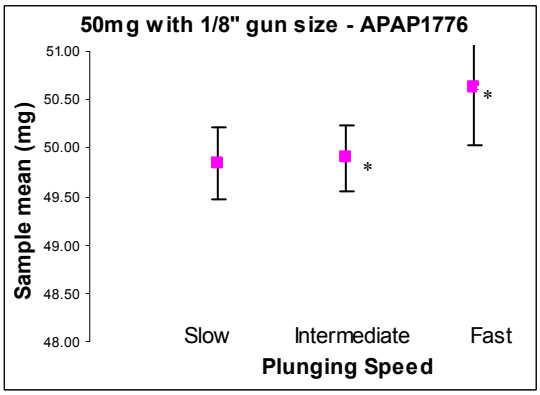

E

* $\overline{X}_{Int}$ and $\overline{X}_{Fast}$ are significantly different.

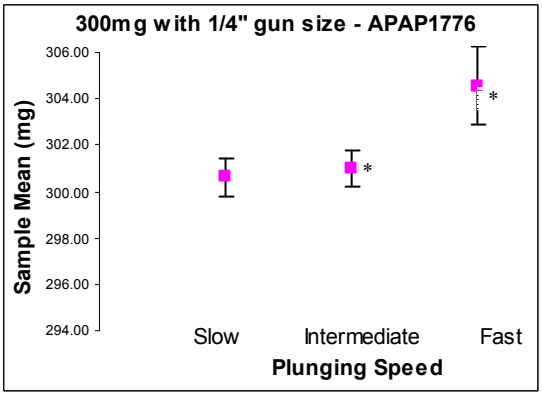

F

* $\overline{X}_{Int}$ and $\overline{X}_{Fast}$ are significantly different.

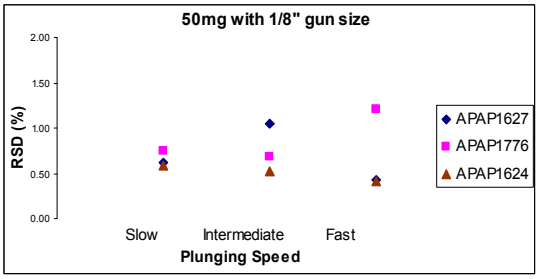

G

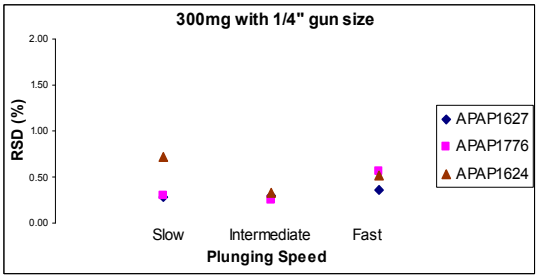

H

Figure 32 - Figure showing the change in sample mean with increasing collection speed for 3 sizes of APAP at fill weights of 50 mg and 300 mg. Also, figures G & H show the change in RSD with collection speed for the same materials at 50 mg and 300 mg fill weights.

3.4.1.4 Effect of collection speed on materials with different sizes - discussion

Prior to carrying out this investigation, it was hypothesised that the accuracy and precision of the dose weight would be unaffected by the speed of powder collection. The results have shown that this is not the case because in some experiments, the mean fill weight has been shown to increase with plunging speed, while with others, the mean fill weight has decreased with increasing collection speed. On analysing the results, the trends do not follow a clear pattern and the results do not seem to be linked to any of the powder properties (e.g. particle size). It is therefore suspected that the manual method used to collect the powder may have introduced other variables that influenced the results. For example, when collecting a powder using a fast collection speed, the gun was inserted to a depth of 2 cm into the powder bed and removed in less than half a second. By carrying this process out by hand, it was very difficult to ensure that the depth was precisely 2 cm for each dose. If the depth was a few millimetres greater, then it is possible that the powder inside the gun became over compacted and conversely, if the depth was less than 2 cm, then the powder may have packed more loosely giving a lower dose weight. The overall effect of this is greater variability in the RSD and also greater variability between sample means. To obtain more reliable data, the method of powder collection could be improved by ensuring that the powder collection depth is precisely the same for all experiments. Another improvement to the method would be to ensure that the collection speed is controlled more carefully and is more repeatable. One solution would be to use a robotic arm to carry out the powder collection process which would solve both the bed depth and the speed issues. However, despite these limitations, acceptable % RSDs were always achieved, indicating the robustness of the approach.

3.4.2 The effect of collection speed on materials with different flow characteristics

In this section, the following comparisons are carried out to show the effect of collection speed on materials with similar particles sizes, but different flow characteristics:

- ACR180 versus SUR180
- ACR355 versus SUR355
- IBU1618 versus lactose and Avicel

3.4.2.1 Effect of collection speed on ACR180 and SUR180

At 50 mg fill weight, the results for ACR180 (Figure 30(A)) show no trend with increasing collection speed but with SUR180 (Figure 31(A)) there is a tendency for the mean fill weight to increase as the collection speed increases i.e. the more cohesive material gives an increased fill weight when collected using a fast speed. At 400 mg fill weight, neither material is greatly affected by the collection speed (Figure 30(B) and Figure 31(B)).

3.4.2.2 Effect of collection speed on ACR355 and SUR355

The results of ACR355 (Figure 30(C)) and SUR355 (Figure 31(C)) at 50 mg fill weight are very similar to each other because the mean decreases as the collection speed increases. Both these materials consist of relatively large particles and it is possible that the dosing gun requires a slightly longer period of time inside the powder to pack the particles in a tight arrangement. Nevertheless, this is not detrimental to the precision of the instrument, as shown by % RSD (Figure 30(E) and Figure 31(E)). At a fill weight of 400 mg, the trends for ACR355 and SUR355 are opposite to each other (increasing mean for ACR355, decreasing mean for SUR355). This is very interesting, especially because in section 3.4.2.1, the mean for SUR180 at 50 mg increased with collection speed, therefore it would be reasonable to expect that SUR355 may behave similarly, however this is not the case.

3.4.2.3 Effect of collection speed on IBU1618, lactose and microcrystalline cellulose (Avicel)

Figure 33(A) and (B) show the results for IBU1618 at fill weights of 50 mg and 300 mg respectively. At both fill weights, there is no clear trend as the collection speed increases

therefore IBU1618 is not greatly affected by a change in the collection speed. Note however the large error bars; it must be acknowledged that such inter-sample variability for ibuprofen makes identification of statistically significant differences more difficult. Figure 33(C) shows the results for lactose at 50 mg fill weight. There is no statistically significant difference between the adjacent means. At 300 mg fill weight (Figure 33(D)) there is no trend as the collection speed increases. The results for Avicel at both 50 mg (Figure 33(E)) and 300 mg (Figure 33(F)) fill weights show that there is again no trend with increasing collection speed. The results for these three materials are as hypothesised because the speed of collection should not affect the dose weight.

The RSD values for all three materials at 50 mg fill weight are shown in Figure 33(G). The RSD values for Avicel and IBU1618 are relatively high compared to lactose, the reasons for this were discussed in section 3.3.2.3. In general, the RSD values are more variable than in previous experiments where the collection speed was kept constant. This is probably because the dose collection procedure was very difficult to repeat exactly for each dose. The important outcome is that the RSD for lactose is very low at both fill weights and does not vary a great deal with collection speed. For IBU1618 and Avicel, the RSD is generally higher and closer to the 2 % limit, therefore care must be taken when using these materials to ensure that the collection procedure is identical for each dose.

3.4.2.4 Effect of collection speed on materials with different flow characteristics – discussion

The results for IBU1618, lactose and Avicel were largely as expected i.e. there was no significant effect of collection speed on the mean fill weight at both 50 mg and 300 mg target weights. With the materials ACR180, ACR355, SUR180 and SUR355 some statistically significant effects were seen. As the collection speed increased, the sample mean increased for SUR180 at 50 mg fill weight and ACR355 at 400 mg fill weight. A decreasing trend was seen with ACR355 at 50 mg fill weight and SUR355 at both 50 mg and 400 mg fill weights. These trends could not be readily linked to any powder properties. As in section 3.4.1.4, it is recommended that the method for collection is standardised. From an industrial point of view however, the results have shown that the FC Powder Filler can pick-up all the selected materials with a very short actuation time. This outcome is crucial to the future use of this technology because it confirms that a

filling gun could potentially operate at high speeds to delivery many powder doses per minute.

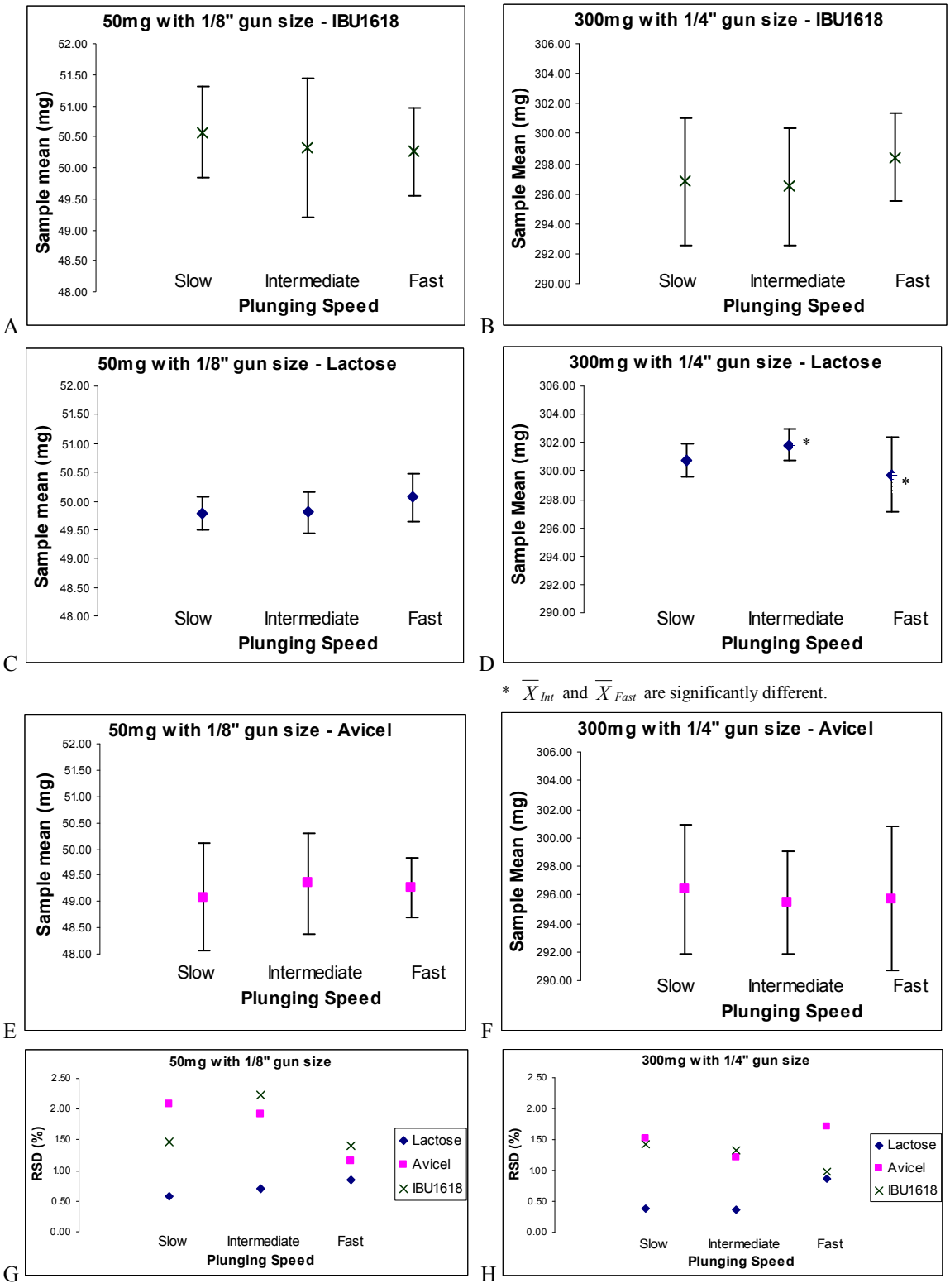

Figure 33 - Figure showing the change in sample mean with increasing collection speed for IBU1618, lactose and Avicel at fill weights of 50 mg and 300 mg. Also, figures G & H show the change in RSD with collection speed for the same materials at 50 mg and 300 mg fill weights.

3.4.3 Recommendations

In light of the results obtained the recommendation when using the FC Powder Filling Machine is to use a constant dosing speed for all dosing purposes. When using manually (i.e. by hand) it is not recommended that a "fast" collection speed is used because it is very difficult to carry out the process in a repeatable manner. For manual operation, care must be taken to ensure that the gun is inserted to the same depth for each dose. It is not yet known how the fill weight uniformity is affected by collecting from different powder bed depths (e.g. 2 cm, 4 cm, 8 cm) and this could be the subject of further investigation. Finally, it has been demonstrated with all the materials that a fast collection speed can be used to collect powder and deliver doses accurately and with a precision of lower than ± 2 %. It is therefore recommended that robotic motion is utilised to automate the dosing process to take the two-stage dosing investigation to the pilot scale.

3.5 Conclusions

The FC Powder Filling Machine has been shown to be capable of delivering accurate 50 mg and 400 mg doses of model drug particles (sizes between 100 μm-500 μm) with high precision (RSD <2 %). The strength of vacuum used to collect the powder was seen to affect the dose weight for certain materials more than others and the magnitude of this effect was shown to be linked to the Carr's Index. The speed of powder collection was also investigated; it is recommended that the method for powder collection be standardised. The dosing equipment was shown to be capable of collecting doses rapidly (< ½ second), hence being suitable for a potential, future automated process.

4 THE CONTROL OF SURFACE CHARACTERISTICS

4.1 Introduction

In this chapter, a discrete scientific topic is investigated, but it is based on the same pharmaceutical dosage form described in section 1.1. In the manufacture of a proprietary fast dissolving dosage form (FDDF), the formulation may consist of a biopolymer such as gelatine and a saccharide such as mannitol in an aqueous solution. The formulation is then dosed into preformed blisters and subsequently frozen in a cryogenic tunnel before being freeze-dried. Under certain process conditions and with certain formulations, imperfections (also called nodules) may occur on the surface of the freeze-dried units. In this chapter, the occurrence of nodules is investigated by studying the cause and effect of various freezing conditions and formulations.

The aims for this chapter are:

- To create freeze-dried tablets in the university using laboratory freezing methods (shelf freezing and blast freezing).
- Create extreme freezing conditions and formulations in the university laboratory to create experimental nodules.
- Compare the freezing rates achieved in the laboratory with typical freezing rates from an industrial manufacturing process.
- Create extreme freezing conditions and formulations in a cryogenic freezing tunnel to create experimental nodules.
- To develop an overall understanding of the effect of formulation and freezing conditions on the occurrence on nodules.

4.1.1 Gelatine

Gelatine is produced by the partial hydrolysis of collagen extracted from bones, connective tissues and organs of animals such as cattle and fish. It is commonly used in food, pharmaceutical, photography and cosmetics manufacturing (Bailey *et al*, 1989).

The benefits of gelatine are that it provides strength and structure in a product and can be used as a stabiliser, a thickener or a texturiser. The most common pharmaceutical application is the formation of gelatine capsules for oral drug administration.

Gelatine is a protein made up of approximately 14% hydroxyproline, 16% praline and 26% glycine (Figure 34). The protein is made up of peptide triplets, glycine-X-Y, where X and Y can be any one of the amino acids but proline has a preference for the X position and hydroxyproline the Y position (Bailey *et al*, 1989).

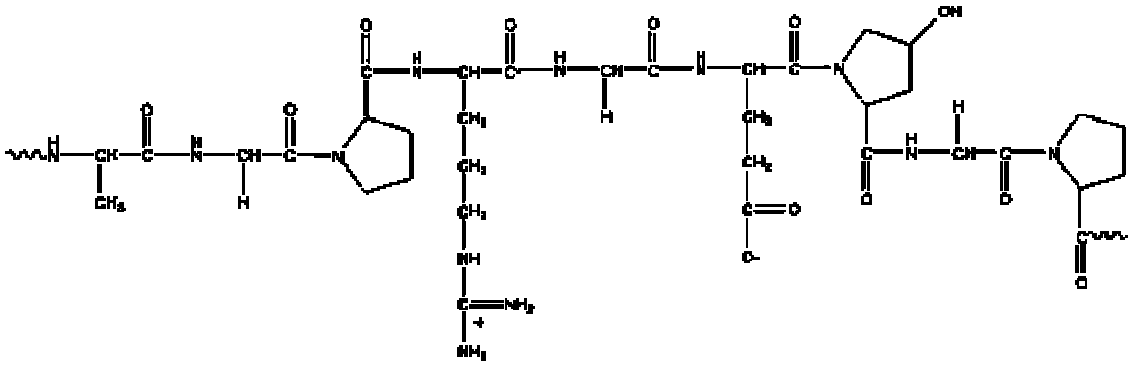

Figure 34 – Gelatine has a large percentages of glycine, proline and hydroxyproline. A typical structural unit of gelatine may consist of -Ala-Gly-Pro-Arg-Gly-Glu-4Hyp-Gly-Pro-. Source: Chaplin *et al*, 2009.

There are two main types of gelatine, type A and type B. Type A gelatine is derived from collagen with exclusively acid pre-treatment whereas type B is the result of an alkaline pre-treatment of the collagen (Cole *et al*, 1999). The acid process is mainly used with pig skin and fish skin whereas the alkali process is used commonly on bovine hide and sources where the animals are relatively old at slaughter (Cole *et al*, 1999).

An important property of gelatine is its thermally reversible gelling property with water. The stability of a gelatine solution depends on temperature and pH. The strength of a gel increases with low temperature and the optimal pH for strength is in the range of 5 to 7. In the manufacture of confectionaries, gelatine is usually combined with sugar and glucose syrups. It is compatible with such substances as well as polyhydric alcohols (e.g. glycerol or mannitol). In general, the lower the mean molecular weight (MW) of gelatine, the lower the gel strength and viscosity is of its solution (Francis *et al*, 1999).

If a gelled jelly is frozen, the product will be affected by syneresis (expulsion of liquid from the gel) and after thawing, the clear jelly will disintegrate with the loss of water (Cole *et al*, 1999). However, if water containing a small amount of gelatine (e.g. 0.5%) is frozen, the water will freeze into many tiny discrete crystals, instead of forming a single solid block of ice. This effect is desirable in confectionaries such as ice-cream to obtain a smooth product with small crystals and can also be highly beneficial for the same reason in the formation of fast-dissolving pharmaceutical tablets.

Around 50 % of gelatine produced worldwide is sourced from cattle. Another common source is pigskin (46 %, GME, 2008). However, with both types of mammalian gelatines, concerns exist (e.g. religious, vegetarianism, and health issues such as BSE) in certain markets with regard to their usage (Asher *et al*, 1999 and Schrieber *et al*, 2007).

A substitute to mammalian gelatine is gelatine produced from collagenous fish (Gilsenan *et al*, 1999; Nagai *et al*, 2000 and Wasswa *et al*, 2007). One advantage of fish gelatine is that it is not associated with BSE. Furthermore, it is acceptable for religions such as Islam, Judaism, and Hinduism. A great deal of work has been carried out on the extraction of gelatine from various varieties of fish (Karim *et al*, 2009).

A major difference between fish and mammalian gelatine is that fish gelatines have lower concentrations of proline and hydroxyproline. This also varies between cold water and warm water fish. The proline and hydroxyproline contents are approximately 30% in mammalian gelatines compared to 22-25% for warm-water fish and 17% for cold-water fish gelatine (Muyonga *et al*, 2004). The result is that fish gelatines have lower gelling and melting temperatures. There is also a structural difference between the two types of gelatines. Mammalian gelatines have greater molecular weights and a greater amount of cross linking between protein chains that result in greater gel strength. Typical gelling and melting points range from 20-25°C and 28-31°C respectively, whereas for fish gelatines, these are 8-25°C and 11-28°C respectively (Karim *et al*, 2009). Studies carried out to compare the rheological properties of fish and mammalian gelatines (Gilsenan *et al*, 2000) showed that samples from cold-water fish had a lower melting point than mammalian gelatine whereas samples from warm-water fish had properties quite similar to mammalian samples.

4.1.2 Mannitol

Mannitol is a sugar alcohol, known as a polyol, and is widely used in the food and pharmaceutical industries because of its unique functional properties. It is a sweet tasting substance and is often used as a substitute for sucrose in "sugar-free" foods and confectionaries such as chewing-gum. The chemical structure of mannitol is shown in Figure 35.

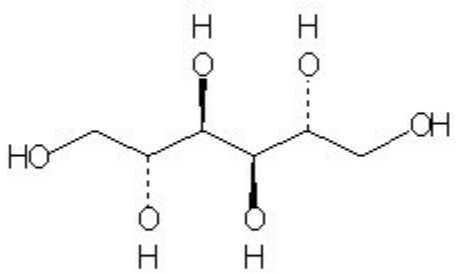

Figure 35 – Chemical structure of mannitol. Source: merck-chemicals.com

One of the functional advantages of mannitol is that it does not pick up moisture from the atmosphere (non-hygroscopic) which makes it very useful for foods and pharmaceuticals. It has a high melting point (165-169°C), is very stable and has a pleasant taste. It is also readily soluble in water, a process which is endothermic; the benefit of this is that it provides a cooling sensation when mannitol dissolves in the mouth.

Mannitol generally occurs as a crystalline excipient but it can exist in at least three polymorphic forms. A number of studies have shown that three types of polymorphs exist (α, β and δ) (Walter-Levy *et al*, 1968 and Jones *et al*, 1970). It is known that conversion from one polymorphic form of an excipient to another can be caused by heat, friction or other processing procedures (Yu *et al*, 1998). However, the forms of mannitol are quite stable and do not easily change under mechanical stresses.

Mannitol is also known to be a cryoprotectant i.e. it can be used to prevent damage to biological tissues caused by freezing by inhibiting the formation of large ice crystals. It also tends to crystallise readily during freezing and freeze drying (Cavatur *et al*, 2002).

4.1.3 Freezing

Freezing is caused by the removal of heat from water which results in a phase change from liquid to solid. The freezing rate is the rate at which heat is removed to cause the

phase change. The rate of heat removal is governed by the heat transfer coefficient between an object and the cooling medium and it may be affected by the intrinsic properties of the object or the type of freezing system used. As well as heat removal, nucleation (formation) of ice crystals and crystal growth are also required for freezing. These depend on the composition and physical state of the material (Erickson *et al*, 1997).

As the temperature of a material is lowered, the mobility of particles is reduced. For the solid phase to occur, small solid particles must first form (nucleation). Nucleation can occur spontaneously in super-cooled pure water at -40°C, however in most aqueous systems, very minute amounts of impurities exist which act as a catalysts for the onset of nucleation. As the heat continues to be removed, the crystals grow from the nucleation points until all the liquid is in the solid phase. The size of the ice crystals is largely dependent on the cooling rate. A slow cooling rate promotes larger crystals whereas a fast cooling rate promotes the formation of many small crystals (Russell *et al*, 1999; Cogné *et al*, 2003; Drewett *et al*, 2007). However, when freezing a gelatine solution, the cooling rate alone does not determine the crystal size. The presence of protein chains in the solution provides boundaries which cause the water to freeze into many small discrete crystals instead of large blocks of ice. This effect is desirable in confectionaries such as ice-cream to obtain a smooth product. It is also beneficial for the same reason in fast-dissolving pharmaceutical tablets.

As mentioned, the freezing process is greatly influenced by the rate of heat removal and the characteristics of the sample. In practice, this means the differences between types of freezers and products. Heat transfer rates are dependent on the heat transfer coefficient between the product and the cooling medium. This in turn is dependent on the contact between the product and the cooling medium and the ability of the cooling medium to carry away heat. Three types of cooling medium are often encountered. Firstly, a boiling cryogen on the surface of a product; the cryogen (e.g. liquid nitrogen) will have the combination of a low temperature as well as a high heat capacity since the nitrogen will be vaporising and thus absorbing a latent heat of vaporisation. The second type of cooling is that supplied by a cooled solid object such as a pipe or a shelf which in turn is cooled by some other mechanism (e.g. the circulation of a cooling liquid). The heat transfer in this type of system would occur through conduction and would be highly dependent on a good contact between the product and the cooled object. The third type of

cooling medium is a cooled gas, such as air which removes heat by convection. Gases generally have a lower volumetric heat capacity, and so heat can be removed rapidly only when large volumes of the gas come into contact with the surface of the product.

4.1.3.1 The effects of freezing parameters on ice crystal size

As mentioned earlier, the size of crystals formed during freezing is affected by the rate of cooling and hence rate of freezing. In the freezing of foods, the size and distribution of ice crystals influences the final texture. Low freezing rates give rise to large ice crystal sizes and fast freezing rates generally give smaller crystal sizes.

Most investigations of freezing rate distribution within the bulk of aqueous material have shown that the fastest freezing occurs at the outermost and in the central region of the sample with the slowest freezing occurring in the intermediate regions. Persidsky *et al* (1975) challenged this idea by presenting detailed experimental evidence on the distribution of the ice phase across gelatine gels. The results of the study indicated that the rate of freezing in the central region of a specimen varies, but is most frequently, the lowest of all and is dependent on the gel concentration, freezing temperature and the specimen size. Furthermore, the freezing curves for gelatine gels showed that the freezing plateau formed an increasingly saddle-shaped form as the concentration of gelatine increased from sample to sample. The explanation suggested for this was that super-cooling within the gelatine samples can persist long after the onset of freezing. In order to explain how the interior of a sample can remain in the super-cooled state while being surrounded by a converging ice front, a graphical representation for the temperature changes within the specimen is presented.

The drying kinetics and quality of the dried units is also critically dependent on the ice crystal size distribution, since it influences the nature of the pores left behind by the subliming crystals (Mellor *et al*, 1978). Even though it is widely recognised that the ice crystal size distribution generated during freezing is dependent on freezing rates, there are relatively few studies that have focused quantitatively on their interrelationship. An investigation was carried out into the relationship between freezing rate and mean ice crystal size for coffee extracts (Pardo *et al*, 2002). The method was to determine experimentally the parameters characterising freezing kinetics, such as the rate of fall of temperature and the velocity of the ice front. These were compared with predictions from

Neumann's model (Özilgen *et al*, 1998) for unidirectional freezing and were found to be in agreement. Woinet *et al* (1998, Part I and II) also used Neumann's model to study temperature profiles during freezing and used this to establish the link between freezing kinetics and ice crystal size for low concentration gelatine solutions (1%). In this study, gelatine gels were frozen through contact with a cooled copper plate. It was suggested that crystallisation occurred in three stages: during the first stage very few nuclei appeared suddenly on the surface of the copper plate. During the second stage, surface crystallisation from these nuclei developed rapidly all over the copper plate area and in the third stage, a plane freezing front, parallel to the copper plate surface, migrated into the sample away from the plate. Figure 36 shows a schematic view of the frozen zone. The ice crystals were characterised by first freeze drying the sample, then slicing parallel to the copper plate. A stereomicroscope was used to image the slices and pores were measured using image analysis software. It was found that ice crystal size increased proportionally with the distance from the cooling plate.

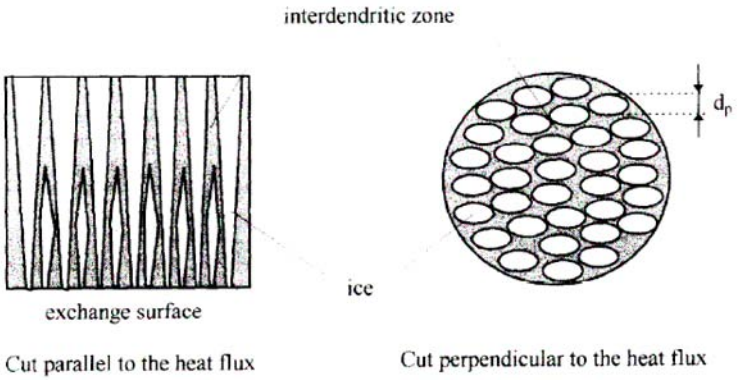

Figure 36 – Schematic structure of a model gel in the frozen state (Woinet *et al* 1998)

A similar study was carried out by Chavalier *et al* (2000a) where cylindrical gelatine gels were frozen with different operating conditions. A method to calculate a local freezing rate was proposed to take into account the variation of freezing rate as a function of the radius. The local freezing rate was related linearly to the radius for all the freezing processes observed. The freezing of the gels also showed a decrease in ice crystal size with an increase in distance to the cooling medium i.e. the mean crystal size was related to its radial position. The freezing at atmospheric pressure was then compared to the pressure-shift freezing of gelatine (Chevalier *et al*, 2000b). For pressure-shift freezing, the size of ice crystals appeared to be more homogeneous in the whole samples and the

mean crystal size had decreased with increased pressure level. This observation was supported by similar work of Zhu *et al* (2005).

4.1.4 Freeze drying fundamentals

Freeze-drying works by first freezing a material and then reducing the surrounding pressure to create a partial vacuum. Heat is then added which causes the frozen water in the material to sublime i.e. evaporate directly from the solid to the vapour phase without entering the liquid phase. Figure 37 shows the boundaries between the various phases in a typical phase diagram and the conditions that must be met to achieve sublimation.

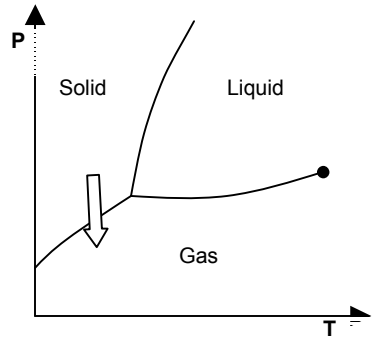

Figure 37 – A typical phase diagram showing the boundaries between solid, liquid and gas. If the conditions of low pressure and temperature are met, then sublimation can occur (indicated by the block arrow).

The most critical phase in the freeze-drying process is the freezing phase. When sublimation occurs during the drying phase, the ice crystals vaporise, leaving behind empty pores of the same volume as the original crystals. Hence, if the freezing creates large crystals, the resulting pores will be large and similarly for small crystals. Therefore, the final microstructure of a product is determined by the initial freezing. The freezing can be carried out using a variety of methods; however typical industrial freeze dryers use the method of shelf freezing, where a product is loaded onto shelves which provide the cooling. Other methods include blast freezing, which is a rapid method of freezing using circulation of chilled air, and cryogenic freezing which uses a cryogen (usually liquid nitrogen) to remove heat.

The drying phase is usually separated into primary drying, and secondary drying. In primary drying, the pressure is lowered typically to a few millibars and the temperature is raised to around 0°C to provide the heat to cause sublimation. In this phase, approximately 95% of the water content is vaporised. The time taken for primary drying

depends on the material type and size and can range from a few hours to several days. The vapour that is removed is usually collected using a condenser, usually a plate or coil, which provides a cold surface for the water vapour to re-solidify on. The secondary drying phase aims to remove unfrozen water molecules that were not removed in primary drying. The temperature in this phase is raised higher than in the primary phase (e.g. to 10°C) and the pressure may also be reduced to break any remaining bonds between water molecules and the frozen material. After secondary drying is complete, the vacuum is broken and the material will be held in an inert atmosphere (e.g. nitrogen) before being sealed.

4.2 Materials & methods

The overall aim for the project is to develop an understanding of the cause of nodules on the surface of a fast-dissolving dosage form and to propose recommendations to minimise their occurrence. The experimental work is thus broken down into the following stages:

1. Create freeze-dried tablets in the Birmingham University laboratory (BH units) using shelf freezing and blast freezing.

    - Characterise BH units and compare them against an industrially manufactured FDDF using DVS, optical microscopy, dispersion tests and X-Ray Micro-CT.
    - Compare nodular material scraped from the surface of an industrially produced FDDF with the bulk material from the same tablet using DVS and microscopy to identify any differences and define a nodule.

2. Create extreme freezing conditions and formulations in the university laboratory to create experimental nodules.

3. Compare the freezing rates achieved in the university laboratory to those achieved in a pilot scale cryogenic tunnel at the site of the sponsoring company.

4. Create experimental nodules using a pilot scale cryogenic tunnel. The following variables will be investigated:

    - The effect of changing the formulation (concentration of major components).
    - The effect of changing the temperature set-point of the tunnel.
    - The effect of temperature fluctuations as product travels through the cryogenic tunnel.

4.2.1 Manufacture of freeze-dried tablets in the laboratory

A Virtis, Advantage+ bench top freeze dryer (Figure 38) was used to create freeze-dried units. The freeze dryer contained a shelf which acted as the medium used to either cool or heat the product placed on the shelf.

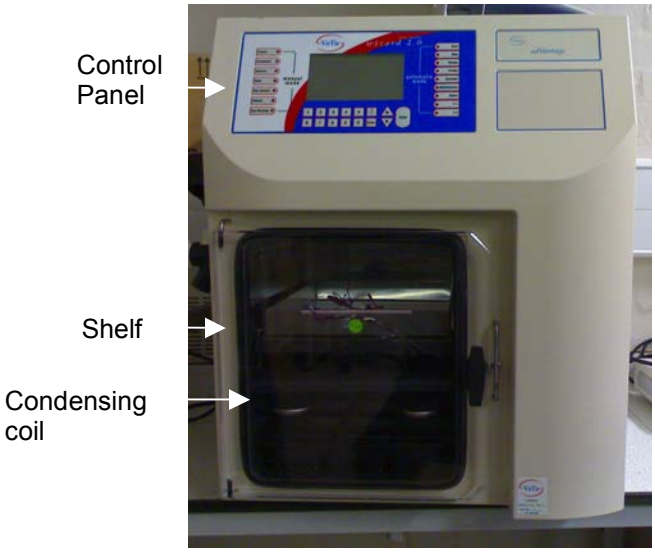

Figure 38 – The Advantage+ bench top freeze dryer, Virtis, UK.

A blast freezer (HC 51.20, Irinox, Italy, Figure 39) was also utilised for rapid freezing prior to transfer into the Advantage freeze dryer for the drying phase. The freezer contained a single chamber with a shelf and was capable of reaching -18°C in automatic mode or temperatures as low as -40°C by using the manual mode to over-ride the thermostatic control.

Figure 39 – Blast freezer used for rapid laboratory freezing (Irinox, Italy)

The formulation consisted of fish gelatine and mannitol with concentrations of 6 % and 5 % respectively. The components were dissolved in water and held at 60°C for 15 minutes before being allowed to cool to room temperature. Two trays with 250 mg blisters were dosed using pipette; one tray was placed into the Virtis freeze dryer with the shelf pre-cooled to -70°C. The second tray was placed in the blast freezer which was pre-cooled to -32°C. After freezing, both trays were then dried in the Virtis dryer. Units

were dried for 6 hours in the freeze dryer with a pressure of 0.5 mbar (370 mTorr) and a temperature of 0°C followed by 15 minutes at 10°C. The trays were finally held at 25°C and 2000 mTorr pressure while waiting unloading.

Both types of freeze-dried unit were compared against each other and against units created in cryogenic tunnel using optical microscopy, X-Ray CT, DVS and dispersion tests.

4.2.2 Optical microscopy

Whole units were placed onto a slide to study the surface using the x4 and x10 magnification lenses. To see the internal structure, units were broken as opposed to being cut with a blade to avoid damaging the fragile internal structure.

4.2.3 X-ray CT micro tomography

A Skyscan 1072 device (Skyscan, Aartselaar, Belgium, Figure 40) was used with a 50 kV, 98 mA x-ray source. It was operated in cone and spiral mode with a 0.90° step random rotation of the sample between scans and 180° total sample rotation. Corrections were made for imperfections in the detector output and for any beam-hardening effects. The raw images were reconstructed using the Skyscan software to create a series of horizontal and vertical cross sectional, binary images (Hancock *et al*, 2005; Appoloni *et al*, 2002). A minimum of three x-ray scans were carried out on independent tablets of each type.

Figure 40 – The Skyscan 1072 x-ray tomography machine.

4.2.4 Dynamic Vapour Sorption (DVS)

A DVS Advantage (SMS Instruments, UK) was used to measure the vapour sorption isotherms of each type of tablet. The sequence for the measurements involved a drying period of four hours with the relative humidity (RH) at 0%. The humidity was then increased in steps of 10% up to 60% before returning to 0%, again in steps of 10%. The sorption isotherms were calculated and plotted as percentage change in mass versus target partial pressure. The scans were carried out for three types of sample; a standard industrially produced FDDF (placebo), nodules scraped from the surface of a similar FDDF and BH units created using shelf freezing. Three scans were carried out for each sample type. In addition, a tablet with a different formulation ("sample C") was also scanned in the DVS to determine whether the DVS instrument was capable of distinguishing between different formulations. The formulation for sample C consisted of 1% fish gelatine and 3% mannitol.

4.2.5 Dispersion tests

Dispersion tests were carried out to compare the dissolution rates of the following three types of sample:

- An industrially produced FDDF.
- An industrially produced FDDF with large nodules.
- BH units.

The tests were carried out in a 1000ml glass beaker containing 600ml water held at 37°C (±0.5°C) in a water bath. The time taken for the unit to fully disperse after being dropped onto the water surface was observed. An assessment of the level of dispersion was carried out visually. Each type of unit was repeated a minimum of 6 times.

4.2.6 Measuring the temperature change achieved for various freezing methods

4.2.6.1 Cryogenic freezing tunnel

An 800 mg fill weight blister was prepared with two thermocouples, one placed inside the blister, and one suspended a few millimetres above the surface of the tablet. The blister was dosed with a control formulation (6 % gelatine, 5 % mannitol) and then placed inside

the cryogenic tunnel. The temperature was -70°C and the residence time was 3 minutes and 15 second. The temperature was recorded automatically using a Pico data-logger.

4.2.6.2 Blast freezer

To measure the temperature change of a tablet in the blast freezer, a blister was prepared in the same way as above and the freezer was pre-cooled to -32°C. The blister was filled with the control formulation and subsequently frozen. The temperatures were recorded every 20 seconds.

4.2.6.3 Virtis Advantage freezer

An 800 mg fill weight blister was prepared with two thermocouples, one touching the base of the blister and one suspended in the centre of the unit (Figure 41). The blister was filled with the control formulation and placed onto the Virtis freezer shelf which was pre-cooled to -70°C. The temperatures were recorded every 20 seconds.

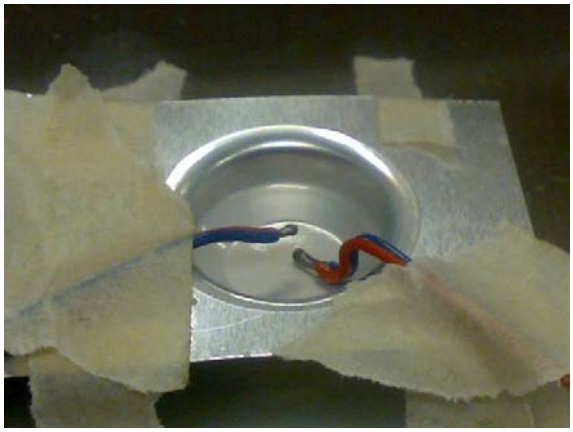

Figure 41 – The preparation of a blister with thermocouples prior to temperature measurement.

4.2.7 Mapping of the cryogenic tunnel with temperature probes

The pilot scale studies were carried out using a cryogenic tunnel provided by the sponsoring company. The tunnel was equipped with a conveyor belt to pass product through and a series of fans to promote efficient heat transfer. Liquid nitrogen was sprayed into the tunnel through a spray bar located close to the tunnel exit. The tunnel temperature was monitored and controlled via a temperature probe. Prior to usage, the tunnel was mapped with several temporary type-T thermocouples to measure the temperature profiles during the experiments (Figure 42).

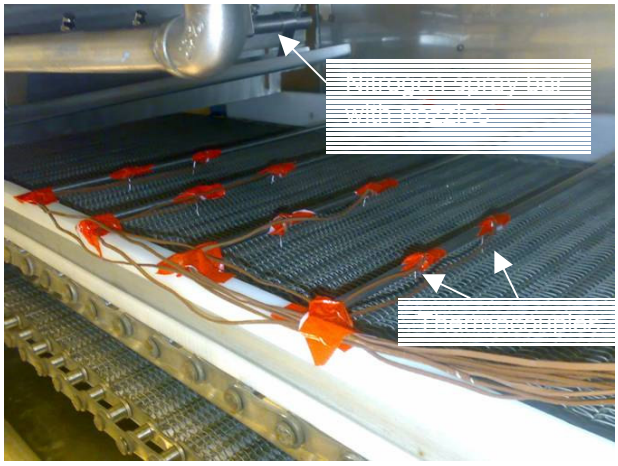

Figure 42 – A photograph showing the thermocouples in one section of the cryogenic tunnel and the nitrogen spray bar in the background.

4.2.8 Creation of tablets with experimental formulations

Four formulations were used in these experiments with varying amounts of fish gelatine and mannitol (Table 12).

Table 12 – Table showing the formulations used for pilot scale investigations to create experimental nodules.

Formulation	Fish gelatine	Mannitol	Formulation purpose
A	6%	5%	Control
B	4%	1%	Effect of very low mannitol content
C	1%	3%	Effect of very low gelatine content
D	4%	6%	Effect of very high mannitol content

By using different formulations, it was expected that one formulation would give rise to more nodules than the others. Formulations B and C were chosen to investigate the effect of low mannitol and gelatine content. Formulation D was chosen to investigate the effect of a very high level of mannitol compared to gelatine.

Large, 800 mg fill weight blisters were used because of the larger surface area compared to smaller blisters and hence an increased likelihood of seeing nodules.

The trays were cut into three sections. Each row in the small tray was then dosed with one of the four formulations A-D. The trays were placed into the freezing tunnel with the orientation as shown in Figure 43. Many trays (at least 30) were frozen with the tunnel

operating under steady conditions with a temperature set-point of -70°C and a residence time of 3 minutes and 15 seconds. The procedure was later repeated with a set-point of -90°C.

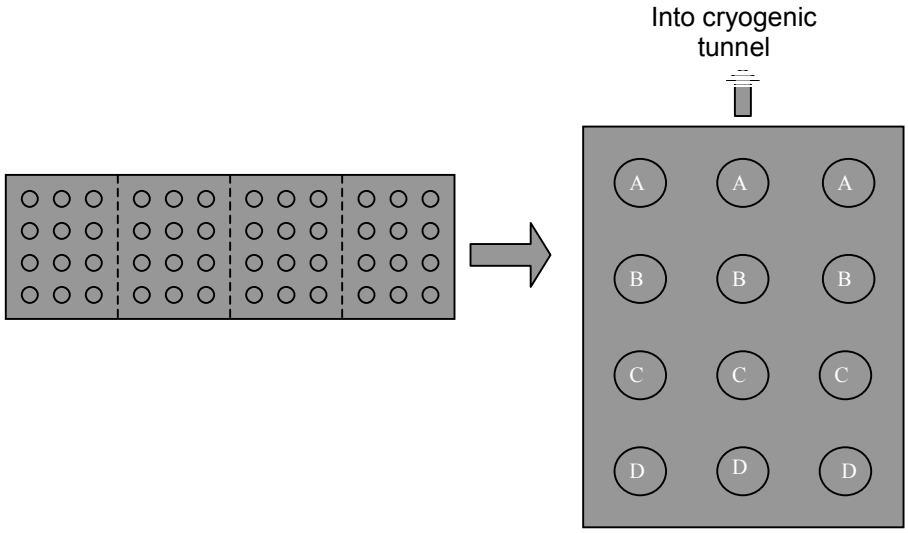

Figure 43 – Diagram showing the dosing method for each tray and orientation when placed into the cryogenic freezing tunnel

The frozen trays were held in an intermediate freezer before being dried at the end of the day with a 0.5 mbar pressure and at 0°C for 6 hours. Dried units were analysed visually and categorised according to the descriptions in Table 13. The numbers of tablets in each category were presented in a bar chart.

Table 13 – Nodule categorisation criteria.

Nodule category	Description
1	No nodules
2	One or two small nodules less than 1 mm diameter each
3	Three or more small nodules. Total affected area less than 3x3 mm.
4	One or more large nodules greater than 1 mm diameter each. Total affected area less than 3x3 mm.
5	Total affected area greater than 3x3 mm.

4.2.9 Investigating the effect of temperature fluctuation in the cryogenic tunnel

In the above experiments, the temperature of the freezing tunnel was maintained relatively constant using automated feedback control. The purpose of this investigation was to intermittently disrupt the flow of liquid nitrogen into the tunnel in order to create a random and fluctuating temperature profile. This was carried out by first allowing the tunnel to reach a steady operating temperature of -70°C. The cryogen supply was then turned off and a tray of product was placed into the tunnel. A short time later (between 30-90 seconds) the nitrogen supply was turned back on to decrease the temperature very rapidly. This made it possible to create large temperature fluctuations and hence, very inconsistent freezing rates. The frozen trays were dried as described in section 4.2.8, categorised according to Table 13 and the results were presented in a bar chart.

4.3 Results & Discussions

4.3.1 Optical Microscopy

Figure 44 shows the macroscopic appearance of nodules on a freeze-dried unit. Figure 45 shows images of a unit produced using the freezing tunnel. Figure 46 is an image of a BH unit frozen using the shelf freezing method (Virtis). The oval shaped structures in both images are the voids that remained after the ice had sublimed from the surface. The appearance of the tablets is quite similar however the size of the voids are different; in Figure 45 (left), the average length of 20 randomly selected voids is 123 μm whereas in Figure 46, the average void length is 174 μm. This difference is likely to be as a result of a slower freezing rate experienced in the Virtis freezer which leads to a larger crystal size. Both types of tablets used the same concentrations of gelatine and mannitol and difference in colour is due to the natural variability that exists in fish gelatine batches.

Figure 47 shows a much more ordered pattern in the structure when blast freezing was employed. The star shapes present are a result of the faster freezing achieved with the high wind chill in the blast freezer. Crystals formed in the blast freezer are smaller (52 μm average length), higher in number and tend to form in an ordered array which appears as a star shape. Visually, BH units frozen in the Virtis freezer more closely match those created using the cryogenic tunnel.

Figure 44 – Image of nodules on a freeze-dried unit.

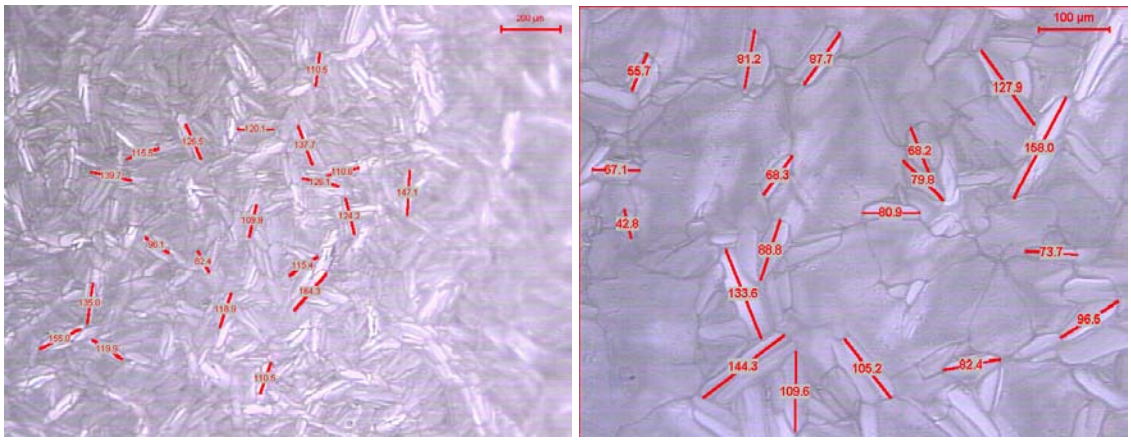

Figure 45 – Surface image of a cryogenically frozen unit. Left: x4 magnification; right: x10 magnification.

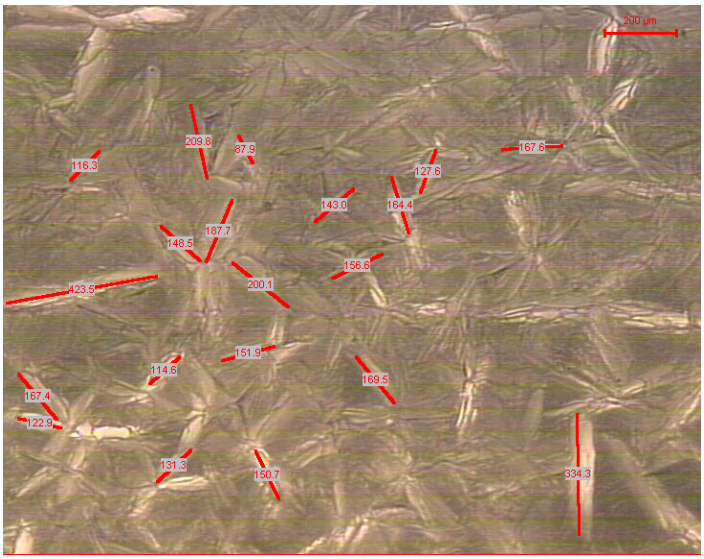

Figure 46 – Surface image of a BH unit frozen using the Virtis freezer (shelf freezing) (x4)

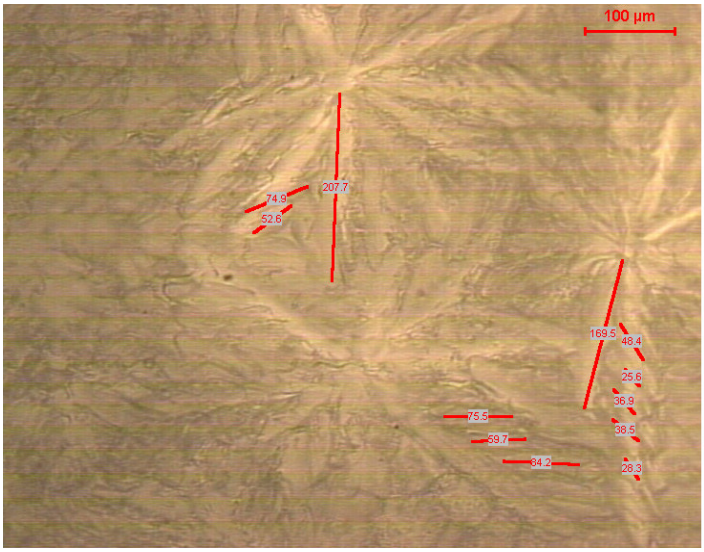

Figure 47 – Surface image of a BH unit frozen using blast freezer (convective) (x10).

Figure 48 and Figure 49 are both images of a cross section of a unit produced in the cryogenic tunnel. The flaky structure with long narrow voids where ice crystals once formed is characteristic of a typical unit frozen in this manner. The average size of the crystals in Figure 49 is 63 µm with a typical "flake" width of around 500 µm. In contrast, Figure 50 and Figure 51 show the cross section of a typical nodule. The voids are circular in shape and much smaller, with an average diameter of 22 µm. This suggests that the local freezing rate in a nodule is greater than the freezing rate in the remainder of the tablet because faster freezing leads to smaller crystal structure (Drewett *et al*, 2007; Cogné *et al*, 2003; Russell *et al*, 1999,).

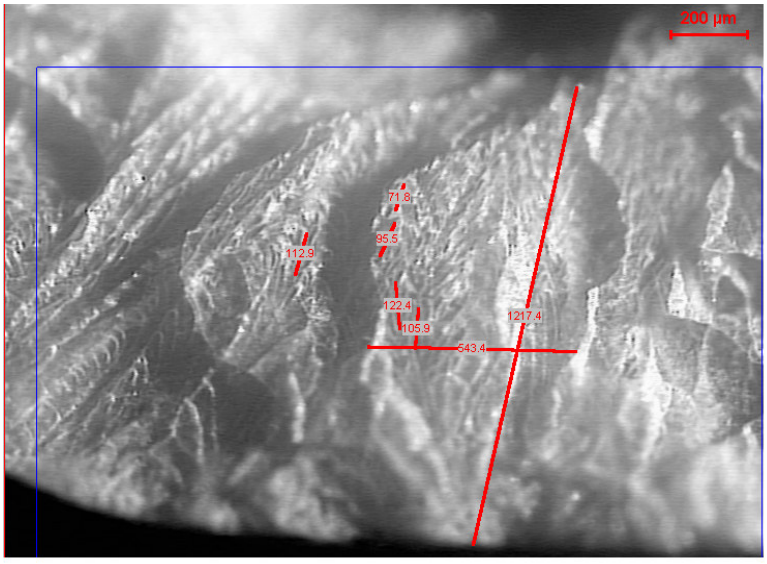

Figure 48 – Flaky structure with long, thin voids in a typical cryogenically frozen unit (x4).

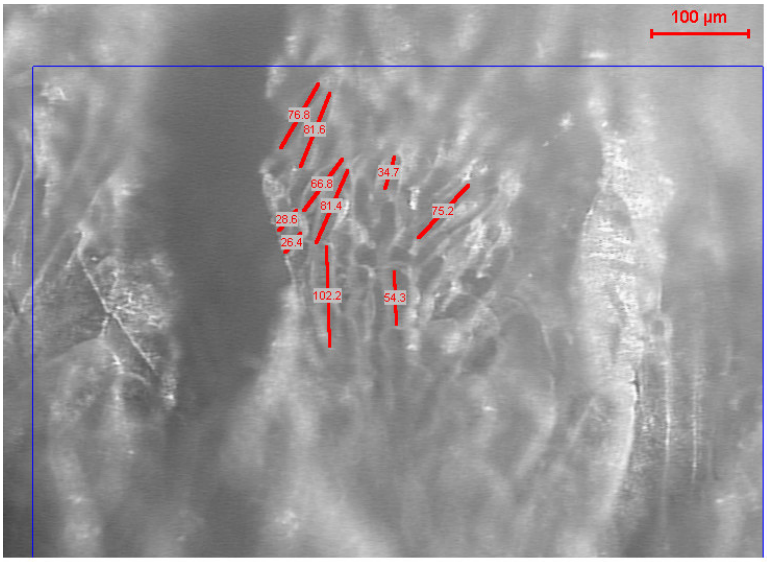

Figure 49 – Flaky structure with long, thin voids in a typical cryogenically frozen unit (x10).

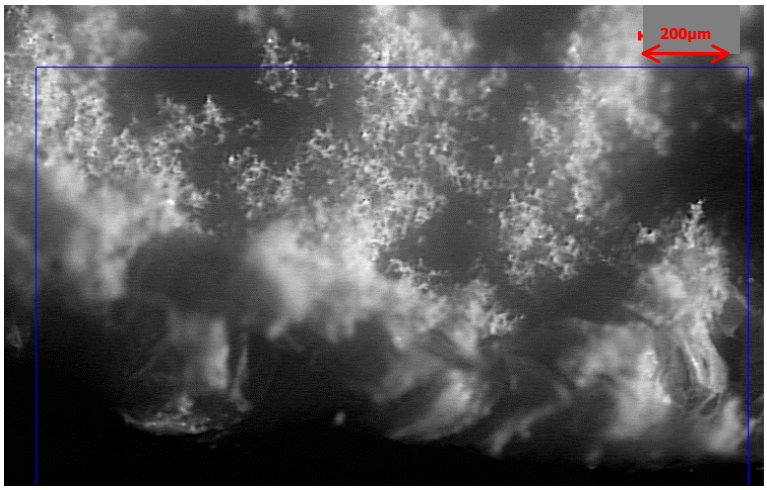

Figure 50 – Cross section of a nodule using reflected light microscopy (x4).

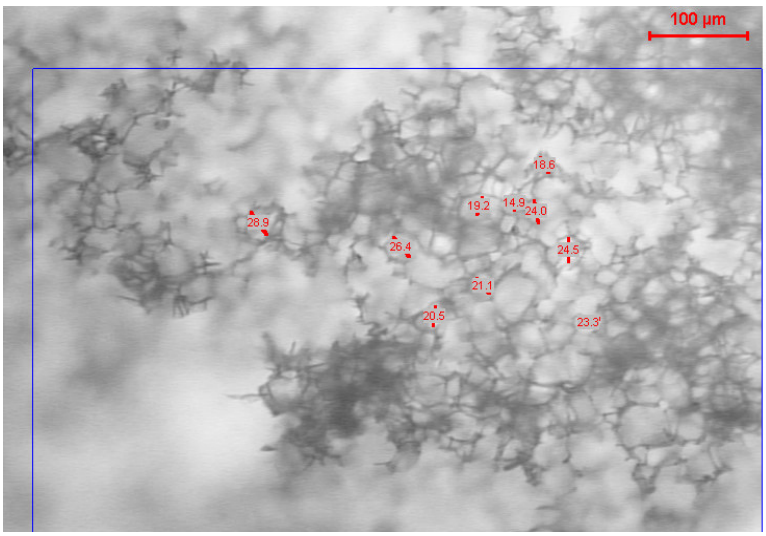

Figure 51 – Cross section of a nodule using optical microscopy (x10).

4.3.2 X-ray CT micro tomography

Figure 52 shows the cross section of a tablet created using the cryogenic freezing tunnel. The irregular-shaped structure seen on the surface is a nodule. The colour and texture of the nodule is clearly different to the remainder of the unit which consists of long rod-like voids (darker areas). The densest areas appear lighter coloured. The nodule is defined from the bulk of the tablet by a line separating the two regions, with two different structures on either side. Figure 53 shows a unit frozen in the Virtis using shelf freezing. It comprises smaller rod-like voids towards the base of the unit and on the surface and larger voids towards the centre. This is because rapid freezing creates small crystals on the outer regions and the central region freezes more slowly giving larger crystals (Chevalier *et al*, 2000a; Woinet *et al*, 1998; Part I and II). Figure 54 shows a unit frozen in the blast freezer. This tablet is generally lighter in colour which suggests it is denser than the other two tablets. It also has a very light coloured (i.e. very dense) surface layer. This is likely to be as a result of the very fast freezing encountered in the blast freezer which leads to smaller crystal size and a denser surface and internal structure. Of the two BH units, it seems that shelf freezing produces the closest structural resemblance to the unit produced in the cryogenic tunnel.

From the evidence in the three images, particularly with the size of the pores in each tablet, it appears that the largest crystals were formed in the cryogenic tunnel with the pore length up to 2 mm. The smallest crystals were formed in the blast freezer. It is therefore reasonable to suggest that the rate of freezing was the slowest in the cryogenic tunnel and the fastest in the blast freezer. Freezing rate will be considered later also in section 4.3.5.

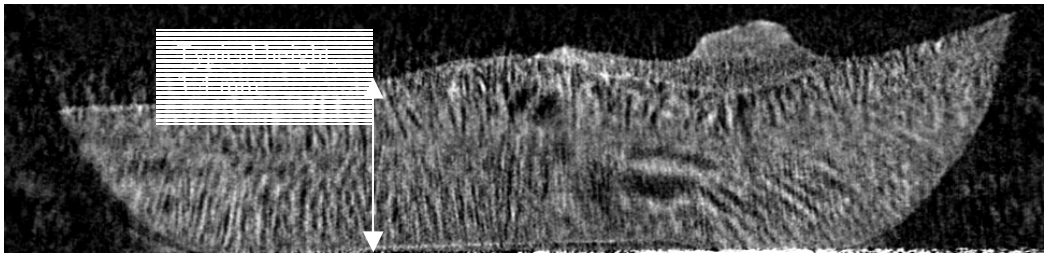

Figure 52 – X-Ray scan showing the cross-section of a unit frozen in the cryogenic tunnel with a nodule on the surface

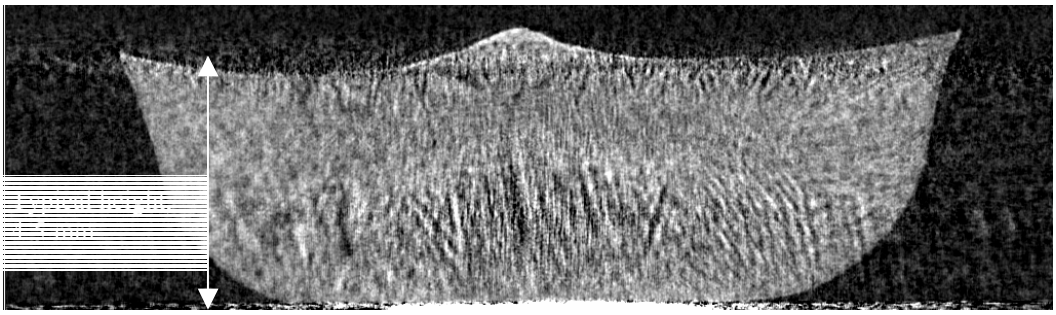

Figure 53 – X-Ray of the cross section of a unit made in Birmingham using shelf freezing (Virtis)

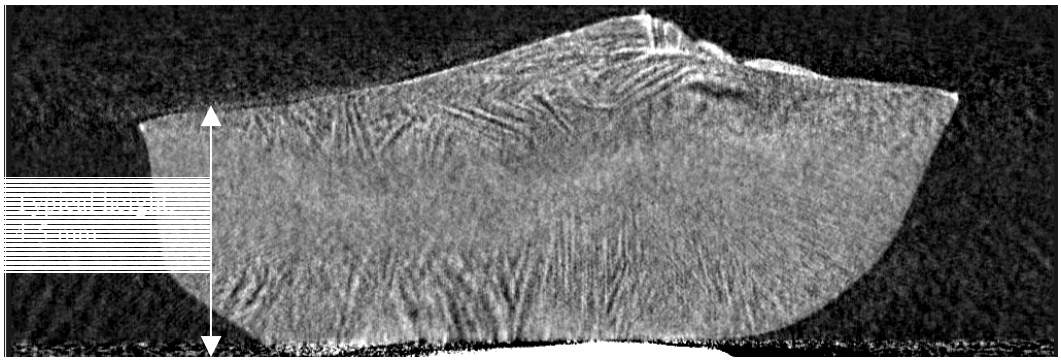

Figure 54 – X-Ray of the cross section of a unit made in Birmingham using a blast freezer

4.3.3 Dispersion tests

The dispersion test was carried out on a minimum of six tablets of each type. The observations (Table 14) show that BH units frozen in the Virtis freezer are the closest to cryogenically frozen units with respect to dissolution rate whereas the units frozen in the blast freezer took slightly longer to disperse. The dissolution of the skin for these tablets was similar to the dissolution of a nodule, with both materials taking several seconds to fully disperse.

Table 14 – Dissolution test observations

Unit Type	Observation
Cryogenically frozen, no nodules	Units dispersed fully within one second (~0.25 second)
Cryogenically frozen with large nodules	Bulk of the unit dispersed immediately. The nodule material often remained for 1-10 seconds
BH units frozen in the Virtis freezer	Immediate dispersion, not distinguishable from cryogenically frozen units
BH units frozen in the blast freezer	Dispersed approximately 0.5 second slower than cryogenically frozen units. The top skin surface occasionally remained for ~5 seconds

4.3.4 Differential vapour sorption (DVS)

Figure 55 shows the three repeats for BH tablets created using shelf freezing. The figure demonstrates the reproducibility of the results using DVS and also the reproducibility of the sample tablets. The reproducibility is the same for typical cryogenically frozen tablets and for nodular material scraped from the surface of such tablets. Figure 56 shows the isotherms for three samples, cryogenically frozen tablets, BH tablets and nodular material. The isotherms for the three samples are indistinguishable. Sample C was a freeze-dried tablet created in the Virtis freeze dryer. It consisted of 1 % fish gelatine and 3 % mannitol as opposed to the control formulation (6 %:5 %). The isotherm for sample C is shown on the same axes to demonstrate the ability of the DVS instrument to distinguish between formulations that are significantly different. The results show that the sorption of vapour is not dependent on internal structure, but is dependent on the composition of the sample. Moreover, it is dependent on the gelatine concentration because mannitol is known to be non-hygroscopic. The first three samples contain the same formulation and therefore the same sorption isotherms are seen. Sample C takes up less moisture than the other samples because it contained only 1 % gelatine.

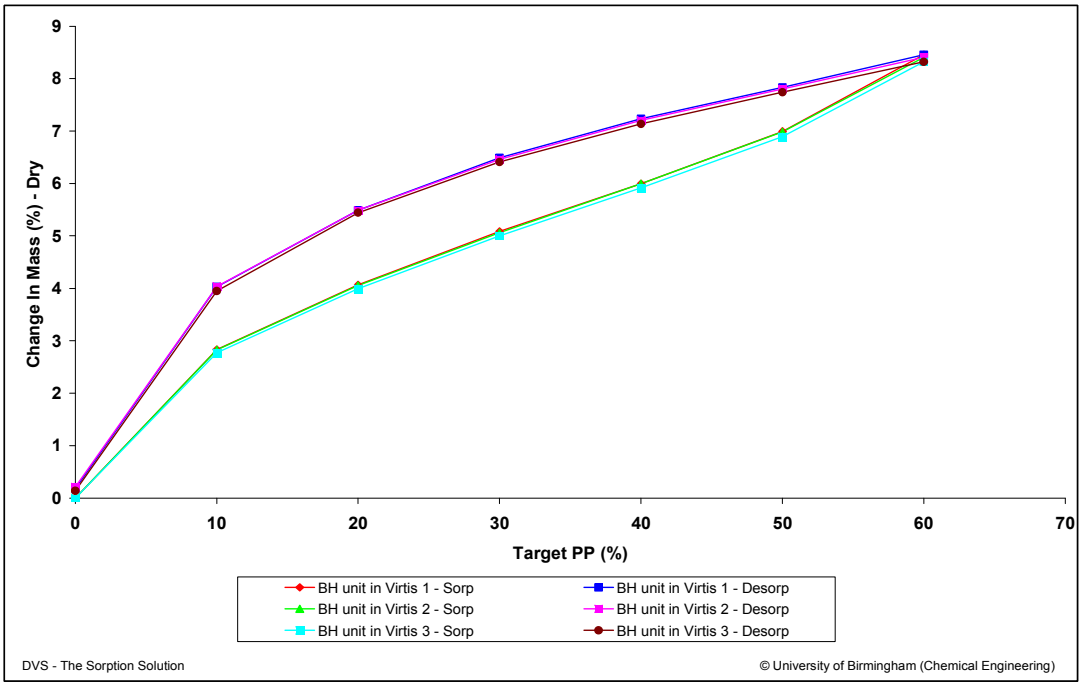

Figure 55 – DVS isotherm plots for three independent tablets created in the Virtis freeze dryer using shelf freezing. PP is the partial pressure of water vapour (synonymous with relative humidity).

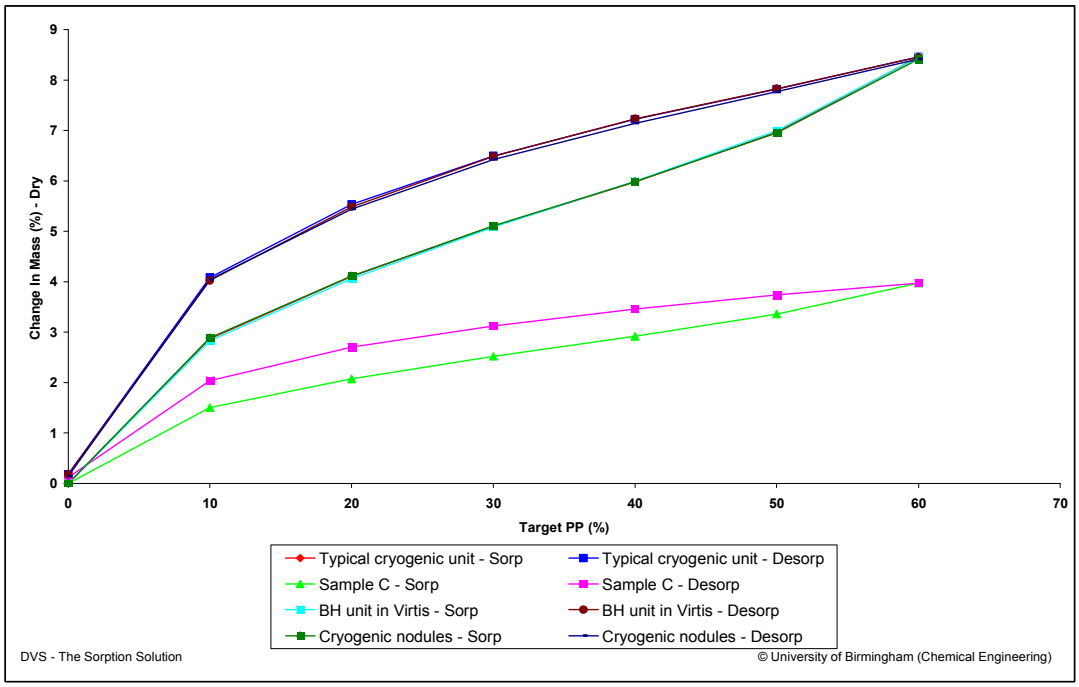

Figure 56 – DVS isotherm plots for a typical cryogenically frozen tablet, cryogenic nodules, a BH tablet created via shelf freezing and a tablet containing 1% gelatine, 3% mannitol.

4.3.5 Comparison of freezing rates achieved for various freezing methods

Each freezing trial was repeated at least three times. The average temperature data was calculated before plotting time versus temperature. Figure 57 shows the average

temperature data of a unit frozen in the Virtis freezer with the shelf pre-cooled to -70°C. The Virtis freezer uses conduction as the heat transfer method and depends on the contact of the blister pocket with the shelf. Therefore, the unit cools from the bottom upwards. Hence the slight differences in T1 and T2 in Figure 57 where the centre of the unit takes a few seconds longer to reach the same temperature as the bottom.

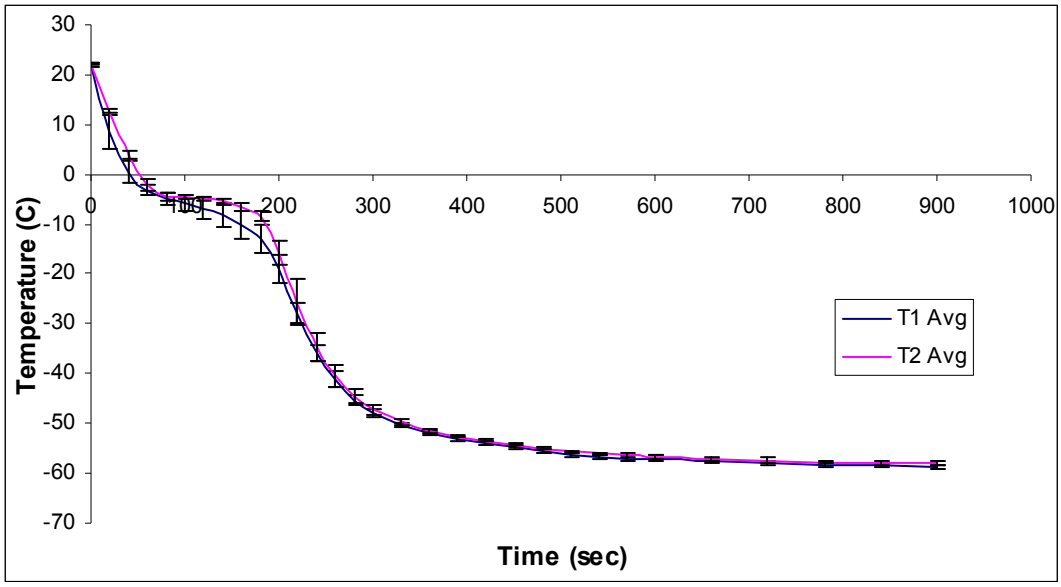

Figure 57 – Average temperature profiles for a unit frozen in the Virtis freezer at -70°C. T1: tablet base; T2: tablet centre.

Figure 58 shows the temperature profile in the centre of a tablet frozen in the blast freezer. The air temperature rose slightly at the beginning of the run when the freezer door was opened, but gradually returned to the lowest value. The unit begun to freeze at around 70 seconds and was completely frozen just after 150 seconds when it began to cool to the surrounding temperature. The temperature remained at zero through the freeze step because freezing is exothermic i.e. heat is released during freezing which maintains the temperature at 0°C.

The comparison of the two freezing methods is shown in Figure 59. The initial cooling of the units was very similar for both methods, with the Virtis being slightly faster. However, in the Virtis freezer the temperature of the unit dropped to below 0°C during freezing i.e. super-cooling occurred before nucleation occurred. Super-cooling did not appear to occur in the blast freezer. The reason for this may be that in the blast freezer, nucleation of ice crystals occurs much earlier than in the Virtis freezer. Consider a blast of chilled air at -30°C creating turbulent air flows on the surface of a blister filled with

liquid. Fast air currents create a considerable chill effect and are more efficient at heat transfer than stagnant air (Coulson *et al*, 1999). The air chill would likely result in ice nucleation on the surface of the liquid. It is quite possible that nucleation occurred on the surface even before the bulk of the liquid had reached 0°C thereby starting the exothermic stage of freezing. As a result, any further cooling would be counterbalanced with the heat released through ice crystal growth and the temperature would remain constant until the unit has completely frozen through.

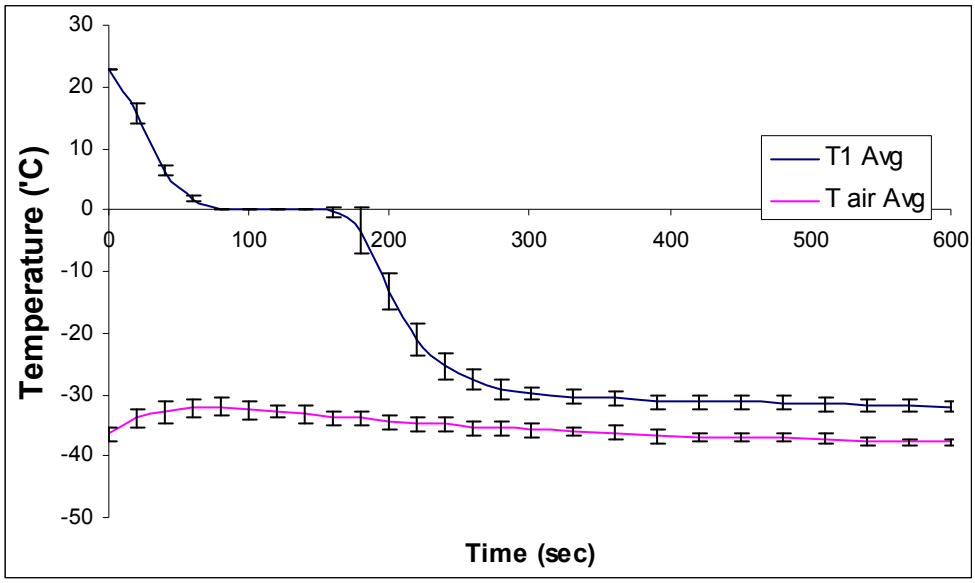

Figure 58 – Average temperature profile for a unit frozen in the blast freezer.

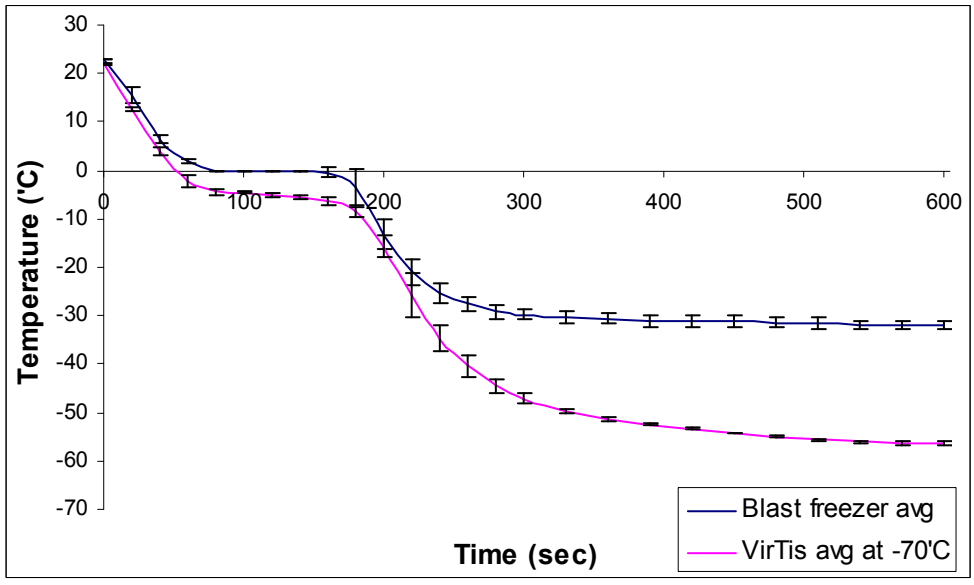

Figure 59 – Average temperature profiles for two units; one frozen in the Virtis and one frozen in the blast freezer.

Figure 60 shows the temperature profile of a typical unit as it freezes in the cryogenic tunnel. It shows that the air temperature along the tunnel varies from around 10°C, close to the tunnel entrance, to a low of around -80°C. Also the drop in air temperature is not steady. The product drops below 0°C after around 90 seconds when crystallisation begins. The freezing completes after approximately 150 seconds.

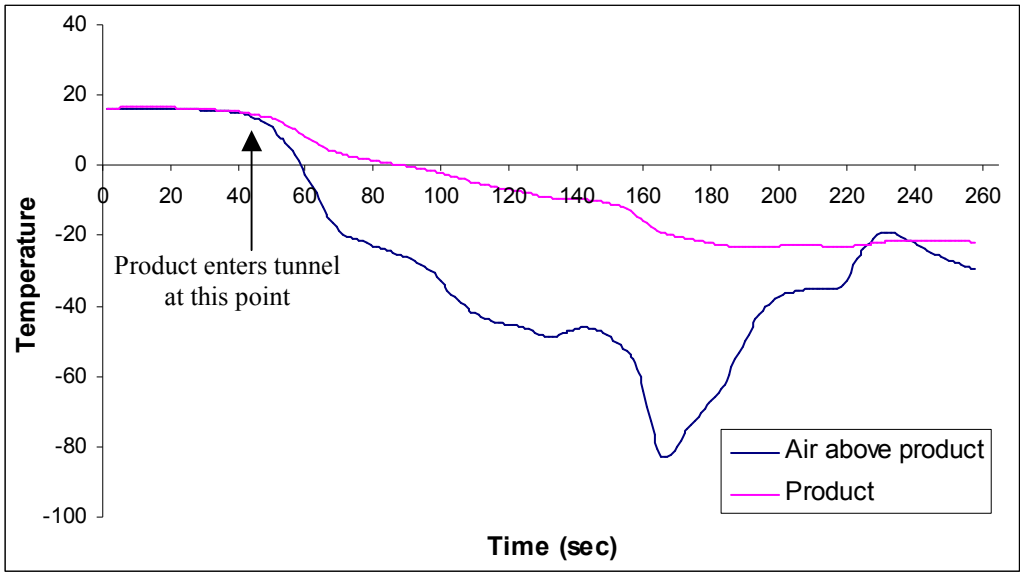

Figure 60 – Temperature profile of a typical 800mg unit frozen in the cryogenic tunnel set to -70°C.

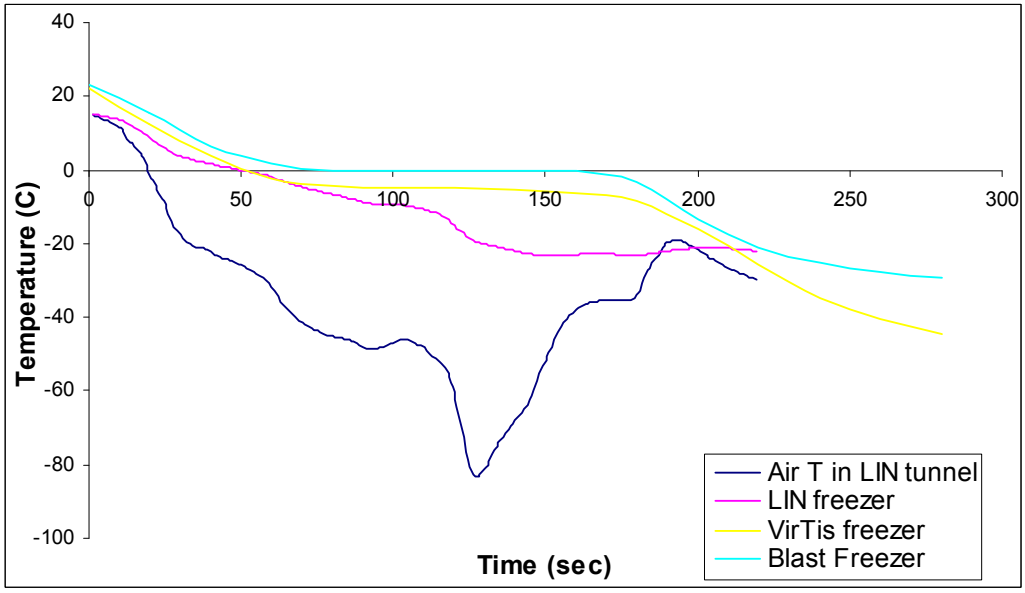

Figure 61 – Comparison of temperature profiles achieved in Virtis freezer, Blast freezer and cryogenic tunnel.

Figure 61 compares the two freezing rates achieved in the laboratory with the freezing rate achieved in the pilot scale cryogenic freezing tunnel.

The unit frozen in the cryogenic tunnel seemed to be completely frozen approximately 125 seconds after entering the tunnel. In contrast, the units in the Virtis and blast freezer took approximately 190 seconds to freeze completely. The initial cooling rates for the first 50 seconds were similar for all three methods however the significant change happened after 50 seconds. The blast freezer and Virtis freezer can be considered as isothermal, in that the freezing temperature (of the air or the shelf) is relatively constant thus providing a steady freezing rate. However, the cryogenic tunnel provides dynamic freezing rates i.e. the freezing temperature is dependent on the position inside the tunnel because the tunnel does not evenly distribute the coolant, liquid nitrogen. As Figure 61 shows, the temperature at the inlet to the tunnel (at time=0) was around 15°C. As the unit moved further into the tunnel, after 50 seconds, the air temperature was approximately -25°C. Further down the tunnel between 100-125 seconds, the air temperature dropped suddenly when the unit was almost completely frozen.

4.3.6 Mapping of the cryogenic tunnel with temperature probes

The cryogenic tunnel was mapped with a series of thermocouples which were used to record the temperature over time in several locations within the tunnel, as shown in Figure 62.

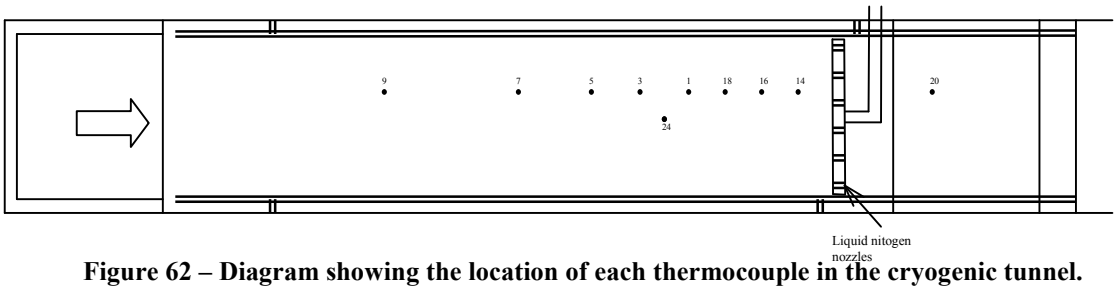

Figure 62 – Diagram showing the location of each thermocouple in the cryogenic tunnel.

Under typical operating conditions with the temperature set to -70°C, the tunnel would reach what may be termed as a steady state with the temperature being relatively steady in each location. Figure 63 shows the temperature profiles as measured by selected thermocouples during steady state operation over a period of around 3 minutes. The selected thermocouples correspond to a straight line path that a typical blister would make through the tunnel. The graph illustrates the fact that temperature varied considerably from one location in the tunnel to another. As a result, the cooling rate of a blister would have varied also, similar to that shown earlier in Figure 60. Although most of the

temperature curves in Figure 63 are around the -80°C mark, two thermocouples measured a much lower temperature. Thermocouple 18 measured a steady temperature of approximately -190°C indicating that the thermocouple was constantly sprayed directly with liquid nitrogen. Thermocouple 1 also measured a steady low temperature, around -110°C. Again, this was located close to the spray bar and close to thermocouple 18. Either side of these two thermocouples, the measurements at location 3 and 16 were much higher, around -80°C. This suggests that a small region existed around location 18 where liquid nitrogen was being directly sprayed onto the product.

By mapping the tunnel with thermocouples in this way, it was possible to understand the degree of temperature variation in the cryogenic tunnel.

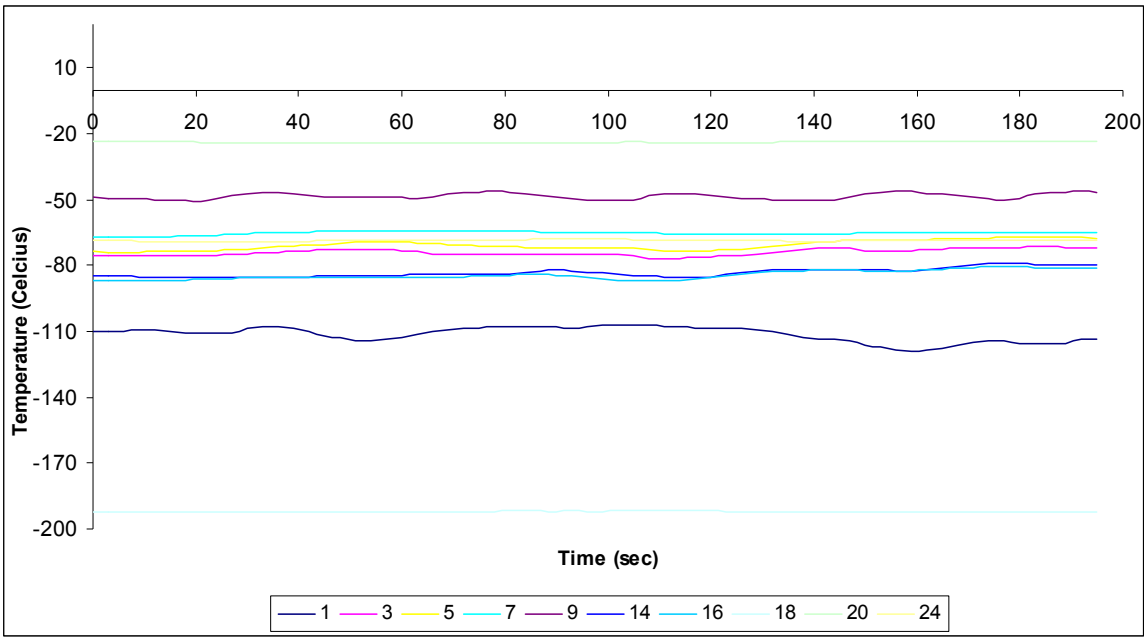

Figure 63 – Graph showing the temperature profile measured by selected thermocouples in the cryogenic tunnel. Each line shows the temperature variation at a specific location over a period of 3 minutes. These temperature profiles are typical for steady state operation.

4.3.7 Creation of tablets with experimental formulations

Experimental formulations were used to create freeze-dried tablets to establish whether one formulation is more likely to result in the occurrence of nodules. The formulations used were:

- A: 6% fish gelatine, 5% mannitol
- B: 4% fish gelatine, 1% mannitol

- C: 1% fish gelatine, 3% mannitol
- D: 4% fish gelatine, 6% mannitol

The results for the first trials at -70°C are shown in Figure 64 and Figure 65. Figure 64 shows that small nodules (up to 3x3 mm area affected; nodule categories defined in Table 13, section 4.2.8) were quite frequent. The control formulation (A) showed the least nodules whereas formulations C and D were affected the most with over 60 % of the tablets showing small nodules. Figure 65 shows the tablets that were affected by large (category 4 and 5) nodules. Again, formulations C and D were more prone to large nodules, however the difference between the four formulations was much less.

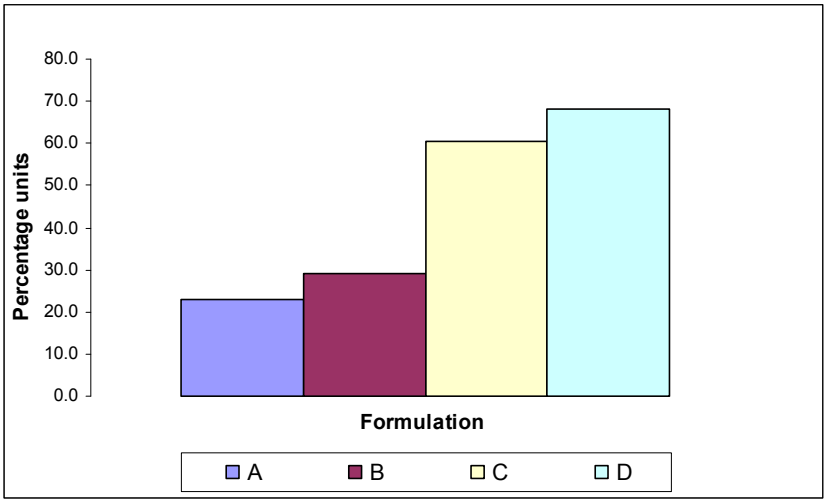

Figure 64 – Figure showing the percentage of tablets with category 2 or 3 nodules. The operating temperature was -70°C.

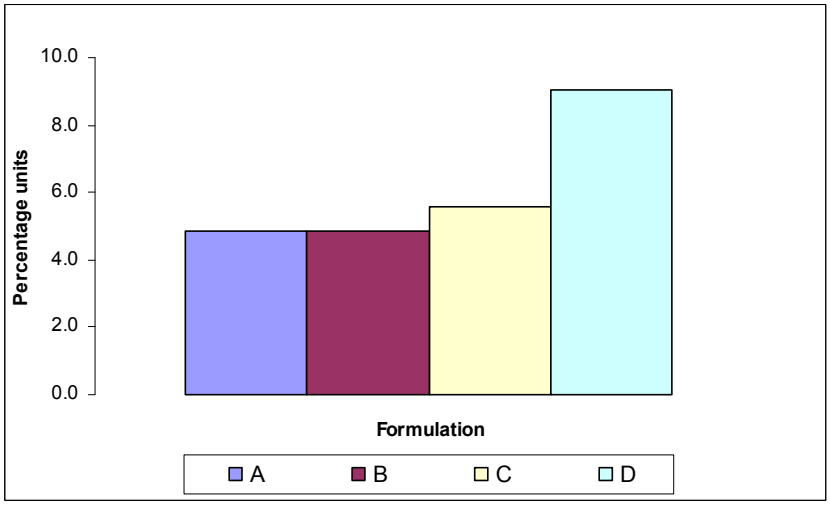

Figure 65 – Figure showing the percentage of tablets with category 4 or 5 nodules. The operating temperature was -70°C.

At -90°C, the results were similar to those at -70°C. Figure 66 shows that formulations C and D were very prone to small nodules with almost 70 % of the tablets being affected. However, formulations A and B were affected very little with only around 10% of the units showing small nodules. Figure 67 shows that large nodules were less frequent than small nodules for all formulations. Furthermore, formulation C was the one affected the most with around 6% of the tablets comprising large nodules. Again, formulation A was the least affected.

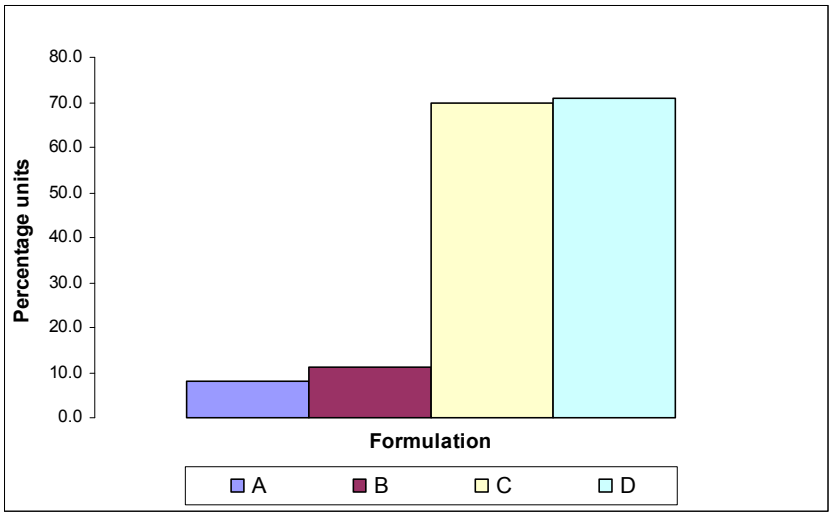

Figure 66 – Figure showing the percentage of tablets with category 2 or 3 nodules. The operating temperature was -90°C.

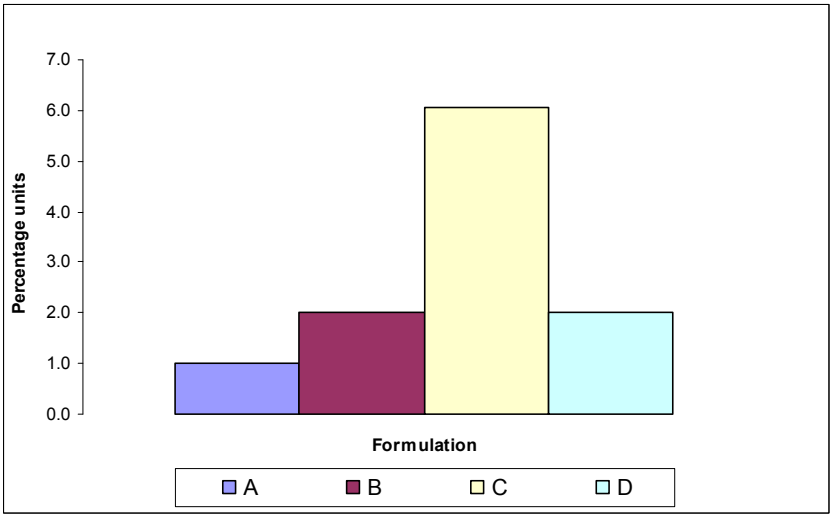

Figure 67 – Figure showing the percentage of tablets with category 4 or 5 nodules. The operating temperature was -90°C.

From the four figures shown above, one particularly important observation can be made. For formulations C and D, at both temperatures, small nodules are very common, with

around 60-70% of the tablets being affected. This is much greater than for formulations A and B. When considering large nodules however, the frequency of occurrence is not so different between the formulations. The presence of small nodules is greater with formulations C and D because the mannitol content in both formulations is greater than the respective gelatine content. If formulations B and D are compared, the gelatine contents in both are identical (4%) however the greater mannitol content in formulation D causes more nodulation. It is not clear why this is the case, but it is clear that a balance is required between the two major components to create the correct matrix structure. In the case of large nodules, these do not appear to be linked to formulation, therefore their presence must be linked to a processing condition.

4.3.8 Investigating the effect of temperature fluctuation in the cryogenic tunnel

The effect of temperature fluctuation was investigated by turning the nitrogen supply off and on intermittently while passing trays through the cryogenic tunnel. The temperature profile for a typical tray that experienced this is shown in Figure 68. The temperature measurements in this graph correspond to the thermocouple positions shown in Figure 62. If this graph is compared with Figure 63 earlier, the differences in temperature can clearly be seen. When the nitrogen supply was turned on, a sudden drop in temperature was experienced in all parts of the freezing tunnel. It was suspected that this type of sudden drop is responsible for the formation of nodules.

The results of these trials are shown in Figure 69 and Figure 70. Figure 69 shows the occurrence of small nodules. For formulations C and D, the frequency of occurrence is similar to the results seen earlier (Figure 64). However, with formulations A and B, the percentage of tablets with small nodules is quite high (over 30%) when compared to the numbers in Figure 64. Similarly for large nodules, Figure 70 shows that the percentages for formulations A and B are relatively high.

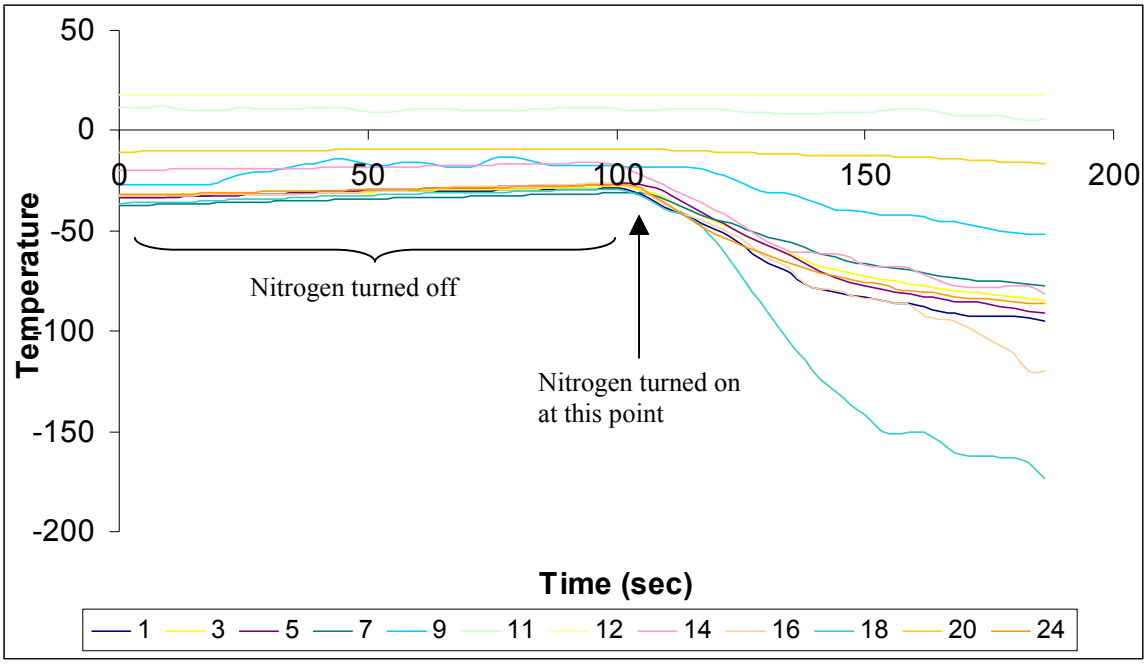

Figure 68 – Temperature profiles at selected points in the cryogenic tunnel (see Figure 62 for details of thermocouple positions). The nitrogen supply was off to begin with and was turned on after approximately 100 seconds.

In both figures, it is clear that formulations C and D are affected the most by both small nodules and large nodules. With formulations A and B, a much greater percentage of units contain nodules than with previous "steady-state" trails.

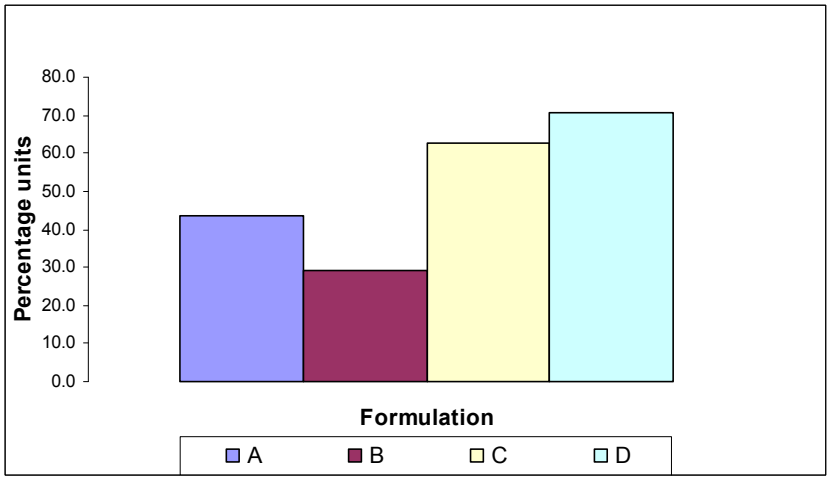

Figure 69 – Figure showing the percentage of tablets with category 2 or 3 nodules. The nitrogen supply was intermittently turned off and on to create temperature fluctuations.

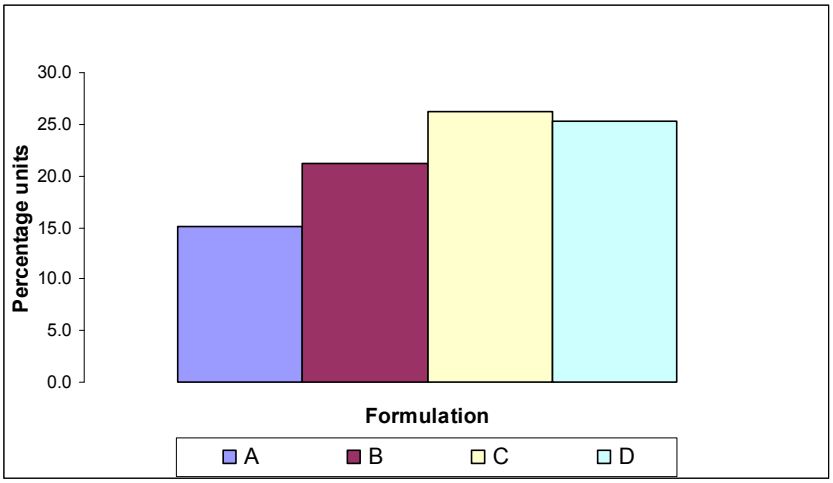

Figure 70 – Figure showing the percentage of tablets with category 4 or 5 nodules. The nitrogen supply was intermittently tuned off and on to create temperature fluctuations.

To summarise the effects of temperature fluctuations, it is easier to look at one formulation under a range of conditions. Figure 71 shows formulation A when frozen under steady state operation at -70°C and -90°C and also when the temperature was caused to fluctuate. The number of units with nodules was relatively low (10-20%) under steady freezing conditions, however under fluctuating temperature conditions, the number of units with nodules went up to 50%. Although formulation was shown to have some effect with formulations C and D being more susceptible to nodules, the temperature fluctuation seems to produce a more pronounced effect on all the formulations.

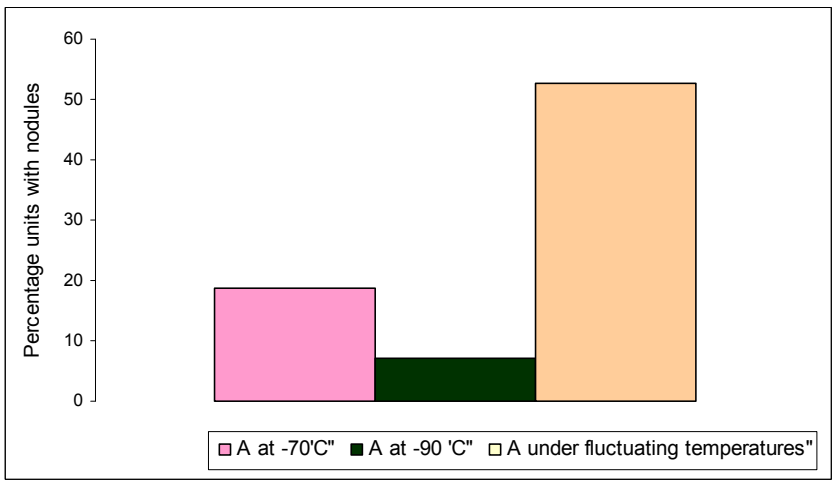

Figure 71 – Figure showing the how formulation A is affected by various freezing conditions

Further evidence to support that nodules are created by fluctuating temperature profiles is shown in Figure 72. The image is of the tray that corresponds to the temperature profiles

in Figure 68 and it shows that every tablet in the tray, regardless of formulation type has nodules present.

It is hypothesised that as a unit is being cooled and begins to freeze, a steady freezing rate will result in a homogeneously frozen tablet with a clean surface. However, if the freezing rate suddenly drops at the semi-frozen stage as in Figure 68, the remaining unfrozen material will freeze at a much faster rate. Faster freezing is known to create smaller crystal structure (Cogné *et al*, 2003; Drewett *et al*, 2007), therefore the remaining material will freeze with a very small crystal size and will appear as a nodule. This hypothesis is also supported by the optical images seen in section 4.3.1 which showed that nodules consist of much smaller crystals than the bulk of the tablet.

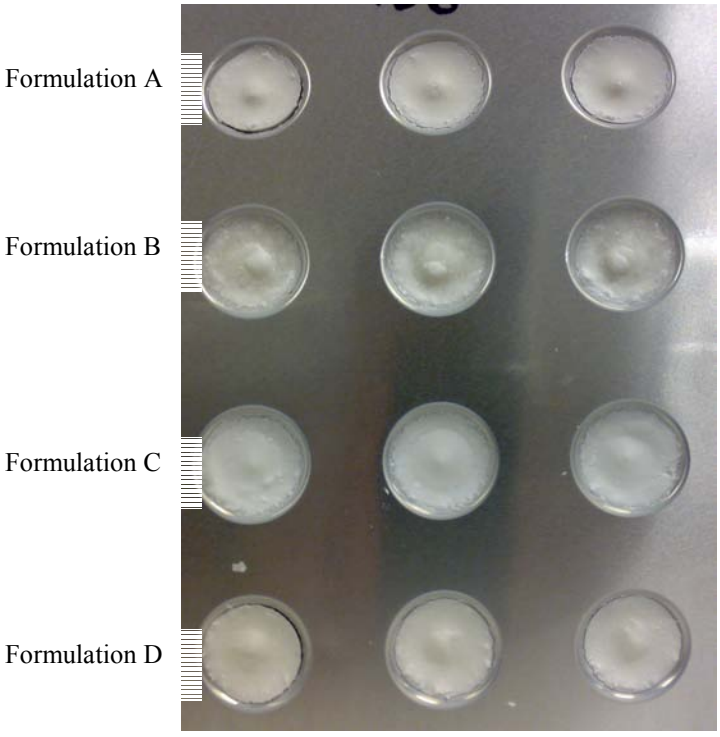

Figure 72 – Image of a tray that was subjected to fluctuating temperature conditions. The tray corresponds to the temperature profiles in Figure 68.

4.3.9 Summary & conclusions

Freeze-dried tablets were created in the laboratory (BH units) using a formulation consisting of 6% gelatine and 5% mannitol. The units were compared to tablets frozen using a cryogenic tunnel. The tablets were characterised and compared with cryogenically frozen units using a range of techniques. The following observations were made:

- Optical images showed that from the units created in the Virtis shelf freezer and the blast freezer, the Virtis tablets more closely resembled cryogenically frozen tablets. It was also seen that nodules consist of smaller pores than the bulk of a cryogenically frozen tablet which suggests that the local freezing rate of a nodule is much faster than the bulk of the tablet.

- X-Ray images also showed that Virtis tablets more closely resembled cryogenically frozen tablets and supported the microscope images.

- Dispersion characteristics of the tablets showed that there was no observable difference between cryogenically frozen tablets and BH units frozen on the Virtis shelf. Blast frozen tablets took slightly longer to fully disperse.

- DVS data showed that the vapour sorption isotherms are near identical for the three types of tablets. This indicates that all the samples with the same formulation (6% fish gelatine, 5% mannitol) are indistinguishable with DVS. This could be expected since the gelatine content of all the samples was the same. A freeze-dried unit containing 1% gelatine, 3% mannitol (sample C) showed a clear difference in sorption behaviour. This was because the gelatine content was much reduced thus limiting the amount of moisture sorption. The mannitol is known to be non-hygroscopic therefore a change in mannitol content would not be expected to have as great an effect on the sorption isotherm as gelatine.

In conclusion, the method of creating fast dissolving tablets in the Virtis freeze-dryer using shelf freezing was successful and produced tablets with similar microstructure and with almost identical dispersion properties as tablets frozen cryogenically. Blast freezing however created tablets which had a very different microstructure and hence did not have the same dispersion rate.

The pilot scale trials were aimed at developing an understanding of the combinations of formulations and freezing conditions that promote the formation of nodules on the surface of freeze-dried tablets. In summary, the following observations were made:

- Formulations C and D were more prone to small nodules under steady operating conditions than formulations A and B. Approximately 60% of C and D units were

affected by small nodules however around 20-30% of units A and B were affected.

- Formulations C and D were also more prone to large nodules than formulations C and D however the difference between the two groups was less than for small nodules; approximately 5% of units A and B were affected and 5-10% or units C and D were affected by large nodules.
- Under fluctuating temperature conditions, all formulations were subject to increased nodulation. The difference between formulations A/B (15-20% affected) and C/D (20-25% affected) was reduced greatly.

In conclusion, the fluctuation of temperature during the freezing stage is shown to have a considerable effect on the occurrence of nodules. It is hypothesised that a sudden drop in the freezing rate of semi-frozen units is the major cause for nodules. The concentration of the major constituents also influences the presence of small nodules however this is not thought to be the main cause. To minimise nodule occurrence it is recommended that the operation of the cryogenic tunnel is monitored closely to ensure that the temperature remains constant and is not allowed to fluctuate. The operation of the cryogenic tunnel and the distribution of cryogen may be the subject of further investigation. Other future work may involve studying the effect of spraying small amounts of liquid nitrogen onto the surface semi frozen tablets.

4.4 References

Appoloni C R, 2002. Characterisation of Porous Microstructure by X-ray Microtomography, X-ray Spectrometry 31, pp 124-127.

Alexande G R, Brown W H, Escullon E C, 1999. Cross-feed auger and method, US Pat. 5996855, 7th Dec. 1999. Assign: Material Sciences Corpn. Lll.

Aronson T F, 1972. Method and apparatus for measuring and dispensing predetermined equal amounts of powdered material, US Pat. 3656518, 18th April 1972, Assign: Perry Ind. NY.

Bentejac R, 1994. Freeze-drying, in the Handbook of Powder Technology, Volume 9, Elsevier, pp257-271.

Bridson R H, 2007. *DVS*, Measurement Techniques Module Notes, University of Birmingham

Brown R L, Richard J C, 1970. Principles of Powder Mechanics, Oxford, Pergamon pp 184-486.

Caillet A, Cogné C, Andrieu J, Laurent P, Rivoire A, 2003. Characterisation of ice cream structure by direct optical microscopy. Influence of freezing parameters. Lebensmittel-Wissenschaft und-Technologie, Vol. 36, Iss. 8, pp743-749.

Carpenter J F, Chang B S, Garzon-Rodriguez W, Randolph T W, 2002. Rational design and stable lyophilized protein formulations: theory and practice. Pharm. Biotechnol. 43, pp 109-133.

Carr R L, 1965. Evaluating flow properties of solids, Chem. Eng. 72, pp 163-168.

Cavatur R K, Vemuri N M, Pyne A, Chrzan Z, Toledo-Velasquez D, Suryanarayanan R, 2002. Crystallisation behaviour of mannitol in frozen aqueous solutions. Pharmaceutical Research 19 (6), pp 894-900.

Chaplin M, 2009. Gelatin, http://www.lsbu.ac.uk/water/hygel.html, accessed on 10/2/09.

Cheng Y F, Guo S J, Lai H Y, 2000. Dynamic simulation of random packing of spherical particles. Powder Technology 107, pp 123-130.

Chevalier D, Le Bail A, Ghoul M, 2000a. Freezing and ice crystals formed in a cylindrical food model: Part I. Freezing at atmospheric pressure. J of Food Eng. 46, pp 277-285.

Chevalier D, Le Bail A, Ghoul M, 2000b. Freezing and ice crystals formed in a cylindrical food model: Part II. Comparison between freezing at atmospheric pressure and pressure-shift freezing. J of Food Eng. 46, pp 287-293.

Chulia D, Cohard, C, Gonthier Y, Verain A, 1985. A correlation between flowability and tapping variation rates of powders, Int. J. Pharm. Tech and Prod. Mfr. 6, pp 10-16.

Cogné C, Laurent P, Andrieu J, Ferrand J 2003. Experimental data and modelling of ice cream freezing. Chem. Eng. Research and Design 81, pp 1129-1135.

Coulson J M, Richardson J F, 1999. Chemical Engineering Volume 1: Fluid Flow, Heat Transfer and Mass Transfer, 6th Edition, Butterworth Heinemann.

Coulson J M, Richardson J F, 1991. Chemical Engineering Volume 2: Particle Technology and Separation Processes, 4th Edition, Pergamon Press, pp 1-54.

Craik D J, Miller B F, 1958. The flow properties of powders under humid conditions, J. Pharm. Pharmacol. 10, 136T-144T.

Cumberland D J, Grawford R J, 1987. Handbook of powder technology, Volume 6, The packing of particles, Elsevier.

Dean J A, 1995. *The Analytical Chemistry Handbook*, New York. McGraw Hill, p15.1-15.5

Deleuil M, Chulia D, Pourcelot Y 1994. Particle and Powder Dynamics, in: Powder Technology and Pharmaceutical Processes, Elsevier, Amsterdam, pp115-163.

Dinius H B, 1987. Powdered material apportioning apparatus, US Pat. 4671430, 9th June 1987, Assign: Eli Lilly lnd. USA.

Drewett E M, Hartel R W, 2007. Ice crystallization in a scraped surface freezer. J of Food Eng. 78, pp 1060-1066.

DSC, 2008. http://www.pslc.ws/mactest/dsc.htm. Differential Scanning Calorimetry, department of polymer science, University of Mississippi 2005. Accessed 19.1.2008.

Dullien F A L, 1997. Structural properties of packings of particles. In: Handbook of Powder Science & Technology, 2nd edition, Chapman & Hall, pp 53-90.

Erickson M C, Hung Y C, 1997. Quality in Frozen Food. Chapman & Hall, 1997.

Faydi E, Andrieu J, Laurent P, 2001. Experimental study and modelling of the ice crystal morphology of model standard ice cream. Part I: Direct characterisation method and experimental data. J. of Food Eng. 48, pp 283-291.

Fayed M E, Otten L, 1997. Handbook of Powder Science & Technology, 2nd edition, Chapman & Hall.

Francis F J, 1999. Wiley Encyclopedia of Food Science and Technology, 2nd Edition, John Wiley & Sons, pp 1183-1188.

Gaalswyk M K, Owens M A, 1999. Concentric auger feeder, US Pat. 5871081, 16th Feb. 1999, Assign: Easy Systems Inc. Minn.

Gilsenan P M, Ross-Murphy S B, 2000. Viscoelasticity of thermoreversible gelatin gels from mammalian and piscine collagen. Journal of Rheology, 44, pp 871–882

Gilsenan P M, Ross Murphy S B, 1999. Structure and rheology of gelatine gels. In B. T. Stokke, & A. Elgsaeter, Polymer networks group review series, vol. 2, pp 237–273. Chichester: Wiley

Harnby N, Edwards M F E, and Nienow A W, 1985. Mixing in the Process Industries, Butterworth, London.

Hancock B C, Mullarney M P, 2005. X-ray Microtomography of solid dosage forms, Pharmaceutical Tech, pp 92-100.

Hass H, 1916. Tool for taking samples, US Pat. 1205888, 21st Nov. 1916.

Hawkins A E, 1990. Characterizing the single particle, in: Principles of powder technology, John Wiley & Sons Ltd, pp 9-31.

Hofer U, 1983. Trockene fullguter. In: Fahrig, W., Hofer, U. (Eds.), Die Kapsel, Grundlagen, Technologie und Biopharmazie einer modernen Arzneiform. Wissenschaftliche Verlagsgesellschaft mbH, Stuttgart, Germany, pp 83-111.

Hottot A, Nakagawa K, Andrieu J 2008. Effect of ultrasound-controlled nucleation on structural and morphological properties of freeze-dried mannitol solutions.

Iinoya K, Masuda H and Watanabe K, 1988. Powder and bulk solids handling processes, Marcel Dekker, New York.

Ionadi F, 2000. Screw feeder dosage unit provided with stirring device, US Pat. 6062720, 16th May, 2000. Assign: Anadntex SpA Italy.

Irwin G M, Dodson G J, Ravin L J, 1970. Encapsulation of clomacran phosphate. I. Effect of flowability of powder blends, lot-to-lot variability, and concentration of active ingredient on weight variation of capsules filled on an automatic filling machine. J. Pharm. Sci. 59, pp 547-550.

Israelachvili, J N, 1991. Intermolecular and surface forces, 2nd edition, Academic Press, London.

Jenike A W, 1964. Storage and flow of solids, Utah Eng, Exp. Stn. Bull. 123, pp 1-194.

Jones B.E, 1987. The history of the gelatine capsule. In: Ridgway, K. (Ed.), Hard Capsules, Development and Technology, The Pharmaceutical Press, London, pp 1-12.

Jones B.E, 2001. The filling of powders into two-piece hard capsules, I. J. Pharmaceutics 227 (2001), pp 5-26.

Jones D, 2002. Pharmaceutical Statistics, The Pharmaceutical Press, London.

Jones F T, Lee K S, 1970. The optical and crystallographic properties of three phases of mannitol. Microscope 18, pp 279-285.

Karim A A, Bhat, R, 2008. Fish gelatin; properties, challenges and prospects as an alternative to mammalian gelatins, Food Hydrocolloids 23, pp 563-576.

Kaye B H, 1997. Particle size characterisation. In: Handbook of Powder Science & Technology, 2nd edition, Chapman & Hall, pp 1-32.

Klous M G, Nuijen B, Van den Brink W, Van Ree J M, Beijnen J H, 2004. Process characterisation, optimisation and validation of production of diacetylmorphine/caffeine sachets: a design of experiments approach, Int. J. Pharma. 285, pp 65-75.

Knight J B, Fandrich C G, Lau C N, Jaeger H M, Nagel S R, 1995. Density relation in a vibrated granular material, Phys. Rev. E Stat. Phys. Plasmas Fluids Relat. Interdiscip. Topics 51 (1995) 3957-3963

Krogerus V E, 1959. New model of a powder measure for dispensing, Farm. Aikak. 68, 124-126.

Kurihara K, Ichikawa I, 1978. Effect of flowability on capsule-filling-weight-variation. Chem. Parm. Bull. 26, pp 1250-1256.

Leuenberger H, Zimmerman Y, 1976. Electrostatic charges of granulates and free flowing powders, Acta Pharm. Technol. 22, pp 255-266.

Li Q, Rudolph V, Weigl B, Earl A, 2004. Interparticle van der Waals force in powder flowability and compactibility. Int. J. of Pharmaceutics 280, pp 77-93

M & O Perry Industries Inc. Description of the Perry "Accofil" principal of vacuumetric powder filling, 412 N. Smith Avenue, Corona, CA 92880, USA.

Mellor J D, 1978. Fundamentals of Freeze Drying, Academic Press, London, UK

Miyake Y, Shinoda A, Nasu T, Furukawa M, Uesugi K, Hoshi K, 1974. Packing properties of pharmaceutical powders into hard gelatine capsules (in Japanese), Yakuzaigaku 34, pp 32-37.

Molerus O, 1982. Invited Review; Flow Behaviour of Cohesive Powders, Chem. Eng. Commun. 15, pp257-289.

Molerus O, 1993. Principles of Flow in Disperse Systems. English edn. Chapman and Hal, London, pp197-235.

Morris J P, 1989. Powder dosing apparatus, US Pat. 4850259, 25th July 1989, Assign: Eley Ltd. UK.

Muyonga J H, Cole C G B, Duodu K G, 2004. Extraction and physico-chemical characterisation of Nile perch (Lates niloticus) skin and bone gelatine. Food Hydrocolloids, 18, 581-592.

Nagai T, Suzuki N, 2000. Isolation of collagen from fish waste material – skin, bone and fins. Food Chemistry, 68, pp277-281.

Nail S L, Jiang S, Chongprasert S and Knopp S A, 2002. Fundamentals of freeze drying. Pharm. Biotechnol. 14, pp 281-360.

Nakagawa K, Hottot A, Vessot S, Andrieu J, 2006. Influence of controlled nucleation by ultrasounds on ice morphology of frozen formulations for pharmaceutical proteins freeze-drying. Chem. Eng. and Proc. 45, pp 783-791.

Özilgen M, 1998. Food Process Modelling and Control, Gordon and Breach Science Publishers, Amsterdam, The Netherlands.

Pardo J M, Suess F, Niranjan K, 2002. An investigation into the relationship between freezing rate and mean ice crystal size for coffee extracts. Food & Bioproducts Proc. Vol. 80, issue 3, pp 176-182.

Parnell J B, 1934. Improvements in or relating to the delivery of charges of powdered or granular materials, UK Pat. 443377, 29th Aug 1934.

Persidsky M D, Luyet B J, 1975. Analysis of the freezing process across temperature gradients within gelatine gels. Cryobiology, Volume 12, Issue 4, pp 364-385.

Piersma H D, 1963. Disposable sample probe for bulk chemicals, US Pat. 3080760, 12th March 1963, Assgn: American Cyanamid.

Reier G, Cohn S, Rock S, Wagenblast J, 1968. Evaluation of factors affecting the encapsulation of powders in hard gelatine capsules, I. J. Pharm. Sci. 57, pp 660-666.

Rhodes M J, 1990. Pneumatic Conveying, in Principles of Powder Technology, John Wiley & Sons Ltd.

Russell A B, Cheney P E, Wantling S D, 1999. Influence of freezing conditions on ice crystallisation in ice cream. J. of Food Eng. 39, pp 179-191.

Schulze D, 1994. Storage, feeding, proportioning, in Powder Technology and Pharmaceutical Processes, Elsevier, Amsterdam, pp285-316

Schulze D, 2008. Flow properties testing with Ring Shear Testers, RST-01.01, RST-01.pc and RST-XS. Version 1.6, Dietmar Schulze.

Seville J P K, Tüzün U, Clift R, 1997. Processing of particulate solids, Chapman & Hall.

Skoog D A, Holler F J, Nieman T A, 1998. Principles of Instrumental Analysis, 5th Edition, New York.

Sutton H M, 1976. In: Parfitt G D, Sing K S W (Eds.), Characterisation of Powder Surfaces, Academic Press, London, pp107-158.

Svarovsky L, 1990. Characterization of powder, in: Principles of powder technology, John Wiley & Sons Ltd, pp 35-68.

Takagi K, Sugihara M, Kimura S, 1969. Studied on filling properties in automatic filling machine (in Japanese). Yakuzaigaku 29, pp 245-249.

Tay B Y, Evans J R G, Edirisinghe M J, 2003. Solid freeform fabrication of ceramics, Int. Materials Review 48, pp 341-370.

Thomson F M, 1997. Storage and flow or particulate solids, in: Handbook of powder science and technology, Chapman & Hall, New York.

Wasswa J, Tang J, Gu X, 2007. Utilization of fish processing by-products in the gelatin industry. Food Reviews International, 23, pp 159-174.

Webb M D, Davis I L, 2006. Random particle packing with large particle size variations using reduced-dimension algorithms. Powder Technology 167, pp 10-19.

Williams J C, 1990. Mixing and segregation in powders, in: Principle of Powder Tech., John Wiley & Sons Ltd, pp 71-90.

Woinet B, Andrieu J, and Laurent M, 1998. Experimental and theoretical study of model food freezing. Part I. Heat Transfer Modelling. J. Food Eng. 35, pp 381-393.

Woinet B, Andrieu J, and Laurent M, Min S G, 1998. Experimental and theoretical study of model food freezing. Part II. Characterisation and modelling of the ice crystal size. J. Food Eng. 35, pp 395-407.

Yang S, Evans J R G, 2007. Metering and dispensing of powder, the quest for new solid freeforming techniques, Powder Technology 178, pp56-72

Yokoyama T, 1991. In: Inoya K, Gotoh K, Higashitani K, (Eds.), Powder Technology Handbook, Dekker, NY, pp127-138.

Yu A B, Feng C L, Zou R P, Yang R Y, 2003. On the relationship between porosity and interparticle forces. Powder Tech. 130, pp 70-76.

Yu L, Reutzel S M, Stephenson G A, 1998. Physical characterization of polymorphic drugs: an integrated characterization strategy. PSTT 1, pp 118-127.

Zhu S, Ramaswamy H S, Le Bail A, 2005. Ice-crystal formation in gelatin gel during pressure shift versus conventional freezing. J of Food Eng. 66, pp 69-76.

APPENDIX I
IDENTIFICATION OF POWDER FILLING TECHNOLOGY

Introduction

The overall aim of the project was to identify and test a system capable of carrying out the dosing as required on a small (laboratory) scale. If successful, this approach may in the future lead to the development of a fully automated production machine that incorporates the same basic principles developed in the laboratory.

This chapter describes the equipment options that were available. Each technology was subject to a theoretical appraisal against a set of requirements. The technologies that satisfied the requirements on paper underwent an experimental assessment with one equipment option eventually chosen for procurement.

Equipment requirements (acceptance criteria)

The equipment must be able to deliver accurate and precise doses. The measure for precision commonly used in the pharmaceutical industry is the relative standard deviation (RSD). This is simply the standard deviation (SD) of a sample of doses expressed as a percentage of the sample mean.

$$RSD = \frac{SD}{mean} \times 100$$

For example, in a sample of 20 doses, if the mean weight is 50.00mg and the standard deviation is 0.5mg, the RSD is therefore 1%. For this application the industrial sponsors' requirement is that the equipment must deliver doses with a precision of RSD ±2% or better.

The powder equipment must be able to deliver particles in the size range of 100μm-500μm diameter with fill weights between 50mg-400mg. This particle size range was chosen for several important reasons:

- Materials greater than 100μm diameter are relatively free-flowing when compared to very fine materials (<<100μm).
- Materials greater than 100μm are easily coated using fluid-bed coating methods. With smaller materials, problems such as clumping and agglomeration can occur

with individual particles being difficult to separate in the fluidised bed (Richardson *et al*, 2002).

- Materials less than 500μm do not leave a gritty mouth-feel when used in an oral dosage method.
- Materials in this size range are large enough to minimise surface forces (such as van der Waal's forces, electrostatic attraction and the effect of moisture) which can give rise to substantial attraction between particles and cause agglomeration.

The fill weight range of 50mg-400mg was chosen to meet the typical fill weight range for a pharmaceutical drug (e.g. in tablets). Furthermore, fill weights in this range are large enough to be delivered with the required precision but small enough to potentially be formulated into a freeze dried dosage form.

The throughput of the equipment must also be considered. Although at the laboratory scale, it is not necessary for the equipment to deliver several dozens of doses per minute, a fully automated production machine would be expected to meet requirements of this scale. Therefore, there must be the potential for the chosen equipment (when fully automated) to deliver at high speeds such as would be required in a manufacturing process. To satisfy this need, the collection, measurement and dispensing of the powder must therefore be very rapid processes that can be carried out within a few seconds.

Option 1 – Powdernium, Symyx Technologies Inc.

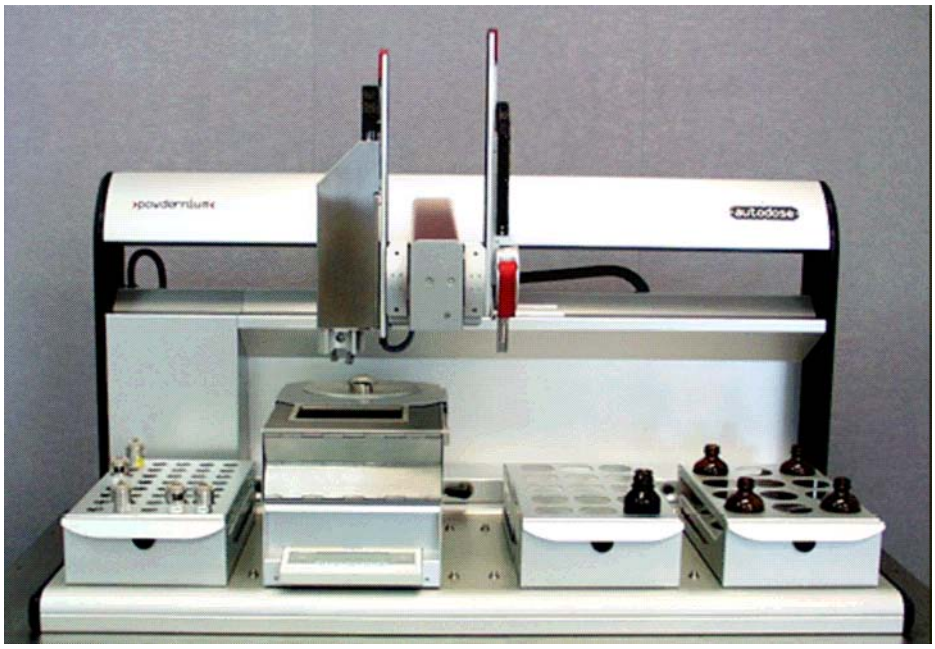

Figure 73 – The Powdernium® powder filling workstation

The Powdernium (Symyx Technologies, Santa Clara, USA) is a fully automated powder dispensing workstation that is capable of dosing a wide range of materials. It operates by using a very precise balance that weighs each powder dose before dispensing. According to the manufacturer, the major benefits of this technology are:

- Flexibility with regard to materials. Materials with a wide range of physical properties can be used, including low density, free-flowing, cohesive and micronised.
- Accuracy and precision. Capable of RSD between 1-5% depending on flow properties of the powder.
- Compatibility with many types of receiving container, (e.g. all sizes of capsules, vials etc).
- Many different powders can be stored on the machine, on line (up to 200)
- Capability of fill weights as low 20mg.
- Self regulating. The workstation is capable of monitoring powder properties online and optimising the filling process accordingly.

The major disadvantages of the Powdernium are:

- Inability to handle full size blister trays.
- Slow throughput. The workstation measures the dose by mass, i.e. it uses a very accurate balance to weigh each dose, a process which can take between 20-60 second per dose. This is considerably slower than would be practical in a manufacturing process where the collection, measurement and delivery of a dose would need to be carried out within two or three seconds.
- High cost. The budget for a bench scale powder dosing system was £35 000. The minimum cost of the Powdernium was quoted at $120 000 (£80 000).

Assessment of Powdernium - Conclusion

The Powdernium workstation is designed as a lab based research tool which is capable of dosing under full automation with a wide range of materials. However it is not feasible for potential manufacturing application because of slow throughput and high cost. Furthermore, it is capable of dosing into many types of small containers; however it cannot be used with full sized blister trays.

Option 2 – Micro-Fill auger, All-Fill Technology

A  B 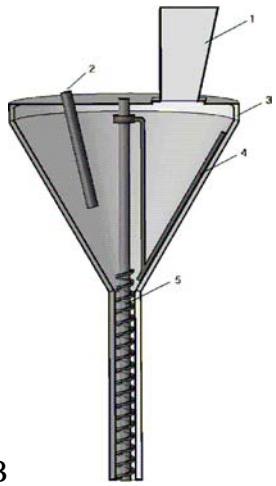

Figure 74 – (A) Series 1 Micro-Fill auger, All-Fill Technology. (B) Diagram of an auger filling system. (1) Opening with funnel for filling powder into hopper; (2) Product sensor; (3) Plexiglass hopper; (4) Agitator; (5) Auger. (taken from Klous *et al*, 2004).

The Series 1 Micro-Fill is an auger (screw) type powder filling machine. As shown in Figure 74B, the equipment is essentially a funnel with an automated screw (auger). The funnel is filled with powder and the dosage size and rate is controlled by the rotation of the auger. It is designed for precision dosing of powders and granules either by volume or by weight. In the latter method, the auger will dose onto a precise balance that weighs the dose before delivering the dose. The Micro-Fill is controlled by a touch screen display panel and is very simple to operate. The screw size is changeable which makes the system capable of handling a wide range of powder types (cohesive to free flowing), a wide range of particle sizes and fill weights. The manufacturer claims fill weights from 10mg to 100g with the potential for a very high throughput. Finally, the Micro-Fill can be placed on a bench top for use in a laboratory or incorporated into a pilot line as a free-standing unit (as shown in the image above).

The major benefits with the auger system are:

- The capability to handle a wide range of materials and particle sizes.
- The capability to dose in the required fill weight range.
- The ability to deliver into blister trays.
- The cost. The initial estimate was £12 000.

There did not appear to be any great disadvantage with the Micro-Fill at this stage with the manufacturer claiming it could meet the accuracy and precision requirements. This was promising and so a set of practical tests was carried out (under the instructions of the author) using coated sugar spheres.

Assessment of Micro-Fill auger – Materials and methods

The purpose of the assessment was to see the performance of the auger with coated materials and the accuracy and precision of the doses at 50mg and 400mg fill weights. Assessment of the Series 1 Micro-Fill was carried out by All-Fill Technology technicians in Bedfordshire under instruction from the author. The materials used were sugar spheres coated with Acryleze, with nominal sizes 180µm and 500µm (ACR180 and ACR500 respectively). The procedure was to take 10 doses at a target fill weight, and accurately measure the weight of each dose using a balance. The standard deviation and RSD were then calculated. Two target fill weights were used, 50mg and 400mg. Finally, the auger

dosing head was covered with a plate to minimise the leakage of powder and ensure the best possible accuracy as shown in Figure 75b.

Assessment of Micro-Fill auger – Results and discussion

Table 15 – Assessment of the Series 1 Micro-Fill auger using coated Suglets

Material		ACR180	ACR180	ACR500	ACR500
Target weight		50mg	400mg	50mg	400mg
Dose number	1	48	415	57	403
	2	61	411	60	402
	3	55	410	60	397
	4	59	414	49	394
	5	52	411	64	403
	6	55	418	58	397
	7	63	406	53	402
	8	58	413	63	404
	9	58	420	56	410
	10	53	413	60	397
Sample mean (mg)		56.2	413.1	58.0	400.9
RSD (%)		7.99	0.97	7.80	1.17

The table above summarises the results obtained. For each experiment, the mean fill weight varied somewhat from the target fill weight. This is because the auger was not optimised fully to give a mean of 50mg. However, the presumption is that after optimising the auger, the correct mean fill weight would be achieved. The important observation is that RSD is within the ±2% range when using a fill weight of 400mg. However, with 50mg fill weight, the RSD rises considerably to almost 8%.

Although the auger used a plate to minimise the leakage of powder, the RSD at 50mg was too high. It is suspected that the difference in RSD between low and high fill weights occurs as a result of avalanching behaviour.

Consider a schematic of the auger system. The auger can operate with two types of delivery methods. The first is a simple screw in the orifice of a funnel through which material is conveyed as illustrated in Figure 75a. Using this method to deliver small, very precise doses of powder can be difficult because leakage at the end of the auger can occur. These leakages may only be small (2-5mg), but they are likely to contribute significantly to the inconsistency encountered at low fill weights (e.g. 50mg).

The second delivery method uses a plate to cover the outlet of the auger as illustrated in Figure 75b. As powder builds up on the plate, it flows over the edge to deliver a dose. Although this approach can overcome the problem of leakage, the downfall is that it is only accurate for very free-flowing powders and at larger fill weights (>500mg). With cohesive powders, material tends to build up, and then an avalanche effect occurs, thus delivering a larger dose than expected. This can lead to inconsistent dose weights.

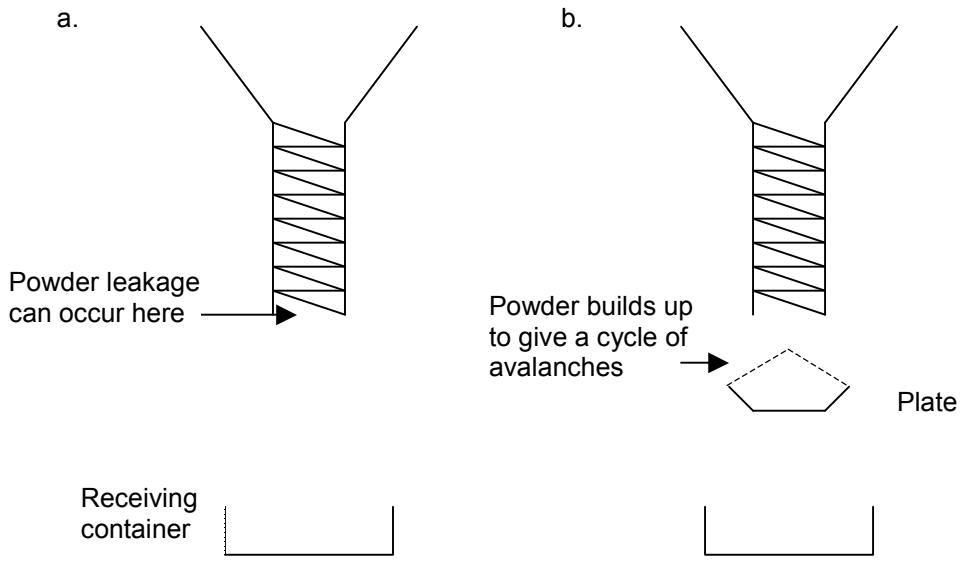

Figure 75 – a) A standard auger; b) An auger with a plate to minimise the effect of powder leakage.

Assessment of Micro-Fill auger – Conclusion

The practical assessment using coated sugar spheres showed that the Micro-Fill auger system is capable of dosing accurately and precisely at 400mg but is not easily capable of very high precision at a fill weight of 50mg. Other factors considered were the practicality of using the auger on a pilot line. Figure 74A shows the bulky nature of the equipment which would make it very difficult to dose into blisters a few millimetres

apart. Hence, it was decided that the Micro-Fill auger would not be considered for further thorough evaluation and experimentation.

Option 3 – Floor Console Powder Filling Machine, M&O Perry Industries

The Floor Console (FC) Powder Filling equipment is based on the pneumatic principles outlined in section 0 and is shown in Figure 76. It consists of two main components, a free standing unit housing a vacuum pump and a powder collecting head known as a filling gun. The schematic of the filling gun is shown in Figure 77.

Figure 76 – The Floor Console Powder Filling Machine, M&O Perry Industries

The filling gun operates by collecting powder in the powder collection chamber using a vacuum and delivering to a container using positive pressure. A filter prevents powder from being entrained into the vacuum pump and the volume of the collection chamber defines the size of the dose. The chamber size can be changed to adjust the fill weight by adjusting the piston position. For large changes in fill weight, alternative gun sizes are available. The table below shows the gun sizes that cover the specified range.

Table 16 – The available fill gun sizes and fill ranges (extract from M&O Perry product brochure)

Fill gun inner diameter (I.D.) in inches	Fill range (mg)
1/16	2 - 6
3/32	4 - 25
1/8	15 - 85
3/16	50 - 200
1/4	125 - 450
5/16	240 - 950

After a theoretical appraisal, the following advantages of the system were identified:

- The manufacturers claim a precision of RSD ±2% for "most" materials.
- The equipment can dose in the range of 50mg-400mg (with a change of filling gun).
- The fill guns are capable of handling a wide range of materials, from free-flowing to cohesive.
- The fill guns are relatively small (compared to the auger system) and operated manually so it may be possible to design a robotic arm for use on the pilot scale.
- The equipment cost is within budget (estimated to be £15 000-£20 000).

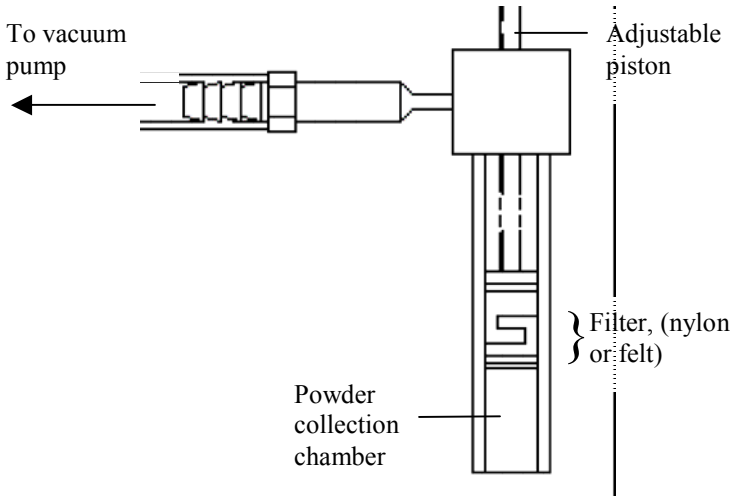

Figure 77 – Schematic of a filling gun from the FC Powder Filling Machine (M&O Perry Industries)

With the FC Powder Filler theoretically meeting the specifications, an experimental assessment was carried out using sugar spheres; some uncoated and some coated with Acryleze and Surelease.

Assessment of the FC Powder Filler – Materials and methods

Coated and uncoated sugar spheres were sent to M&O Perry Industries, California, USA for evaluation with the FC Powder Filler with instructions from the author. The following combinations of powder sizes and coatings were tested:

- 180µm, 355µm and 500µm with Acryleze coating.
- 180µm and 500µm with Surelease coating.
- 355µm, uncoated. (Surelease coating in this size was unavailable at the time).

Three gun sizes were used with 2 fill weights for each material as shown in Table 17.

To dose the powder, the gun was inserted into the bulk supply of powder. Subsequently, during the vacuum cycle of the machine, product was drawn into the barrel of the fill gun forming a mushroom of product on the gun's tip, which was then wiped off using a sharp edged blade prior to dosing. Product was then dispensed into the receiving container by the reversal of the machine's vacuum cycle to a positive pressure cycle which was initiated by depressing a footswitch.

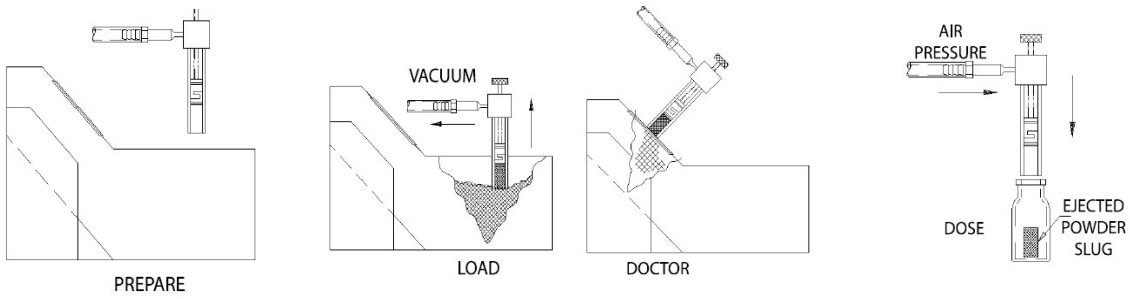

Figure 78 – Diagram showing the operation of a fill gun (Source: M&O Perry product brochure).

The vacuum pressure of the FC machine was set to the highest possible, -24 inches mercury (inHg) to ensure a good pick-up. Note, the equipment dials and measurements were in imperial units therefore the use of these is continued to maintain consistency. Doses were delivered into blisters from a height of less than ½ inch and with the dose pressure between 1.5-3 inHg depending on the gun size. A higher dose pressure would have resulted in spillage of the powder from the blister.

For each experiment, 20 doses were taken and weighed on a balance. The results were used to calculate standard deviation and RSD. A visual assessment of the collection of powder was also made to describe how well a powder picked up, the size of the mushroom on the gun tip and whether or not the powder formed a solid slug.

Table 17 – Table showing the gun sizes evaluated with coated sugar spheres by M&O Perry Ind.

Gun size (I.D.) in inches	Fill range of gun (mg)	Target fill weight (mg)
1/8	15 - 85	50
3/16	50 - 200	50
1/4	125 - 450	400

Assessment of the FC Powder Filler – Results and discussion

The key results are highlighted in Table 18. It must be reiterated that the aim of this assessment was to simply determine whether the equipment can dose the given materials accurately and precisely. The descriptions of pick-up quality and mushroom size are qualitative descriptions made by the operator to describe how the materials behave generally and were not used as quantitative definitions. In analysing the results, it is apparent that most material/gun combinations lead to a "good" pick-up and an RSD value of less than 2%. The only materials that failed to pick up altogether were those with a size range above 500μm.

The general trend in the results is that the smaller materials were better to pick up. As the powder size increased, the observed pick-up quality became weaker and eventually the largest material failed to pick up altogether. The other main trend is that the RSD is lower for 400mg fill weight than for 50mg. This is understandable since a larger dose would result in a lower percentage variation.

Table 18 also shows that 180μm sugar spheres coated with Surelease (SUR180) did not perform satisfactorily with the 1/8th inch gun. The material filled the gun however it was not possible to purge it from the gun with a dose pressure of 3inHg. This observation may be linked to the flow function curve for SUR180 (Figure 22) that showed the materials coated with Surelease became more cohesive under a higher consolidation

stress. It a possible that with the small diameter of the 1/8th inch fill gun, as the gun is dipped into the powder, sufficient consolidation occurs to cause the material to be become more cohesive and therefore cause a blockage.

Table 18 – Table showing the results obtained when assessing the fill guns using various coated and uncoated sugar spheres. ACR: Acryleze; SUR: Surelease.

Gun I.D. (inches)	Material	Target fill weight (mg)	Pick up	Mushroom size	RSD (%)
1/8	ACR180	50	Good	Small	0.60
1/8	SUR180	50	Fail – material clogs in gun		-
1/8	355µm (uncoated)	50	Good	None	1.39
1/8	ACR355	50	Excellent	Fair	1.39
3/16	ACR180	50	Good	Fair	0.60
3/16	SUR180	50	Good	Fair	0.60
3/16	ACR500	50	Material fails to pick up		-
3/16	SUR500	50	Material fails to pick up		-
¼	ACR180	400	Good	Small	0.17
¼	SUR180	400	Excellent	Small	0.20
¼	355µm (uncoated)	400	Good	Fair	0.42
¼	ACR355	400	Excellent	Fair	0.25

Assessment of the FC Powder Filler – Conclusion

It was demonstrated from the experimental assessment that the filling guns were capable of collecting and dosing sugar spheres coated with both Acryleze and Surelease. Furthermore, the accuracy and precision were also shown to be very good for fill weights between 50mg-400mg with RSD values <2%. The guns were however unable to collect the largest powder size (nominally 500µm) from the powder bed.

Summary

The table below shows a summary of the types of dosing methods available. For some of the methods (1, 3 and 4) a bench scale equipment option exists, but for other methods, (2, 5 and 6), only full scale production machines exist. The only technology to satisfy all the requirements is the FC Powder Filling Machine.

Table 19 – A simple summary of the advantages and disadvantages of the FC Powder Filler using Accofil® compared with other types of dosing.

	Dosing Type	Particle size range	Dose range	RSD +/- 2%	Required throughput	Cost	Flexibility	Bench scale option?
1	**By weight e.g. Powdernium**	✓	✓	✓	×	×	×	✓
2	**Volumetric e.g. Zanasi dosator with compression**	✓	✓	✓	✓	✓	✓	×
3	**Vacuum based e.g. Accofil Powder Filler**	✓	✓	✓	✓	✓	✓	✓
4	**Screw/auger e.g. Micro Auger from All-Fill Tech.**	✓	✓	×	✓	✓	✓	✓
5	**Electrostatic**	✓	✓	×	×	-	-	×
6	**Vibratory methods**	✓	✓	×	-	-	✓	×

The three technologies with bench-scale options were compared against each other. The details of the advantages and disadvantages of each are given in Table 20.

Table 20 – Table summarising the equipment options that were evaluated

	Company	Equipment	Advantages	Disadvantages	Outcome
1	Symyx	Powdernium	- Automated powder dispensing system. - Compatible with a wide range of materials and physical properties (inc. low-density, free-flowing, cohesive and micronised). - RSD 1-5% accuracy depending on flow properties of powder etc. - Compatible with different containers. - Minimum dose is 20mg. - Many powders stored on the machine online. - Each powder dose weighed and recorded automatically. - Monitors powder properties and optimises dosing automatically.	- Cannot handle full size blister trays. - Throughput is slow; each dispense will take 20-60 seconds. - Acceptable purely as a lab based research tool however may not be suitable for production. - Cost; cheapest system quoted at $120k. Customised changes will increase the cost.	Not feasible due to slow throughput and high cost.
2	All-Fill Tech, UK	Series 1, Micro-Fill Auger device	- Volumetric dosing system, designed for dosing foodstuffs and pharmaceuticals. - Capable of desired speeds (up to 300 doses/min). - Can be operated manually and automatically. - Capable of dosing into blister trays. - A pocket as small as 10mm diameter can be dosed. - Can be free standing or incorporated into an existing line. - Cost; system can be ordered for £12000-15000. - UK supplier.	- Volumetric dosing may compromise somewhat on the accuracy although company claimed it was very accurate. - Auger not suitable for cohesive powders.	Visited All Fill Tech to see equipment demonstration. Precision of auger did not match the RSD of ±2%.
4	**M&O Perry, USA**	**Floor Console (FC) Powder Filling Machine**	- **Uses "Accofil" dosing principle.** - **A manual system capable of dosing via a needle/gun.** - **Cost; system is cheap (~£5-10k depending on dosing gun options).** - **Can be used as a set of 8 needles to dose multiple containers. System has a precision between 0.5% (free flowing) – 3% (cohesive powders). Guns available in sizes from 1/8", 3/16", ¼" and larger. Dosing weight and particle size both within range of the instrument.** - **M&O Perry held original patent for Accofil® technology.**	- **The fully automated version of the system is designed for dosing into vials, the equipment is not set up to work with blister packs so the company may not be able to supply a fully automated machine in the future.**	**Chosen as the recommended system ahead of KControls because M&O Perry held the original patent for Accofil®.**
5	Kinematic Controls, USA	Semi-automatic dosing device	- Identical system to the Floor Console from M&O Perry, however it was invented by the latter.	- As above.	See above.

APPENDIX II
COATING TYPES

The first coating type used for sugar spheres is Acryleze®. This coating combines a globally accepted enteric polymer (Eudragit® L100-55) with an aqueous based formulation. The enteric polymer protects against acid media and is soluble at pH 5.5.

The second coating type is Surelease®. This is also an aqueous based formulation which uses ethylcellulose specifically for modified release and taste masking purposes. Ethylcellulose is used as a rate controlling polymer membrane, hence the rate of release can be directly controlled by the thickness of the film coating.

APPENDIX III

PARTICLE IMAGES

All images were taken using a x10 magnification lens.

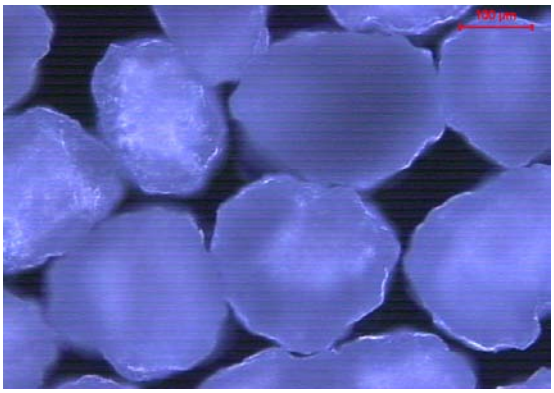

Figure 79 – ACR180, highly spherical

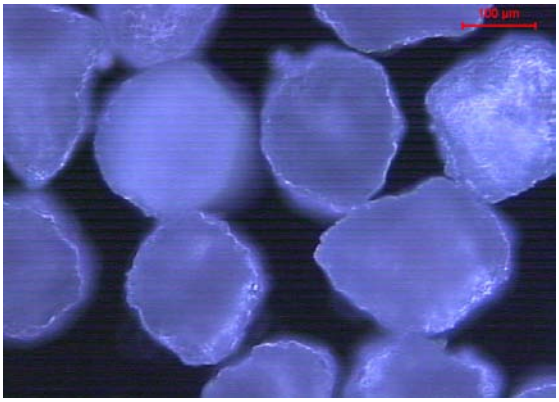

Figure 80 - SUR180, highly spherical

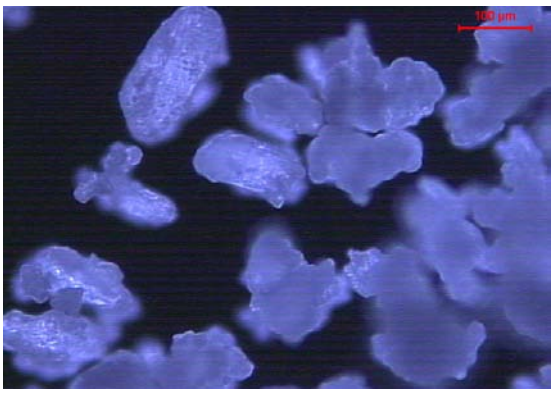

Figure 81 – APAP1627, irregular

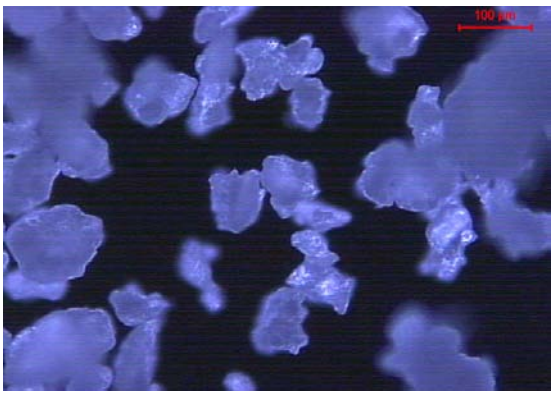

Figure 82 – APAP1624, irregular

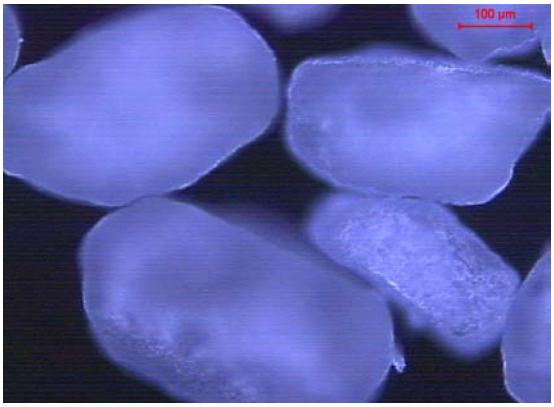

Figure 83 – APAP1776, spherical

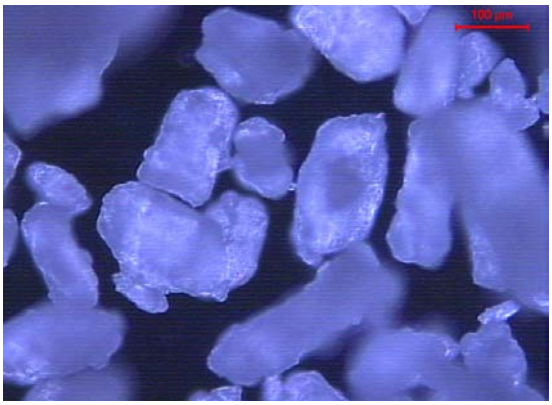

Figure 84 – IBU1618, irregular

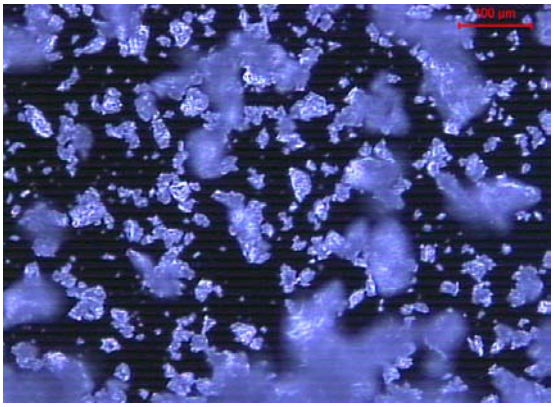

Figure 85 – Lactose, irregular

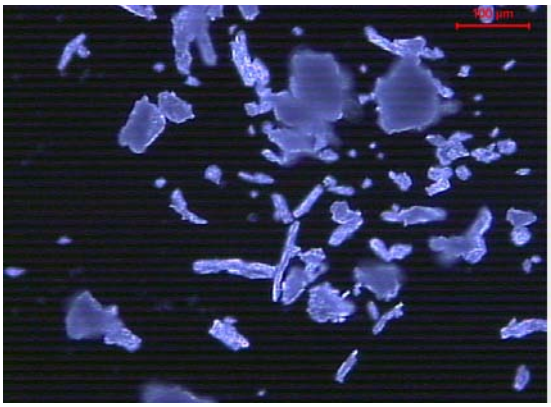

Figure 86 – Avicel, highly irregular, rod shaped

APPENDIX IV

The table below shows the full shear test data for all materials. The material flow functions were calculated and plotted from this table.

Table 21 – Full shear test data

No.	SIGMA1 [Pa]	FC [Pa]	FFC	TAU,C [Pa]	RHOB [kg/m3]	PHIE [°]	PHILIN [°]	PHISF [°]	Bulk solid
1	10076	38	262.31	10	847	36.3	36.2	35	180/250 acryleze
2	10262	135	75.96	37	843	36.1	35.8	35.1	180/250 acryleze
3	10316	52	199.02	14	867	36.3	36.2	35.3	180/250 acryleze
4	21407	184	116.31	48	866	36.9	36.7	36.1	180/250 acryleze
5	20023	248	80.64	67	867	35.9	35.6	34.7	180/250 acryleze
6	20284	307	66.01	83	863	35.9	35.6	34.8	180/250 acryleze
7	29778	516	57.72	142	865	35.4	35	34.3	180/250 acryleze
8	31371	686	45.72	187	867	35.6	35	34.9	180/250 acryleze
9	30758	334	92.21	90	864	36.1	35.9	35.1	180/250 acryleze
						36.1	**35.8**	**35.0**	
No.	SIGMA1 [Pa]	FC [Pa]	FFC	TAU,C [Pa]	RHOB [kg/m3]	PHIE [°]	PHILIN [°]	PHISF [°]	Bulk solid
1	10514	356	29.51	92	829	36.4	35.6	35.5	180/250 Surelease
2	10597	359	29.54	92	817	36.1	35.3	35.4	180/250 Surelease
3	10516	360	29.17	93	815	35.7	34.9	35.1	180/250 Surelease
4	20594	688	29.92	164	827	37.2	36.4	35.8	180/250 Surelease
5	21261	945	22.49	230	823	37.3	36.2	36.3	180/250 Surelease
6	21220	757	28.02	182	826	37	36.1	36	180/250 Surelease
7	29176	2627	11.11	644	823	37.7	35.5	35.3	180/250 Surelease
8	28813	2341	12.31	562	827	37.1	35.2	34.8	180/250 Surelease
9	30556	1782	17.15	451	828	36.4	35	35.2	180/250 Surelease
						36.8	**35.6**	**35.5**	
No.	SIGMA1 [Pa]	FC [Pa]	FFC	TAU,C [Pa]	RHOB [kg/m3]	PHIE [°]	PHILIN [°]	PHISF [°]	Bulk solid
1	10331	0	9999	0	871	37.5	37.5	36.1	355/425 acryleze
2	10523	118	89.32	30	881	37	36.7	35.9	355/425 acryleze
3	10607	132	80.63	35	881	36.8	36.5	35.9	355/425 acryleze
4	20432	314	65.03	82	879	36.8	36.4	35.5	355/425 acryleze
5	20564	140	147.4	35	879	37.6	37.5	36.1	355/425 acryleze
6	20730	127	162.73	33	869	36.6	36.5	35.6	355/425 acryleze
7	31233	757	41.26	198	882	37.6	37	36.2	355/425 acryleze
8	31838	413	77.16	106	880	36.9	36.6	36	355/425 acryleze
9	30277	268	113.15	69	885	37.1	36.9	35.5	355/425 acryleze
						37.1	**36.8**	**35.9**	
No.	SIGMA1 [Pa]	FC [Pa]	FFC	TAU,C [Pa]	RHOB [kg/m3]	PHIE [°]	PHILIN [°]	PHISF [°]	Bulk solid
1	10672	464	23.02	108	802	38.3	37.3	37	355/425 surelease
2	11016	394	27.99	88	813	38.2	37.4	37.3	355/425 surelease
3	10442	390	26.75	94	820	38	37.2	36.5	355/425 surelease
4	21801	1187	18.37	265	810	38.4	37.1	37.3	355/425 surelease
5	21411	1022	20.94	219	815	40.3	39.3	38.2	355/425 surelease
6	22107	1003	22.04	224	826	38.5	37.5	37.5	355/425 surelease
7	31678	2843	11.14	641	818	39.8	37.7	37.7	355/425 surelease
8	31169	2906	10.73	654	818	40.1	37.9	37.6	355/425 surelease
9	31359	2050	15.3	485	823	38.5	37	36.8	355/425 surelease
						38.9	**37.6**	**37.3**	
No.	SIGMA1 [Pa]	FC [Pa]	FFC	TAU,C [Pa]	RHOB [kg/m3]	PHIE [°]	PHILIN [°]	PHISF [°]	Bulk solid
1	10021	161	62.21	41	827	37.3	36.9	35.5	500/600 Acryleze
2	10182	171	59.48	44	831	37.6	37.3	36	500/600 Acryleze
3	10242	75	136.74	19	821	38.1	38	36.3	500/600 Acryleze
4	20922	309	67.73	80	817	35.6	35.3	35	500/600 Acryleze
5	20737	260	79.61	67	833	37.8	37.5	36.3	500/600 Acryleze
6	20635	257	80.26	65	825	38.4	38.1	36.6	500/600 Acryleze
7	29140	304	95.76	77	823	36.6	36.4	34.7	500/600 Acryleze
8	29261	58	504.1	14	827	37.1	37	35	500/600 Acryleze
9	29879	195	153.25	49	822	36.9	36.7	35.2	500/600 Acryleze
						37.3	**37.0**	**35.6**	
No.	SIGMA1 [Pa]	FC [Pa]	FFC	TAU,C [Pa]	RHOB [kg/m3]	PHIE [°]	PHILIN [°]	PHISF [°]	Bulk solid
1	11108	572	19.42	134	767	39.3	38.1	38.1	500/600 Surelease
2	11697	616	18.99	142	766	39.8	38.6	38.9	500/600 Surelease
3				114	765			38.2	500/600 Surelease
4	20981	970	21.64	223	778	38.6	37.6	36.9	500/600 Surelease
5	22239	1068	20.82	231	757	39.2	38.1	38	500/600 Surelease
6	21881	962	22.76	216	776	38.6	37.6	37.5	500/600 Surelease
7	32389	3190	10.15	695	769	40.2	37.9	38.2	500/600 Surelease
8	32408	3903	8.3	852	767	40.8	37.9	38.5	500/600 Surelease
9	33561	2488	13.49	560	778	39.6	37.8	38.3	500/600 Surelease
						39.5	**38.0**	**38.1**	

No.	SIGMA1 [Pa]	FC [Pa]	FFC	TAU,C [Pa]	RHOB [kg/m3]	PHIE [°]	PHILIN [°]	PHISF [°]	Bulk solid
1	9892	587	16.85	149	491	37.9	36.5	35.7	APAP ZM1627
2	10040	570	17.62	144	493	37.4	36.1	35.6	APAP ZM1628
3	10550	525	20.11	133	503	38	36.8	36.6	APAP ZM1629
4	20696	1176	17.6	293	497	38.1	36.8	36.4	APAP ZM1630
5	21147	1132	18.69	277	496	38.8	37.5	37.1	APAP ZM1631
6	21031	885	23.77	222	506	37.9	36.9	36.5	APAP ZM1632
7	31643	1712	18.48	413	510	38.9	37.6	37.2	APAP ZM1633
8	32276	1612	20.02	386	513	39.1	38	37.5	APAP ZM1634
9	32489	1441	22.55	353	516	38.6	37.6	37.3	APAP ZM1635
						38.3	**37.1**	**36.7**	
No.	SIGMA1 [Pa]	FC [Pa]	FFC	TAU,C [Pa]	RHOB [kg/m3]	PHIE [°]	PHILIN [°]	PHISF [°]	Bulk solid
1	11120	160	69.4	40	752	38	37.6	37.2	APAP ZM1776
2	11043	229	48.23	58	758	37.5	37.1	36.8	APAP ZM1776
3	10711	52	204.01	13	766	37.4	37.3	36.4	APAP ZM1776
4	21761	268	81.16	68	758	37.7	37.4	36.8	APAP ZM1776
5	21547	475	45.33	120	757	39.2	38.7	37.6	APAP ZM1776
6	23002	543	42.36	141	751	38	37.4	37.5	APAP ZM1776
7	31687	618	51.27	160	760	37.1	36.7	36.1	APAP ZM1776
8	30660	430	71.38	113	749	36.6	36.3	35.4	APAP ZM1776
9	32894	318	103.45	82	754	37.7	37.5	36.9	APAP ZM1776
						37.7	**37.3**	**36.7**	
No.	SIGMA1 [Pa]	FC [Pa]	FFC	TAU,C [Pa]	RHOB [kg/m3]	PHIE [°]	PHILIN [°]	PHISF [°]	Bulk solid
1	10281	1166	8.82	260	416	41.1	38.4	37.9	Avicel
2	10536	1418	7.43	314	420	42	38.9	38.8	Avicel
3	10616	1396	7.61	302	421	42.3	39.2	39	Avicel
4	21096	2251	9.37	497	422	40.6	38.1	38.1	Avicel
5	21837	2650	8.24	562	427	42.5	39.7	39.6	Avicel
6	21626	2840	7.62	632	425	42.1	39	39.2	Avicel
7	32356	4131	7.83	952	428	41.4	38.4	38.9	Avicel
8	32882	3833	8.58	835	437	42.9	40.2	39.8	Avicel
9	32401	3600	9	779	427	42.1	39.5	39.2	Avicel
						41.9	**39.0**	**38.9**	
No.	SIGMA1 [Pa]	FC [Pa]	FFC	TAU,C [Pa]	RHOB [kg/m3]	PHIE [°]	PHILIN [°]	PHISF [°]	Bulk solid
1	12505	8510	1.47	1661	497	57.7	35.8	47.5	Calcium Carbonate
2	12129	9291	1.31	1868	492	61.1	34	47.6	Calcium Carbonate
3	12190	9130	1.34	1816	486	59.4	32.6	47.3	Calcium Carbonate
4	23189	14834	1.56	2615	539	55.3	35	45.3	Calcium Carbonate
5	23174	15159	1.53	3002	534	54	32.2	44.9	Calcium Carbonate
6	22738	14479	1.57	2424	540	54.7	34.3	44.7	Calcium Carbonate
7	33795	20069	1.68	4225	564	53.2	34.8	44.1	Calcium Carbonate
8	33680	18744	1.8	3927	554	51.5	34.6	43.6	Calcium Carbonate
9	33519	18469	1.81	3760	554	52	35.5	43.6	Calcium Carbonate
						55.4	**34.3**	**45.4**	
No.	SIGMA1 [Pa]	FC [Pa]	FFC	TAU,C [Pa]	RHOB [kg/m3]	PHIE [°]	PHILIN [°]	PHISF [°]	Bulk solid
1	10119	395	25.63	100	544	37.1	36.1	35.5	Ibuprofen
2	10055	340	29.57	83	551	38.8	38	36.4	Ibuprofen
3	10517	317	33.21	77	560	38.1	37.4	36.6	Ibuprofen
4	20453	733	27.91	185	545	37.1	36.2	35.7	Ibuprofen
5	20398	774	26.36	198	543	37.3	36.4	35.8	Ibuprofen
6	20539	567	36.24	142	554	37.3	36.7	35.9	Ibuprofen
7	30922	1158	26.7	293	554	37	36.1	35.7	Ibuprofen
8	29572	1226	24.12	317	545	36.6	35.6	34.9	Ibuprofen
9	31048	1122	27.66	289	559	37.1	36.2	35.8	Ibuprofen
						37.4	**36.5**	**35.8**	
No.	SIGMA1 [Pa]	FC [Pa]	FFC	TAU,C [Pa]	RHOB [kg/m3]	PHIE [°]	PHILIN [°]	PHISF [°]	Bulk solid
1	10133	1686	6.01	365	814	40.9	36.9	37.6	lactose
2	10403	1747	5.96	375	824	41.8	37.8	38.5	lactose
3	10035	1598	6.28	348	827	40.6	36.7	37.3	lactose
4	20281	2570	7.89	574	850	39.7	36.6	37	lactose
5	20064	2547	7.88	570	851	39.3	36.2	36.7	lactose
6	20564	2624	7.84	577	845	39.9	36.8	37.3	lactose
7	30349	3778	8.03	879	862	39.3	36.2	36.8	lactose
8	30348	3883	7.81	911	849	39.2	36.1	36.7	lactose
9	30209	3627	8.33	853	867	38.5	35.6	36.3	lactose
						39.9	**36.5**	**37.1**	
No.	SIGMA1 [Pa]	FC [Pa]	FFC	TAU,C [Pa]	RHOB [kg/m3]	PHIE [°]	PHILIN [°]	PHISF [°]	Bulk solid
1	10189	529	19.27	135	522	37.8	36.6	36	APAP ZM1624
2	10047	520	19.32	134	521	37.1	35.9	35.5	APAP ZM1624
3	10239	480	21.33	121	524	37.8	36.7	36.1	APAP ZM1624
4	20351	921	22.1	241	524	36.6	35.6	35.3	APAP ZM1624
5	19828	941	21.08	248	525	36.8	35.6	35.1	APAP ZM1624
6	20486	857	23.9	218	529	37.4	36.4	35.9	APAP ZM1624
7	31618	1594	19.84	407	528	37.6	36.4	36.4	APAP ZM1624
8	30700	1447	21.22	377	530	36.7	35.6	35.5	APAP ZM1624
9	32225	1783	18.07	453	532	38.4	37.1	37.1	APAP ZM1624
						37.4	**36.2**	**35.9**	

The figures below are the repeats for the flow functions shown in Figure 22.

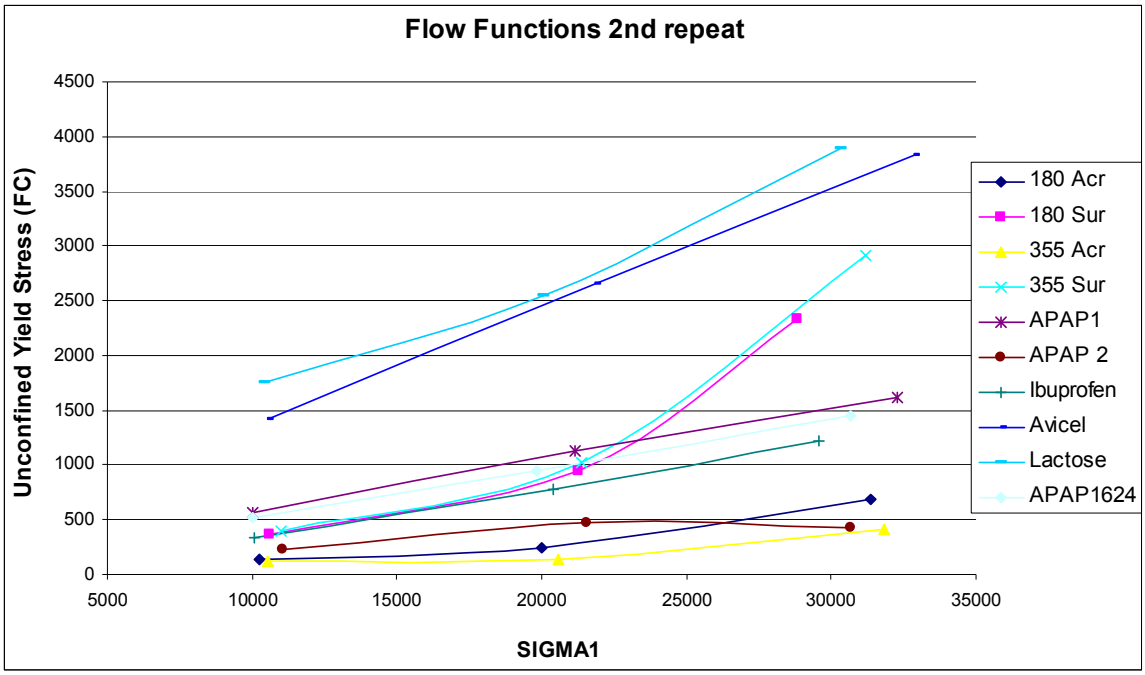

Figure 87 – Flow function curves, 2nd repeat.

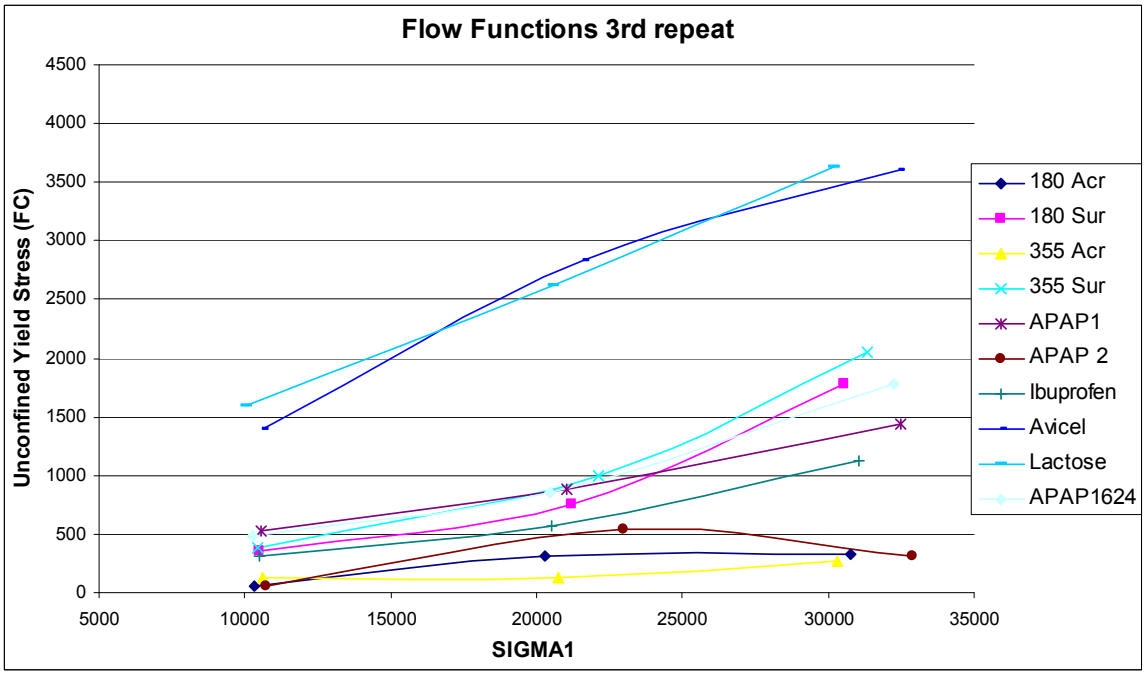

Figure 88 – Flow function curves, 3rd repeat.

APPENDIX V
MEASUREMENT TECHNIQUES BACKGROUND

X-ray CT micro-tomography

X-Ray micro-tomography is a measurement technique that enables the internal structure of a material to be visualised in three-dimensions. The technique is non-destructive and does not require special preparation of the sample. The technique works by taking X-ray images of a sample as it rotates through 360°. The result is a shadow image, as shown on the left in Figure 89. The shadow images are then used to obtain images of horizontal cross-sectional slices using image reconstruction software, as shown on the right in Figure 89. These images can also be used to obtain vertical cross sections for a sample and to create a virtual 3D model.

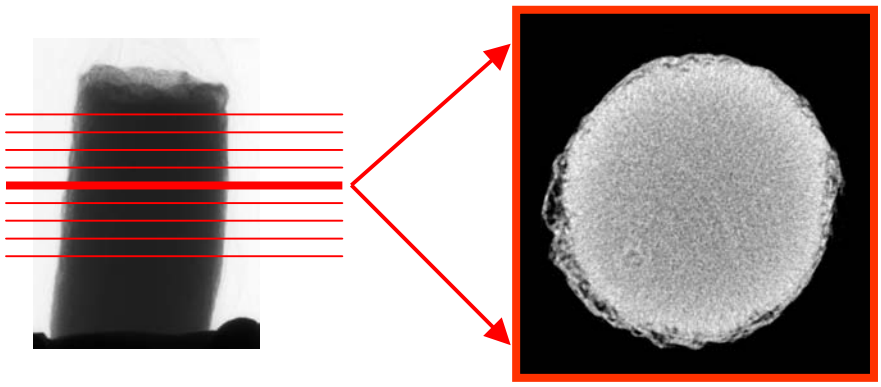

Figure 89 – Diagram showing a typical "shadow" image, and its reconstruction to give a cross sectional image.

Dynamic Vapour Sorption (DVS)

DVS is a characterisation technique that relies on the ability of a sample to sorb water vapour. The physical and/or chemical characteristics of samples can affect the amount of vapour uptake therefore variations in one or more samples can easily be detected by using DVS. The technique is used for quantification of low crystalline and amorphous content in a sample. It can also be used to determine the moisture-induced transition from amorphous to crystalline structure; this is particularly useful for predicting critical storage and process conditions of materials. Other uses for DVS include characterisation of polymorphs and general moisture uptake studies for the prediction of storage conditions and effectiveness of packaging materials (Bridson, 2007).

DVS is a technique in which a sample is subjected to varying conditions of humidity and temperature in a controlled manner. The response of the sample is measured by the change in mass. The equipment essentially consists of a micro-balance and two containers for water and octane. Dry nitrogen flows through the system, and can be directed through either the water or octane depending on the vapour of interest. The microbalance contains a reference sample in one pan and the sample of interest in the other. The relative humidity is then controlled and increased in steps, with the changes in mass of the sample recorded. The technique is extremely sensitive and thus can be used with very small samples (~5mg).

Figure 90 – DVS Advantage, SMS instruments, UK (Bridson, 2007)